Fabrication of single crystalline ultra-thin superlattices by self-assembly via oriented attachment of PbTe nanocrystals

Joep Lodewijk Peters

Student no: 3230465

E-mail: j.l.peters@students.uu.nl

Thesis supervisor: Dr. Dariusz Mitoraj

Second supervisor: Prof. Daniël Vanmaekelbergh

3th of September, 2013

Abstract.

Oriented attachment offers new possibilities to precisely build up complex structures. In this thesis oriented attachment of PbTe and PbS is investigated on an ethylene glycol toluene/hexane interface. While drying a quantum dot solution on a layer of ethylene glycol, the quantum dots attach in three distinct superstructures. Linear attachment is observed for both materials in which the quantum dots attach head to head. Also totally square structures are formed for PbS and a more parallelogram shape for PbTe are observed. For PbTe also patches of siliceen lattices are fabricated. Models were made, to explain how these different structures create.

Content.

1. General introduction.

Developing new materials has always been a main driven force of research in the chemical land and physical world. New materials with new properties has amazed people for hundreds of years. Since the discovery of graphene it was clear that this material has a lot of potential [1]. The regular hexagonal pattern of graphene yields an extremely high electron mobility in the growth direction of graphene. Together with other special properties, these characteristics is also searched on other materials with the same crystal structure. Fabricating the honeycomb pattern by an atomically connection of the colloidal nanocrystal, could yield for example materials with a high spin orbit coupling [2]. Lead chalcogenides and especially PbTe are promising materials also due to its infrared absorption and its inverse bandgap in combination with Sn [3] [4] [5] [6].

In nanotechnology it was already early recognized that if we would like to make practical use of all these new features offered by these new materials, production on a larger scale is necessary. Self-assembly would be a very useful option to create devices of sizes of practical meaning [7]. Recently, a new bottom-up approach is introduced, which yield atomically connected structures [8]. In this process of oriented attachment a very precise building up of large structure is achieved by connecting the individual building blocks [9]. Quantum dots are, in this thesis, the building blocks, in which certain facets attach to each other to form very precise ultra-thin 1D or 2D superlattices.

First the theory on growth and oriented attachment in general will be discussed, followed by the experimental and characterization part. Then the results will be discussed and for every structure found a model is given to explain the arise of the structure. The end of this thesis will consist of the main conclusions and outlook for future work.

2.   Theory.

2.1. The hot injection method.

For most syntheses of quantum dots the hot injection method is used. This method developed by C. Murray et al. is derived following the classical nucleation theory (CNT) and has the goal to get monodispersed particles [10] [11]. The steps in the hot injection method are given in figure 1. Two precursors are made, one for the eventually cation and one for the anion. In most syntheses, the precursors consist of the nonmetal or metalloid dissolved in a coordinated solvent and the metal dissolved in an organic solvent by means of ligands [12] [13]. One of the two is quickly injected in a hot solution of the other ion. Now the nucleation of the nanoparticles occurs rapidly [14]. To get a narrow size distribution a sufficient separation of the nucleation and growth stage is required (both stages are described below) [15]. In general, the nucleation stage determines the number of nuclei formed, which is crucial for the eventual size of the particles; contrary in the growth stage these nuclei grow to the desired size and no new nuclei will be formed. After a typical time span of a few minutes the reaction is quenched rapidly, to prevent Ostwald ripening [16]. The last step is the purification by washing off the organic solvent and residual products, by precipitating of the particles using short chained alcohols. This will be centrifuged and dissolved again in an apolar solvent and repeated two to four times, depending on the purity required.
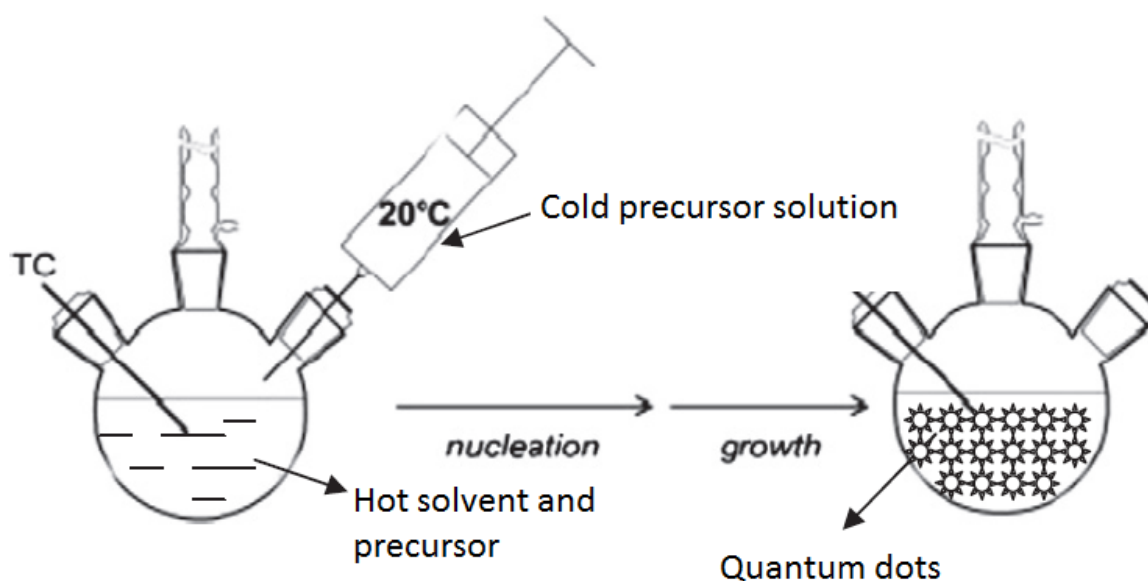

Figure 1. An overview of the of the hot injection method. A cold precursor solution is quickly injected in a hot solution of the other precursor. Nucleation starts immediately and is quickly followed by the growth stage.

It is demonstrated that the washing not only removes residual organic solvent and byproducts, but also a part of the organic shell of ligands [17] [18] [19]. The exact extracted amount of ligands depends on the kind of particles, the kind and amount of short chain alcohols used. For PbSe, washing with ethanol removes about 20% of the oleic aci, commonly used ligands, form the surface of the quantum dots [20]. This is probably roughly the same for all lead containing quantum dots (PbS, PbSe and PTe), due to the fact that oleic acid is bound to lead [21].

2.1.A. Nucleation.

After the quick injection of a precursor solution, the nucleation stage starts [22]. Monomers are formed from the reaction of two precursors. Because of the high Brownian motion and reactivity, the concentration of monomers increases and also clusters of monomers are formed. The shell of ligands around a monomer is very thin, due to the small amount of ligands in this stage. When clusters are formed the volume to surface ratio increases and therefore the amount of ligands available for surface protection arises and the shell gets denser. These clusters or nuclei, can increase in size until the critical nucleus radius is reached in which the probability of further growth and redissolving of nuclei is equal. The concept of a critical radius can be understood be the CNT and the free energy. The energy involving spherical nanoparticles is given by.

$$\Delta G_{Tot} = \left(\frac{4}{3}\right)\pi r^3 \rho \mu + 4\pi r^2 \gamma = \Delta G_V + \Delta G_S$$

in which r is the crystal radius, ρ is the density of the crystal phase, μ is the chemical potential and γ is the interfacial tension between the crystal and solution [23]. The first part explains the free energy decrease caused by the formation of bounds in the crystal nuclei. The second term is surface excess free energy, which is the energy loss by atoms at the outer layer of the nanocrystal due to dangling bounds. Because of the opposite sign, there is a maximum for the ΔG_{total} which is visualized by figure 2. The parameters influencing the critical radius are

$$r_c = -\frac{2\gamma}{\rho k_b T \ln S}$$

In which k_b is the Boltzmann constant, T is temperature and S is the degree of supersaturation.
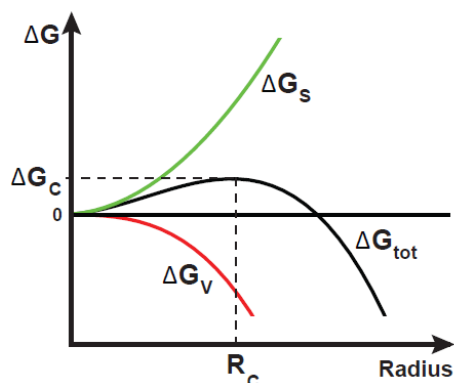
Figure 2. Development of the free energy in the formation of a spherical crystal nucleus. ΔG_c gives the activation energy, ΔG_s gives the surface excess free energy, ΔG_v gives the volume excess free energy and ΔG_{tot} gives the total free energy change.

These critical nuclei are formed in supersaturated solutions of monomers. Also temperature provokes formation of nuclei due to the increase in Brownian motion. In our case, supersaturating is achieved by a sudden increase in monomers by injection of the other ion. While injecting this cold opposite precursor solution the temperature will decrease, which result in a better separation of nucleation and growth stage. These critical nuclei than consume more monomers or the nuclei can growth by coalescence [9]. Meanwhile the amount of monomers and nuclei formed, quickly decreases to concentrations lower than the supersaturating concentration, caused by an increasing rate of consumption compared to formation of monomers [21]. Eventually there is no supersaturated solution anymore and only the particles which reached the critical radius growth further and others redissolve in monomers, which are used in the growth stage.

2.1.B. Growth.

As mentioned above growth of the critical nuclei can proceed by two processes. It can occur by the addition of monomers or by the coalescence of two nanocrystals. It is shown that both growth processes occur and end up with particles of the same size, which is counterintuitive in first thought [9]. This is caused by a form transformation due to surface restructuring after coalescence, which even reduces the size, but makes the particle more spherical [24]. When considering growth in general two distinct regimes can be indicated. The particles (or monomers) should approach each other, in which diffusion is the driver and the particles should be incorporated into each other. These two regimes are called the diffusion controlled regime [25] and reaction controlled regime respectively [21] [26], depending on which process is rate determinative. In the initial growth stage, the growth will be primarily determined by the incorporation of the monomers or the reaction rate of the monomers (or particles) and the nanocrystal. The high temperature and the high monomer concentration are

8

responsible for the high availability of monomers. This growth stage depends on the reactivity of both monomers and nanocrystal, and their ligands, but also on crystallographic orientation of the facet and the site on the facet (corner for example), because all monomers must be incorporated into the crystal lattice [14] [21]. Steric hindering of ligands does not play a prominent role here due to the low volume to surface ratio and the high temperature. In the last stage, growth will primarily be determined by the diffusion speed of the particle (or monomer) to the nanocrystal, due to the lower concentration and Brownian motion. Even though, the particles are in this stage completely surrounded by ligands, which provide protection by steric hindering, temperature is often high enough to overcome this barrier. In this stage there is an excess of ligands due to the increase in particle size and the decrease in surface volume ratio. In other words; there is less surface availably than ligands can occupy. Ligand will than, if the temperature is high enough, etch monomers from the surface which they can redeposit on other particles [27] [28], which can lead to Ostwald ripening [23]. But it is also shown, for mostly metallic particles, that this etching can be used to transform polydisperse particles towards monodispersed particles, by a process called digestive ripening [29] [30] [31] [32] [33] [34] [35] [36]. Two competing processes should occur at that time; particles are minimizing there surface energy by increase in size and the ligands try to decrease the size of the particles so the ligands can occupy more surface [37] [38] [39].
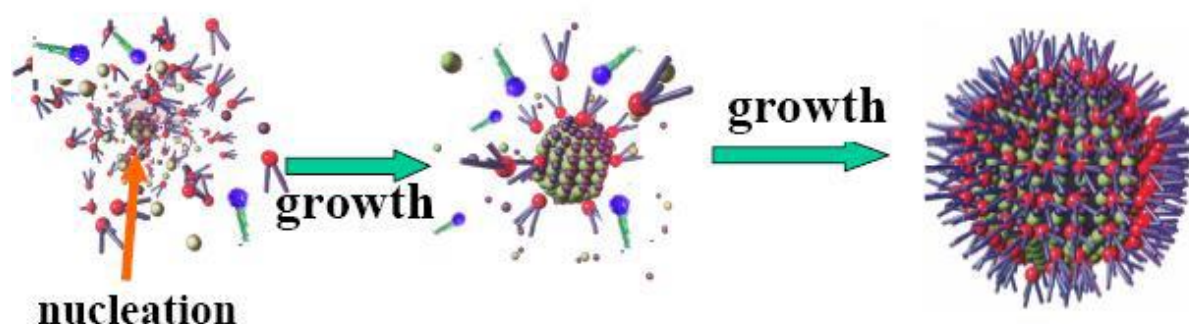

Figure 3. Schematic representation of the formation of quantum dots, starting from the nucleation followed by the growth stage. Reprint of ,C. de Mello Donegá, Universiteit Utrecht, Lectureslides 'Preparation', Nanomaterials Course 2009-2010, 11

2.2.   Oriented attachment.

2.2.A. Introduction.

In nanotechnology two approaches can be uses to build up new materials, the top down or the bottom up method. The main difference between the two approaches introduced by the Foresight institute is how new material will be made [40] [41]. Starting from the bulk and decrease in size, to get the special properties which make nanotechnology so interesting or start from the building blocks and build the material up to the desired form [42]. To manufacture these new materials by the bottom up approach it is impracticable to build it up by hand. Self-assembly offers a solution for this problem [7] [43]. In this process, the building blocks form a material of micro-meso or macro dimensions by itself due to the responsible forces like electrostatic, hydrophobic, magnetic or van der Waals forces [23]. These new building blocks are not atomically connected, but they are separated by ligand shells. A more recent process involves the real attachment of these building blocks in new structures; this process is called oriented attachment [44] [45] [46]. Growth in this process occurs not by classical crystallization but by precise attachment of the building blocks in such a way that the crystal planes are matched [8] [47] [48]. The crystal planes are than extended over a long area to yield large scale complex materials. In oriented attachment growth never occur by monomer by monomer attachment, but by coalescence of two approaching quantum dots (figure 4). In this process the incorporation of the quantum dots is the rate determining step and is therefore said to be in the reaction controlled regime.

2.2.B. Forces involved.

The forces involved in oriented attachment are not completely understood. Because it is reaction controlled it already means that there must be besides attractive forces also repulsive forces. This balance between repulsive and attractive forces makes this regime so interesting, but also vulnerable for small environmental changes [49]. The layer of ligands around the dots are the only repulsive forces otherwise normal aggregation would take place, in which the surface energy decreases [14]. Attachment will proceed by particles approaching each other and search by rotation for the best crystal plane alignment; when this is found attachment occurs very rapidly [47] [48] [50].
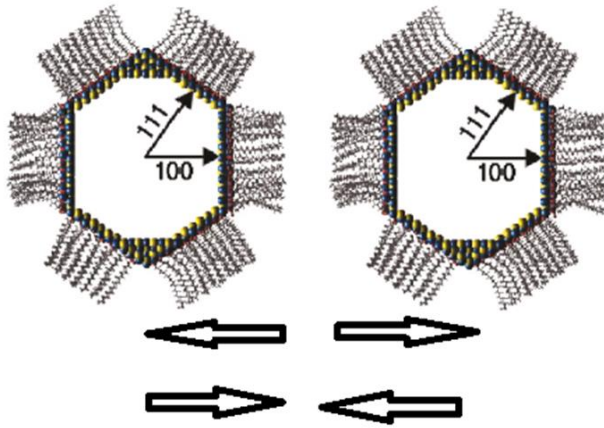
Figure 4. A schematically overview of two approaching quantum dots. Around the quantum dot the repulsive ligand layer is shown [51].

As mentioned in the introduction, matching of the facets is typical for oriented attachment and influenced by energy differences between the facets of a single nanocrystal, in which (for PbSe) the {100} has the lowest energy followed by the {110}, {111} facets [52]. Attachment will therefore preferential start at the facet with the highest energy to minimize its surface energy. Another consideration is that the particle will attach at the crystalline facets with the lowest steric hindering or in other words attached occurs at the facet with the lowest amount of ligand absorbed [53] [54] [55]. It is shown that the amount of ligands bounded to different facets differ and that it also influence the self-assembly [56] [57].

Table 1. An overview of the possible forces involved in oriented attachment.

Direction	Type of force	Source of force.
Repulsive	Steric hindering	Ligand layer around the quantum dot [21] [55].
Attractive	Reduction of surface energy	Differences in surface energy [45] [58]
Attractive	Interatomic electrostatic interactions	Ion nature of quantum dots [59].
Attractive	Dipole moment	Different composition of atom at facets [52] [60].
Attractive	Van Der Waals	dipole–dipole, dipole-induced dipole and London interactions [61].

Which attractive force play the largest role is however not completely clear. Energy calculation predict that long range Coulombic interactions and surface energy are the determined factors and not Van der Waals interactions or dipole interactions. In this article of H. Zhang and J.F. Banfield, predictions of the facet of attachment is done by taking does two factors into account for several quantum dots. They were successful in predicting the right facet in experimental papers. An strong point they make is that in metallic particles the facet of attachment is always the facet with the highest surface energy, since those metallic particles have bonds which are less directional, compared to ionic or covalent bonds [59]. An overview of all attractive and repulsive forces in given in table 1.

2.2.C. Ligands.

Ligands play an enormous important role in the process of oriented attachment and synthesis of nanocrystals. In this part extra attention will be paid to all the functions ligands play. Ligands are amphiphilic organic molecules with a polar head group and a non-polar hydrocarbon tail. The head is coordinated to the metal (lead) in the nanoparticle while the tail interacts with the organic solvent [14]. The chalcogenide-ligand bond is an π-backbonding interaction, which results in electron transfer from the metal (lead) to the C-O bond of the head group [62]. This ligand shell around the nanocrystal plays a central role in the interaction between the nanocrystals and their surroundings. The different functions of ligands are; the control growth during the synthesis, colloidal stability in solution, chemical functionality and optical properties [21] [62] [63] [64] [65] [66].

The colloidal stability is due to the fact that ligands prevents nanoparticles from aggregation by means of steric hindering. Otherwise particles will aggregate, due to van der Waals forces, reduction of surface energy or electrostatic interactions. The stability of quantum dots also increases with increasing length of the hydrocarbon tail. Large tails possess a higher protection, caused by a less Van der Waals interaction between the two approaching particles and larger repulsion by steric hindering [14]. By changing the ligands or functionalize the surface it is possible to use nanocrystals in different environments [67].

In the synthesis of nanoparticles, the bond strength and the availability of ligands play a huge role. A higher binding strength result in more stable monomers and high colloidal stability, but this can result in a slow growth. It also results in less nuclei formed and therefore bigger

particles. A large amount of ligands will have the same effect, by increasing the stability of monomers which results in less nuclei and smaller particles.

Optical properties are also dependent on the nature of the ligand in three ways. A quantum dots tend to lower the surface energy by modification of the surface atoms. A rearrangement or relaxation then results in a lower surface free energy which in turn changes the energy of the surface states [13] [66].

Depending on reaction conditions, ligands can facilitate even opposite processes. An example is Ostwald ripening on one hand and digestive ripening on the other hand. If the temperature is high and the ligands are bound in such way that they can attach or detach monomers from the original quantum dot, but the main driven force will be lowering the surface energy, it will results in the Ostwald ripening principle [23]. On the other hand, if the concentration monomers is sufficient, the temperature is moderated and an equilibrium between detach and attachment of monomers is achieved, size focusing and digestive ripening will occur [68] [37]. In oriented attachment however etching monomers from the surface is not desired, since oriented attachment is based on coalescence of whole quantum dots [49].

2.2.D. Reaction controlled regime.

As mentioned in quantum dot growth section, this growth by coalescence has two regimes. The first regime is the diffusion controlled coalescence in which (almost) every coalescence lead to successful attachment. In this regime the repulsive force by ligands is hardly present or not strong enough due to the high temperature (e.g. in the later stage of the hot injection method). While in the reaction controlled regime the incorporation of the particles is the determining step. In this regime one can have much more control over attachment and make use of energy differences between facets. If two opposing particles approach each other in the reaction controlled regime, the reaction determines the attachment of two particles. Because not every collision leads to a successful attachment only reactions which yields the most energy will occur. This process of very precise attachment is called oriented attachment [8]. The reaction conditions should make it possible to balance the attractive and repulsive forces , thus slow and precise attachment is possible. This process of oriented attachment originates from research on TiO_2 performed by R. Lee Penn et al [45] [8]. In this research the authors discovered that nanocrystalline TiO_2 growths under hydrothermal conditions and sometimes

forms twinned and planer defects while growing. Shortly it was noticed that the reduction of the high surface energy facet played a huge role in which facet will be attached [58]. Later on, more research is conducted on this intriguing process of crystal growth and bio-mineralization [69]. The formation of bio-minerals in nature as well as synthetically manufactured was studied extensively [46] [70] [71]. There are proposed several mechanisms to explain the process of oriented attachment. In figure 5, the main mechanism is shown for two or three D systems [72]. In this mechanism, first a mesocrystal is formed. This is a self-assembled crystal, which consist of unattached building blocks [71] [73]. The ligands prevent attachment of the building blocks after self-assembly, but these ligands are eventually detached from the surface of the individually building blocks. After this detachment the facet are free to attach with the opposite facet and fusion occurs [49]. In the case of 1D materials like wires this process does not hold. It is assumed that the particles are free to move until the binding facet with the highest energy increase is found and attachment occurs [74].
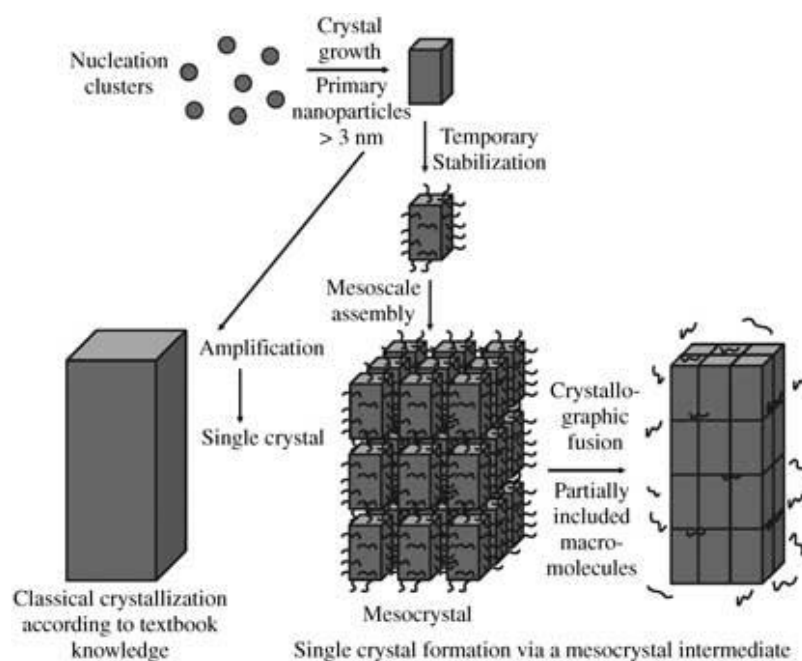

Figure 5. A schematically representation of the classical crystallization process versus the non-classical one. Crystals can grow by direct attachment of the building blocks in the left pathway. In oriented attachment however the right-hand pathway is followed. In this pathway first a mesocrystal is formed by nanoparticles coated with an organic ligand, which can eventually fuse together to form a single crystal [71].

2.2.E. What is done?

In recent years there are several examples of oriented attachment noted in literature. The first discoveries were 1D attachment of quantum dots into a nanorod which is currently reported for several materials (CdSe, Pt_3Fe, ZnO, ZnTe, FeO(OH),CdTe, Ag, Au, ,PbS, PbSe) [75] [74] [76] [46] [77] [78] [79] [80] [81] [82]. An often suggested driven force behind this formation is a small dipole moment in a quantum dot, as discussed in the 'forces behind' section [83] [81] [84] [60]. This is caused by a different compositions of the facets of a single quantum dot [52]. Hong-Gang Liao et al. show in a film by real time TEM in a beautiful way how separate quantum dots attach in a linear manner by dipolar interaction [74]. Although, C. Fang et al. and others doubt if this dipole moment is strong enough to be the cause of linear attachment [52] [85].

2D structures by self-assembly were also discovered with an interfaces as template, like gas-solid [86], gas-liquid [87] [88], liquid-solid [89] and liquid-liquid interface [90]. Examples in which real attached atomically attached structures are made also exist, in which the article of C. Schliebe is the most representative example [91]. In this article ultrathin PbS sheets arise after the authors synthesized PbS quantum dots. These quantum dots, as the authors claim, oriented attach in a planer way to form sheets. S. Ithurria et al. made CdS, CdSe and CdTe nanoplatelets and notice a similar event, but left the exact mechanism open. Also here, quantum dots are visible and nanoplatelets are formed. Another mechanism, which could happen is the dissolution of the quantum dots, followed by monomer-to-monomer attachment on the nanoplatelets [92] [93] [94].

It is already possible to make 3D structures by oriented attachment. [53] [95]. Z. Zhang et al. show that three dimensionally structures arise by oriented attachment of small nanocrystals into an ellipsoidal structure. Although the attachment does not result in a completely filled solid structure, all crystal planes match and a certain specific attachment direction is achieved. It is suggested that this anisotropic growth direction in the order [010] > [100] > [001] is due to the copper rich and therefore ligand rich (the ligand is attach to the copper ion) [001] plane. Because of the steric hindering less collisions are successful and results therefore in slower growth in that direction [53].

3. Experimental.

3.1 List of chemicals.

Chemical	Abbreviation	Manufacturer	Purity	M (g/mol)	ρ (g/mol)
1-octadecene	ODE	Aldrich	90%	252,48	0,789
Trioctylphosphine	TOP	Aldrich	90%	370,94	0,831
Oleic acid	OA	Aldrich	90%	282,46	0,895
Tellurium <250micron	-	ChemPur	99,999%	127,60	6,24
Bis[bis(trimethylsilyl)amino]tin (II)	-	Aldrich	-	439,48	1,136
Tetrachloroethylene	TCE	Aldrich	spectrophotometric grade, ≥ 99%	165,83	1,622
Oleylamine	OLA	Acros organics	80-90%	267,46	0,813
Ethylene glycol	EG	Aldrich	99,8%	62,07	1,1132
Diethylene glycol	DEG	Aldrich	99%	106,12	1,118
Lead(II) acetate trihydrate	-	Aldrich	99,99%	179,33	2,55
Anhydrous methanol	MeOH	Aldrich	99,8%	32,04	0,798
Anhydrous hexane	-	Aldrich	≥99%	86,18	0,655
Anhydrous acetone	-	Merck Millepore	99,9%	58,08	0,791
Anhydrous ethanol	EtOH	Aldrich	99,8%	46,07	0,789
Anhydrous toluene	-	Aldrich	99,8%	92,14	0,87
Chloroform	-	Aldrich	99%	119,38	1,489
Tetrachloromethane	-	Acros organics	99%	153,82	1,587

3.2. PbTe synthesis.

PbTe quantum dots were synthesized following the procedure of J.E.Murphy et al. and J.J.Urban et al. [96] [22]. The synthesis were performed in a Schlenk line or glovebox to establish an oxygen and water free environment. A typical synthesis is performed in a four-neck round-bottom flask. The lead precursor was made by heating lead acetate, oleic acid and ODE for 3 to 4 hours to get rid of the acetate and form lead oleate. The ratio between OA/Pb was about 1 for the smallest particles and 6 for the largest. The Tellurium precursor was made by dissolving fine tellurium in TOP of a concentration of 0.5 M. The actually synthesis was performed in a temperature range from 150°C, for the smallest particles and 180°C for the biggest. The molar ratio of Pb:Te was approximately 2:1 or reversed, which could be adjusted to 1:1 for smaller particles. Rapid injection under vigorous stirring of Te-TOP was crucial to get monodispersed particles which was followed by a decrease in temperature of 120-150°C. After 1 min for the smallest particles and 6 min for the larger particles the reaction was stopped by injection of ethanol or hexane and cooled with ice. Afterward, the particles were washed with ethanol and redispersed in hexane, this was repeated 2-3 times.

3.3. SnTe synthesis.

SnTe quantum dots were synthesized similar as M.V. Kovalenko et al [97]. All experiments were done in an oxygen and water free environment. A TOP-Te solution was made by dissolving elementary Tellurium in TOP and heat it for 2 hours at 100°C. A typical stock solution contained 0.75g Te and 8ml TOP. The tin (II) precursor was a dilution of 0.16 ml (0.4mmol) Bis[bis(trimethylsilyl)amino]tin(II) in 6ml dry 1-octadecene [ODE].

In a typical synthesis, 14ml of a mixture of oleylamine and ODE and 1ml of the TOP-Te stock solution was placed into a 250ml four-neck round-bottom flask and heated to 150°C-180°C. The tin precursor solution was loaded in a injector flash and swiftly injected into the Tellurium solution under vigorous stirring. After injection the temperature dropped to 110°C-150°C and was terminated after 1.5 min by quenching or/and cooling down by ice. After the solution was cooled, 3ml of oleic acid was added to stabilize the particles. A chloroform/acetone mixture (1:1) was added to the crude solution to precipitated the particles which were later collected by centrifugation. The particles were additionally purified by

dissolving them in chloroform and precipitate with acetone. Finally, the particles were dissolved in nonpolar solvent, chloroform, tetrachloroethylene or tetrachloromethane.

3.4. Oriented attachment.

Two dimensional structures made by oriented attachments are grown by drying a strongly diluted suspension of quantum dots in hexane or toluene on ethylene glycol (EG) or diethylene glycol (DEG). In a typical experiment, 1 mL of EG was placed in an open glass vial (Ø 10 mm). 50µl of the suspension was dropped on the EG and evaporated at different temperatures between 7°C-100°C for different times (between 10-180 minutes). After the evaporation, TEM samples were prepared by dipping a TEM grid into the two dimensional solid membrane and put the membrane under vacuum to evaporate the EG. The experiment is shown in a schematic way in figure 6.
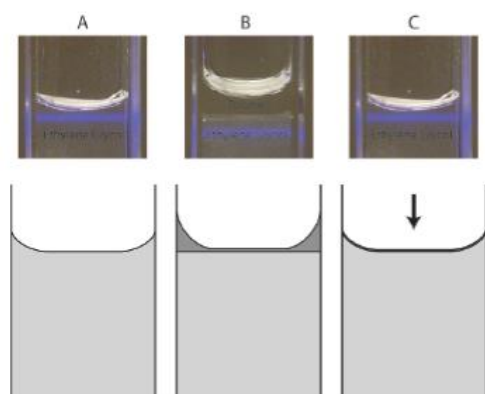
Figure 5. A schematically overview of the oriented attachment experiment. In (B) a strongly diluted quantum dot solution is dropped on 1 mL EG (A). In (C) the solvent is evaporated and the quantum dots form a structure on the surface of the EG. Reprint of [82].

4. Characterization.

4.1. Absorption spectroscopy.

Absorption spectroscopy was performed on a Perkin-Elmer Lambda 950 uv/vis spectrophotometer. The wavelengths chosen was from 1000 nm till 2500 nm for the PbTe samples and 1000 nm till 3000 nm for the SnTe. The samples were diluted so the solution became transparent. To prepare the sample and prevent unwanted distortions in the spectra PbTe samples were diluted in tetrachloroethelyne (TCE). This is done by taking the right amount and evaporating the solvent (hexane or toluene) in vacuum and afterwards dissolving it in 2 ml of TCE. For the SnTe samples, it was often hard to dissolve them properly in TCE, instead carbontetrachloromethane or mixtures of chloroform, TCE or carbontetrachloromethane were used depending on the solvability. The cuvettes were made of quartz which gives no distortion with the light used with a path length of 1 cm.

4.2. Photoluminescence.

Emission spectroscopy is performed at an Edinburgh Instrument with two different detectors. One with a sensitivity up to 1600 nm and the other with a sensitivity up to 2600 nm (R5509-72 and G5852, respectively). The detector R5509-72 is more sensitive compared to the G5852. For all emission measurements the same sample dilution was used as for absorption measurements.

4.3. Transmission electron microscopy.

Measuring quantum dots by TEM was performed in the following way, samples were taken by dropping a small amount of (diluted) quantum dot solution on a carbon coated copper TEM grid. The excess amount of solvent was removed by evaporation in the glovebox, the cup was put under an angle of $\pm 30°$. The samples or the oriented attachment measurements were fished by a tweezers. The TEM measurements were performed on a Fei Tecnai-10 or Tecnai-12.

4.4. Grazing incident small angle X-ray scattering.

Grazing incident small angle X-ray scattering (GISAXS) is performed at the ID-10 beamline of the European synchrotron radiation facility in Grenoble, France, under experiment SC-3537. In the GISAXS setup (figure 6) a x-ray beam of 13.3keV (λ=0.93Å) is scattered on the sample surface. By the reflection one can probe the surface morphology (figure 6A) and get a projection in reciprocal space of the statistical average of the surface [98]. Our experiments were performed in a round Teflon tub with a diameter of 68 mm and a depth of 8 mm filled with EG (22-25 ml). 4 or 5 ml of diluted quantum dot solution was dropped on this layer of ethylene glycol. The measurements are performed in situ to track the scattering from the surface in time while the hexane evaporates. To keep the height of the surface at the same level, EG was injected in the bottom layer. An effort was made to perform the measurement in a nitrogen environment, but this was hard due to several leaks in the setup. The beam searched by moving the sample holder up and down, to find the optimum scattering height of maximum intensity. When this 'height scan' was finished, a longer scan was performed at the maximum intensity height. After the longer scan another run started, by repeating the previous steps. By changes of this height (monitored by the computer outside the camber), it was possible to track the amount of EG necessary to keep the liquid-air interface at the same level.
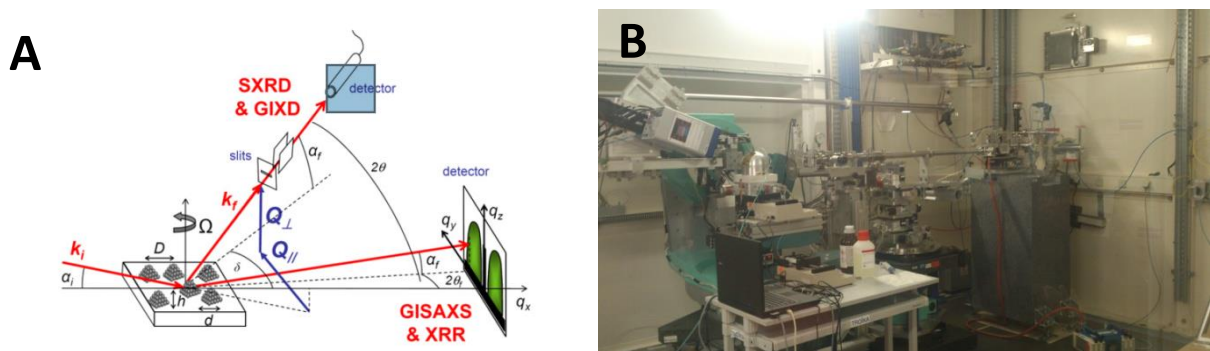

Figure 7. (A) A reproduction of the Grazing incidence X-ray scattering geometry. A detector at small angle (GISAXS) as well an detector at large angles (GIXD) was place, although no signal appeared at large angles [98]. (B) The setup in Grenoble, with in the middle the semicircular closed sample setup. The box with the blue bottom is the detectors for GIXD measurements and the pipe under it, is the GISAXS detector.

5. Results.

5.1 Synthesis of PbTe quantum dots.

PbTe quantum dots of varies sizes, ranging from 3.5 nm till 7 nm (diameter) were successful synthesized (figure 8A and figure 9). This is the range (till ~9.3 nm) where the particles are truncated cubes, caused by the transformation from nucleation which has double pyramid special form, to the cubic structure rocksalt (figure 8C), which is the final crystal structure for PbTe [96] [99] [3]. This spherical (truncated cube) shape is confirmed by TEM images, but the degree of truncation (value of q in figure 8C) is unknown and depends on the amount of oleic acid present and the size of the particle [51] [100].

The black particles show luminescence in the IR range of the light spectrum [3]. Quantum confinement is beautifully shown, in which the absorption and emission of smaller particles lies at higher energies compared to bigger particles (figure 9C). There are several parameters which can be used to influenced the synthesis of PbTe quantum dots. The most common are temperature, concentration of oleic acid (represented by the ratio oleic acid and lead atoms) and reaction time.
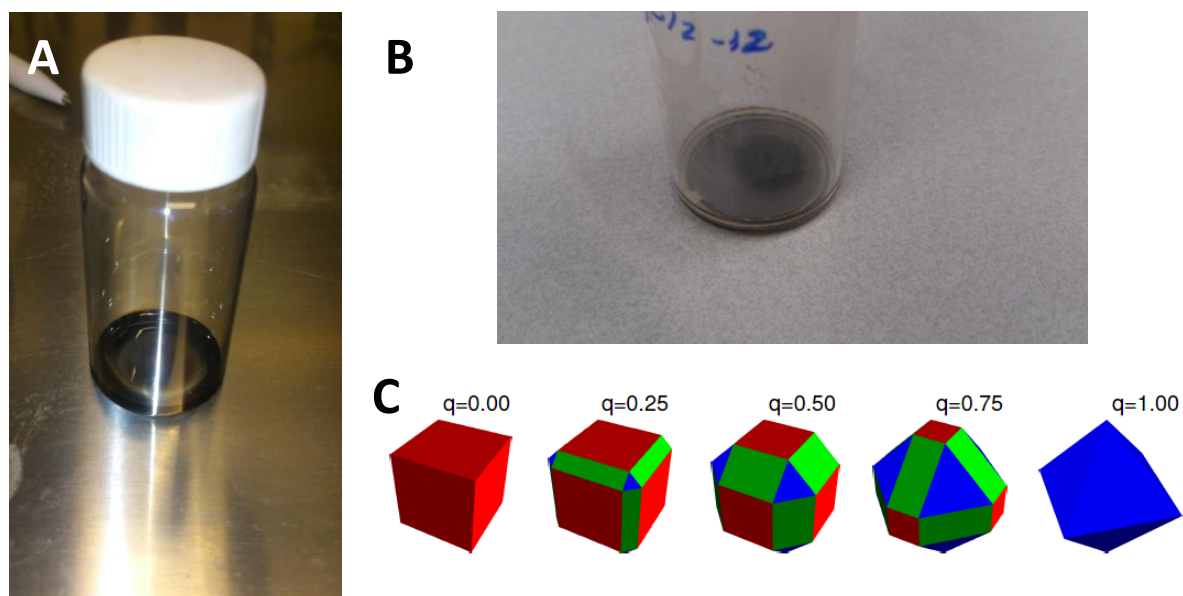

Figure 8. (A) A cup with successfully synthesized black PbTe quantum dot solution. (B) PbTe exposed to one day of air. The solvent is evaporated and a grey layer is covering the degraded quantum dots. (C) The evolution of quantum dot growth. At a q=1.00 the particles is nucleated and formed a double pyramid in which the high surfaces grow to form a truncated cube. Finally when the particle growths even further a cube is formed shown at q=0.00 [82].
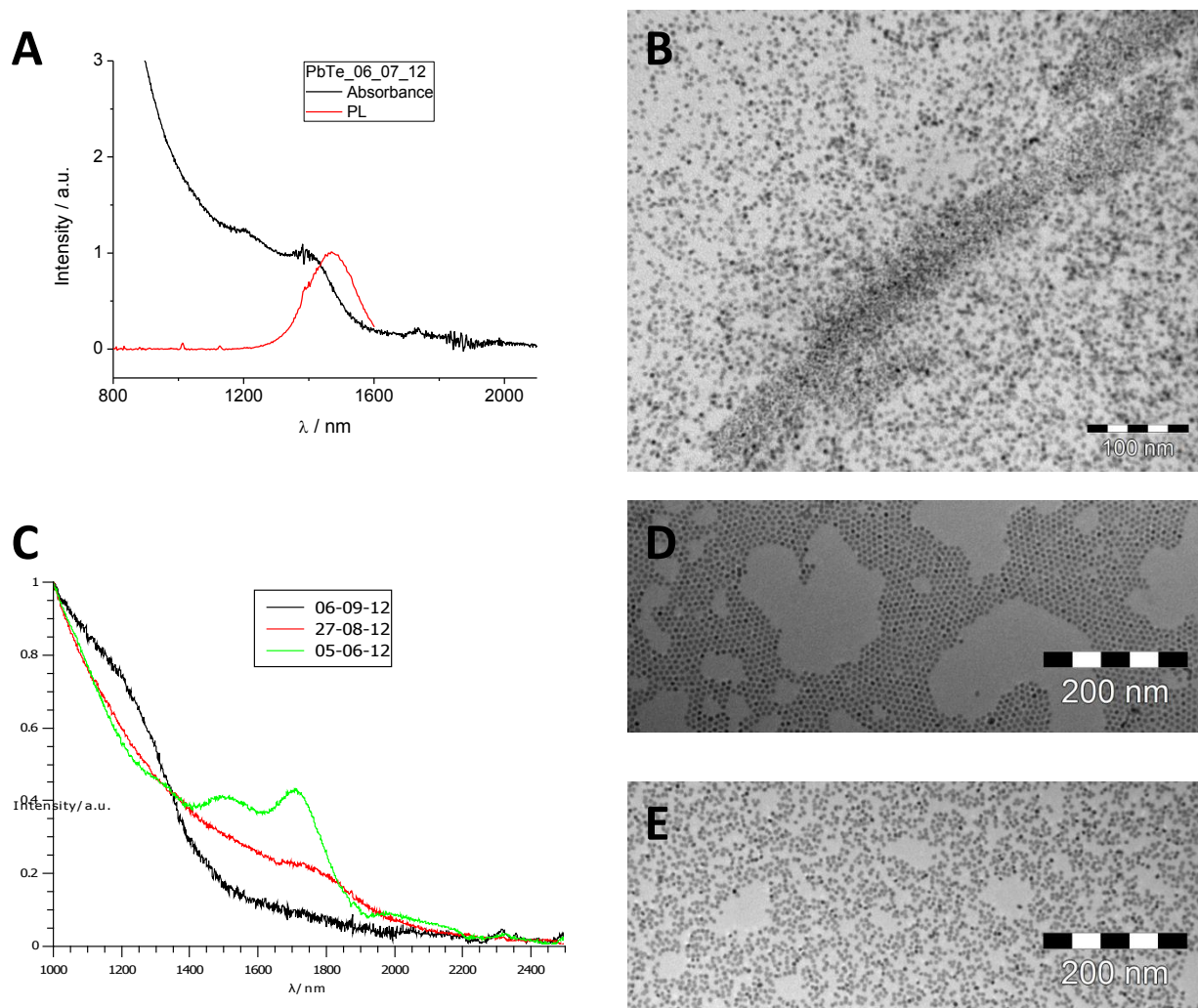
Figure 9. In (A) a absorption and emission spectrum of PbTe 06-07-12 and in (B) the corresponding TEM image for particles of 4.63 ± 0.45 nm. A clear absorption peak is visible in at 1385 nm and the second order peak at 1950 nm. In (C) the absorption peaks of PbTe 06-09-12, 27-08-12 and 05-06-12 is shown and the corresponding TEM images, in (D) PbTe 27-08-12 and in (E) PbTe 05-06-12. The corresponding sizes are 3.62 ± 0.50 nm, 7.02 ± 0.58 nm & 5.86 ± 0.51 nm respectively.

5.1.A. Oleic acid Pb ratio.

The easiest way to control the size of PbTe quantum dots is to vary of the ratio of oleic acid to, lead atoms present [96]. Oleic acid protects the monomers, the quantum dots itself and is therefore crucial in the synthesis and afterwards for the stability of the quantum dots. In the nucleation stage, more oleic acid molecules will protect the lead precursor better what results in less nucleation seeds and eventually in bigger particles because less monomers are used and less seeds are created. This is also reflected by the synthesis performed here. In figure 9C comparison is made between three synthesis. In the synthesis of PbTe 06-09-12, 27-08-12 and

05-06-12 the ratios 1:1, 6:1 and 2:1 respectively are used. It is clear that, as the amount of oleic acid per lead atom increases the size also increases. Although not all conditions were the same in the three synthesis, it is expected that oleic acid is the easiest way to set the size of the quantum dots [22] [96]. Besides oleic acid there is also TOP present, which is the coordinating solvent. In most synthesis protocols it is even in a much higher quantity compared to oleic acid, but is assumed to have less influence on the size [101].

The samples presented in figure 9C were all quenched with ethanol and cooled with ice after 1 or 2 minutes. The particles PbTe 06-07-12 are relatively small and monodisperse with a size of 4.63 ± 0.45 nm, but slowly cooled after 6 minutes (figure 9A). This was likely possible due to the low synthesis temperature of 150 °C and the following decrease during synthesis till 90 °C, which prevented Ostwald ripening. More research on this phenomena would be interesting for industrial purposes, because it simplifies the production process considerably.

5.1.B. Conclusion/discussion.

The synthesis of optical active monodisperse PbTe quantum dots was successful. It was also experienced that the size could be tuned by several parameters in which the concentration of oleic acid was the most important. The scaling up of these particles is probably not an enormous problem. Bottleneck in the large scale production of quantum dots are the necessity of a fast injection, the necessity of quenching and the use of expensive solvents which can harm the environment. In other quantum dots synthesis it was already examined to get monodisperse quantum dots with uniform size and 'green' solvents are used [102] [103] [104]. As shown in figure 9A it is also possible to find reaction conditions in which the fast cooling down criterion was relaxed, which diminishes the fabrication problem even more. Nevertheless fast injection stays an absolute requirement to get monodisperse quantum dots.

For the oriented attachment experiments the sample PbTe 05-06-12 was used with a size of 5.9 ± 0.51 nm.

5.2. SnTe synthesis.

Due to the inverse bandgap of $Pb_{1-x}Sn_xTe$ it would be a very interesting material to synthesize [4] [2] [105] [6]. If the synthesis of this material is controlled it could be used as an infrared absorber. In this thesis two ways were tried to make $Pb_{1-x}Sn_xTe$ in a proper way. The first one is by a one pot synthesis of $Pb_{1-x}Sn_xTe$ using the procedure used by I.U. Arachchige et al. [5]. This procedure failed and did not yield monodisperse quantum dots (appendix 1). The second procedure was to first make SnTe and then perform an incomplete cation exchange with lead to get $Pb_{1-x}Sn_xTe$ [106] [107]. SnTe quantum dots were successfully synthesized, although due to time shortage and due to the difficulties to control the synthesis, cation exchange was not tested. Different sizes were obtained with a reasonable monodispersity showed in table 2. The synthesis is performed using bis[bis(trimethylsilyl)amino]tin(II) complex as tin precursor [97]. SnTe quantum dots absorb in the infrared area, which is shown in the absorption spectra in figure 10 B&D&F. These spectra show a broad absorption band in the infrared region around ˜2300 nm and ˜1750 nm which corresponds to the absorption of the $1S_h$-$1S_e$ excitonic transition of SnTe, which is similar as in lead chalcogenides [97] [108]. This is in agreement with the quantum confinement effect which states that smaller particles absorb at higher energy [109]. The reason that no broad peak is visible in SnTe 01-10-12 can be manifold. The overlap with the increasing absorption peak at ˜1000 nm can be possible. But the most probable explanation is that the sample was too diluted, due to losses in the washing step. The sharp peaks between ˜2750 nm and ˜2850 nm correspond to the $(-CH_2-)_7$ stretching vibration mode of oleic acid bound to the surface of the quantum dot [110] [111]. The numerous of sharp peaks in the SnTe 12-09-12 spectrum are due to the solvent chloroform. It was impossible to dissolve it properly in TCE, thus a mixture of both was used. The noise in the absorption spectra of the SnTe 01-10-12 is caused by the low concentration of the sample.

Table 2. Overview of the peak in absorption measurements, sizes and standard deviation of SnTe

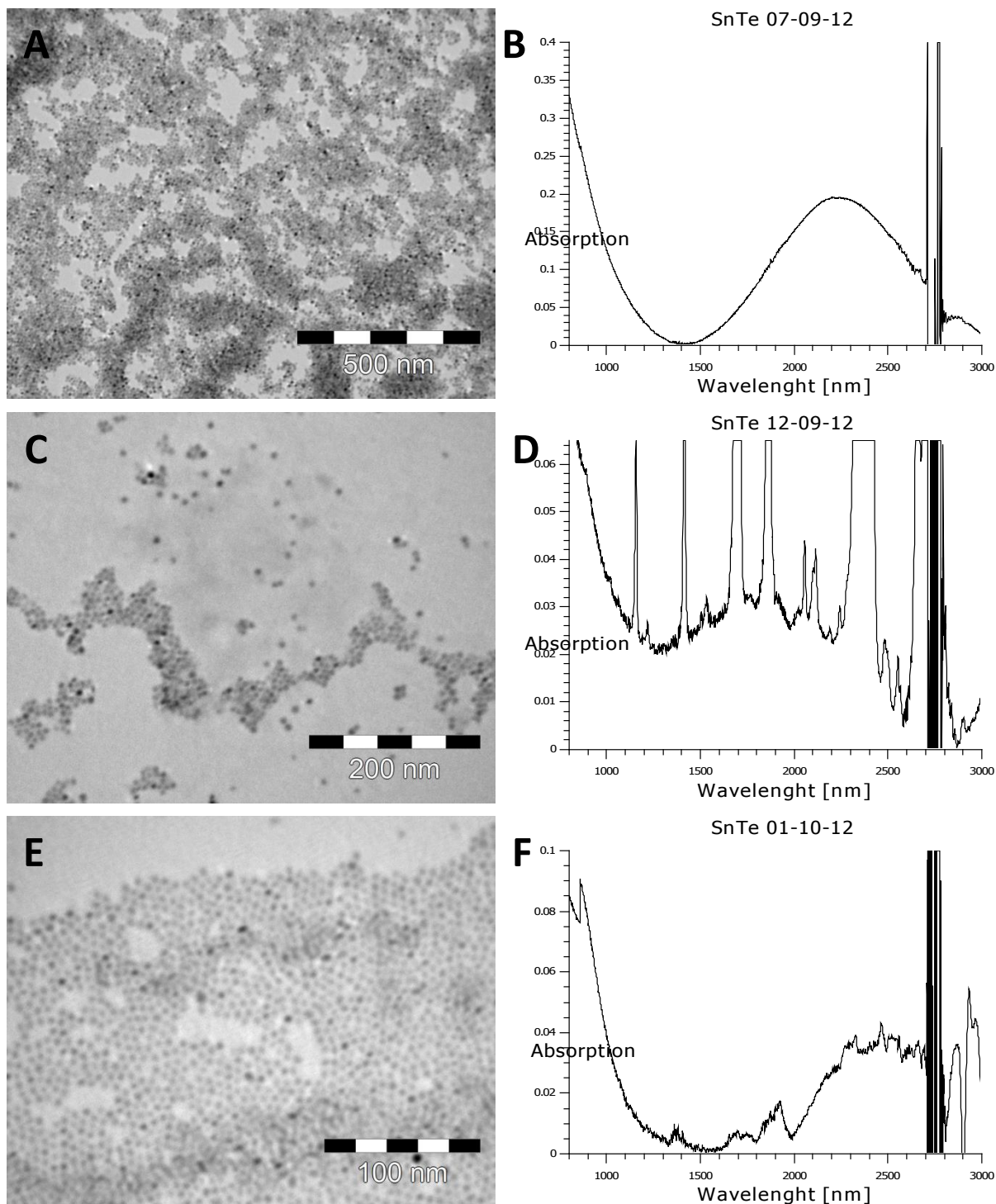| Sample	Peak [nm]	μ [nm]	σ [nm]
07-09-12	2212	8.74	1.13
12-09-12	±1750	6.26	0.74
01-10-12	-	4.15	0.50

Figure 10. TEM images and the appurtenant absorption spectrum of A), B) SnTe 07-09-12, C), D), SnTe 12-09-12, E), F), SnTe 01-10-12. A broad absorption band is visible in B) at 2212 nm and D) at ± 1750 nm but not in F), which is expected at an even higher wavelenght. The sharp peaks around 2750-2850 nm originate from oleic acid bound to the surface. The other sharp peaks in spectra D) originate from chloroform.

5.2.A Conclusion/discussion.

The synthesis and stability of SnTe is very complex. This can be understood by the low synthesis temperature, which makes it hard to separate the nucleation and growth temperature, the high oxidizability [112] and rather weak protection by ligands. Although it is not completely understood why these particles were very unstable, it was noticed that very often after washing the particles aggregated (appendix 1) and were not soluble any more. Another problem is the 'love for glass' of these particles. After centrifuging or drying the quantum dots often stick to the glass vial that it was impossible to redisperse it or even use it again. This resulted in loss of sample, which often caused a problem in measuring absorption. An effort was made fabricate the $Pb_{1-x}Sn_xTe$ by a one pot synthesis, which was even harder than the synthesis of SnTe. A few TEM images of the resulting samples were listed in the appendix 1. This synthesis recipe should give narrowly disperse nanocrystals, but these were not obtained. Although the particles "look worse" compared to SnTe, it seems that the same problems with stability occur, which is visible by the formation of large agglomerates. The next step in this synthesis is therefore finding ligands, which can protect the quantum dots from aggregation.

5.3. Oriented attachment.

Oriented attachment is a very complex process and extremely sensitive for small changes in the environment or composition of the materials used. Very small differences in concentration of the substances, temperature or other environmental parameters could have an enormous effect on the results [49]. In this thesis, I would like to build up the theory of oriented attachment already developed in the past and presented in the theory part of this thesis. Every sample is made by the same simple procedure as described in the experimental section of oriented attachment. From the theoretical section it became clear that the detachment of oleic acid from the surface is a crucial step for oriented attachment, because this layer protects the quantum dots by steric hindering. When the experiment starts, the particles can start 'feeling' each other and by small collisions and the optimal configuration for attachment can be found which gains the most energy by attachment. In the beginning, the steric hindering is large enough to prevent attachment. At a certain moment the attractive forces of the particles are high enough to push the last oleic acid out. Then the surfaces with complementary crystal lattice attach and an almost defect free structure arise.

In this section, relative concentration is used for the PbTe and PbS samples. This is not only for convenience, but also because it would take much time to determine the exact concentration for PbTe, since no article could be found in which the extinction coefficient is determined. For the PbS samples the exact concentrations could be determined and are therefore given [113], but also in this case relative concentrations are provided. However, the relative concentration of PbTe and PbS are not comparable.

In the case of PbTe, hexane is always used as solvent, while in the case of PbS toluene is used. Toluene should give better results although it was impossible to use it for PbTe (this is shown in appendix 2) [82].

I first show the effect of different parameters on oriented attachment. I will start by describing the test at ambient conditions and the temperature effect. After that, the results of the GISAX experiments will be shown, a closer look to the top view will be given and the effect of the ligand. In accordance with the influence these parameters have on the process, the different structures obtained (linear, 'square' and 'honeycomb') will be shown. At the end models will be presented to examine how these structures arise in the sense of facets attached and under which conditions the structures are formed.

5.3.A. Oriented attachment in air.

All lead chalcogenide quantum dots are very oxygen and water sensitive and should be kept in an air free environment, this is also shown in figure 8B. [114] [115]. To investigate the effects of air exposure on the oriented attachment of the quantum dots, oriented attachment is tested in air. This is done for PbS, PbSe and PbTe. In literature, it is suggested that PbS should be the most robust against oxygen, followed by PbSe and PbTe [112] [116]. This is tested for these particles although two considerations should be taken into account. First of all, the sizes are not exactly the same for all three samples, respectively 5.9 nm, 5.4 nm and 5.0 nm. The second consideration is that the amount of oleic acid in not the same in all three samples. This is important, because oleic acid protects the nanocrystals from attachment [53]. This is especially the case for the PbS sample which was provided by Relinde Moes. This sample was not washed extensively like the PbSe an PbTe samples. The PbSe sample was synthesized by Wiel Evers. The concentration is approximately the same in all cases[1]. Figure 11 represents this test, in which PbS was dissolved in toluene (A & B), PbSe was dissolved in toluene (C & D) and PbTe was dissolved in hexane (E & F). TEM images A,C and E were in an open atmosphere and B,D and F are in a system (appendix 3) with a considerable N_2 flow to remove oxygen and water, but the process was definitely not completely. It is clear from picture A, B and C that in open air, no attachment was observed for all lead chalcogenide. Most particles are strongly affected by the exposure to air, whereby the shape is not preserved. In most cases the size of the quantum dots under TEM became smaller. In the system with a flow of nitrogen, shapes are better preserved, but still no attachment is observed for PbS and PbTe. For PbSe a part of the sample contained attached particles, while most of the grid consisted of corroded smaller particles. In the PbTe samples, the particles' size was strongly reduced and non-spherical flakes arose. It is hard to drive the conclusions about PbS, because the particles aggregated a lot, which even resulted in almost empty TEM grids (PbS aggregated on the metal of the TEM grid). PbSe seems less sensible for degradation at least compared to PbTe, which makes it a material of choice. In figure 12 a time trend of the degradation of PbTe by air is visualized, a sample was fished after 30 minutes, 60 minutes and 90 minutes, for figure 12 A,B and C respectively. It is obvious that oxygen and water had

---

[1] The concentration of PbTe could not be determined, but the coverage of a grid was approximately the same as was the case for PbSe and PbS for which the concentration was known. Also the structures formed had the same form in this concentration range.

more time for the degradation of the sample and that after 90 minutes the particles are almost vanished and absolutely no oriented attachment was found.
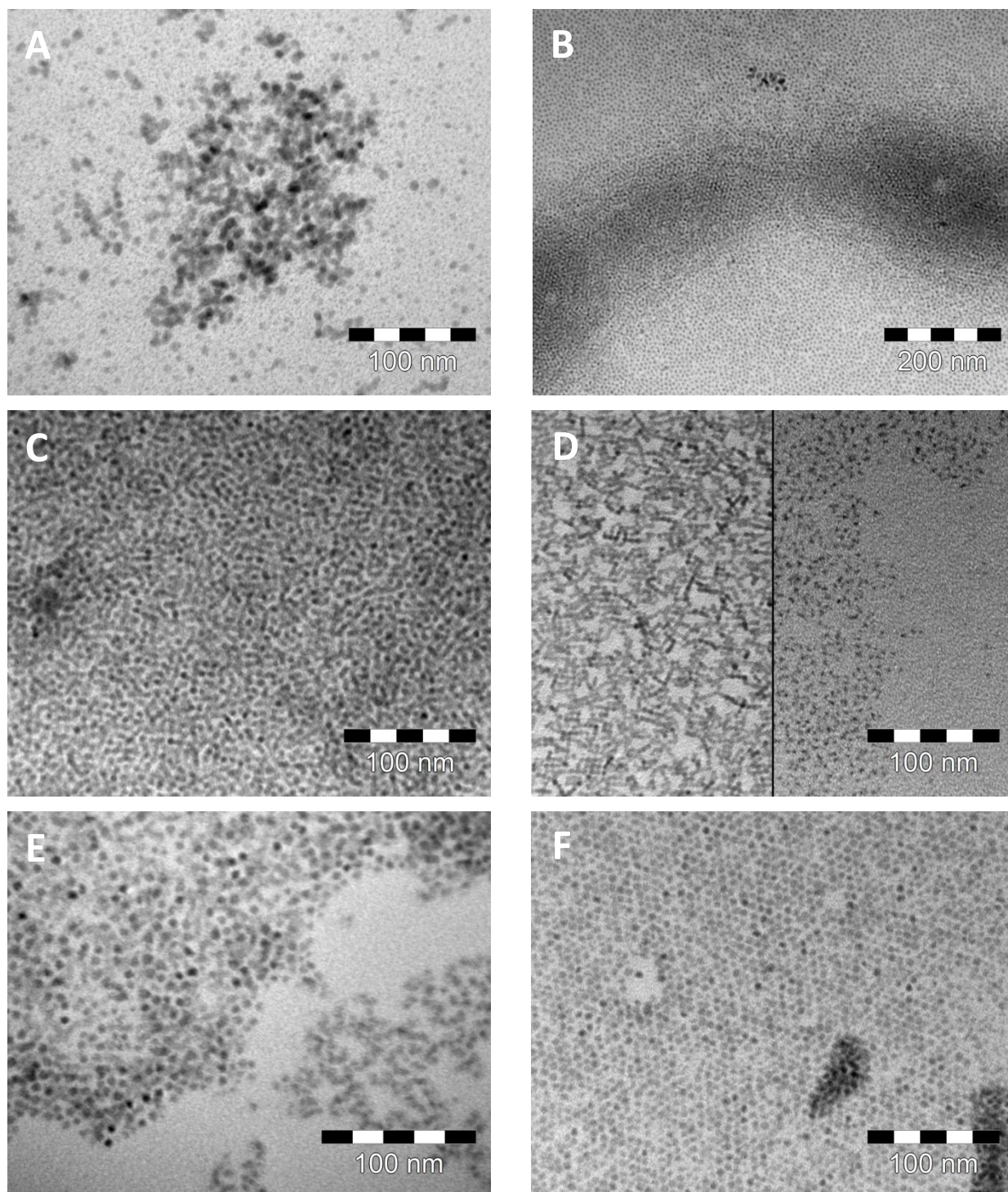

Figure 11. TEM images of A) PbS (5nm), C) PbSe (5.4nm),EC) PbTe (5.9nm) on ethylene glycol in normal atmosphere. TEM images B) PbS, D) PbSe, F) PbTe, the oriented attachement experiment in a special box with a light flow of N_2. (nr. 347&348&349)
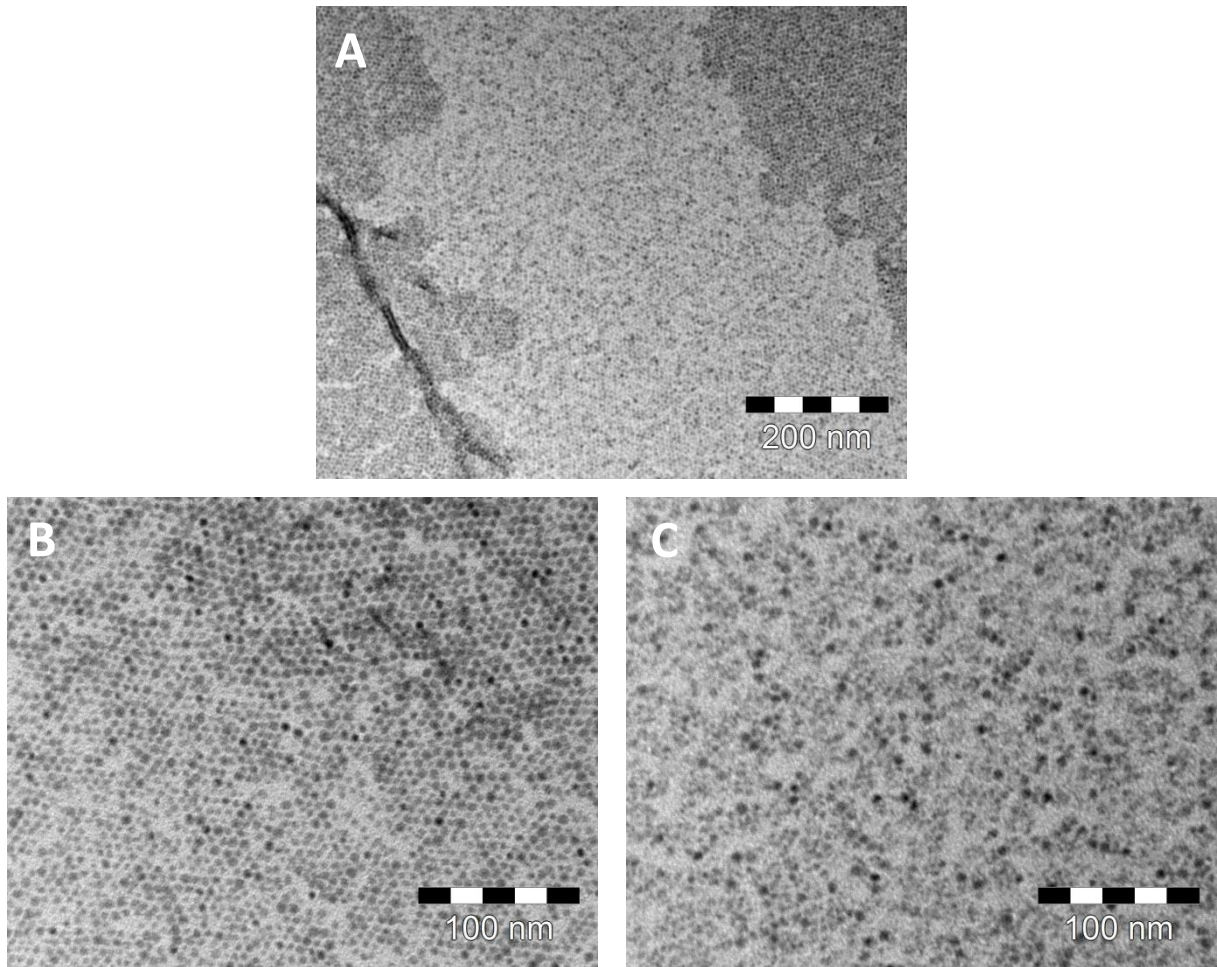
Figure 12. TEM pictures of PbTe quantum dots in normal atmosphere at three times before scooped, A) 30 minutes, B) 60 minutes, C) 90 minutes. It is clearly visible that the quality of the quantum dots reduces with longer air exposure time.

Conclusion.

These experiments are not precise enough to give the oxidation rate, but it is clear that oxidation occurs rapidly and damages the particles discernible. All particles decrease in size when degradation continues and crumble to smaller pieces. The trend suggested in literature is not visible here, PbTe seems to be damaged the most, and for PbS it is hard to conclude due to the aggregation. For PbSe under 'light' air conditions the particles seem to attach for at least a part of the sample.

5.3.B. The effect of temperature on oriented attachment.

The ideal temperature for PbTe oriented attachment is 20 °C or even lower, (until 7 °C), although this was not easy to reach in a nitrogen environment. In figure 13 the temperature dependence is presented, 20 °C (A), 25 °C (B) and 30 °C (C) with the addition of $2 \cdot 10^{-5} \, mol/L$ oleic acid in the EG. In this thesis, I will use the term melting to illustrate the process in which attached particles lose their shape, whereby the original quantum dot could not be recognized any more. Melting does not only depend on the temperature, but also on the amount of oleic acid (see 'The effect of oleic acid'), the composition of the materials used and the glovebox atmosphere. For PbS the temperature in which oriented superstructures were found is around 30 °C. This will be further discussed in the sections about the three superstructures.
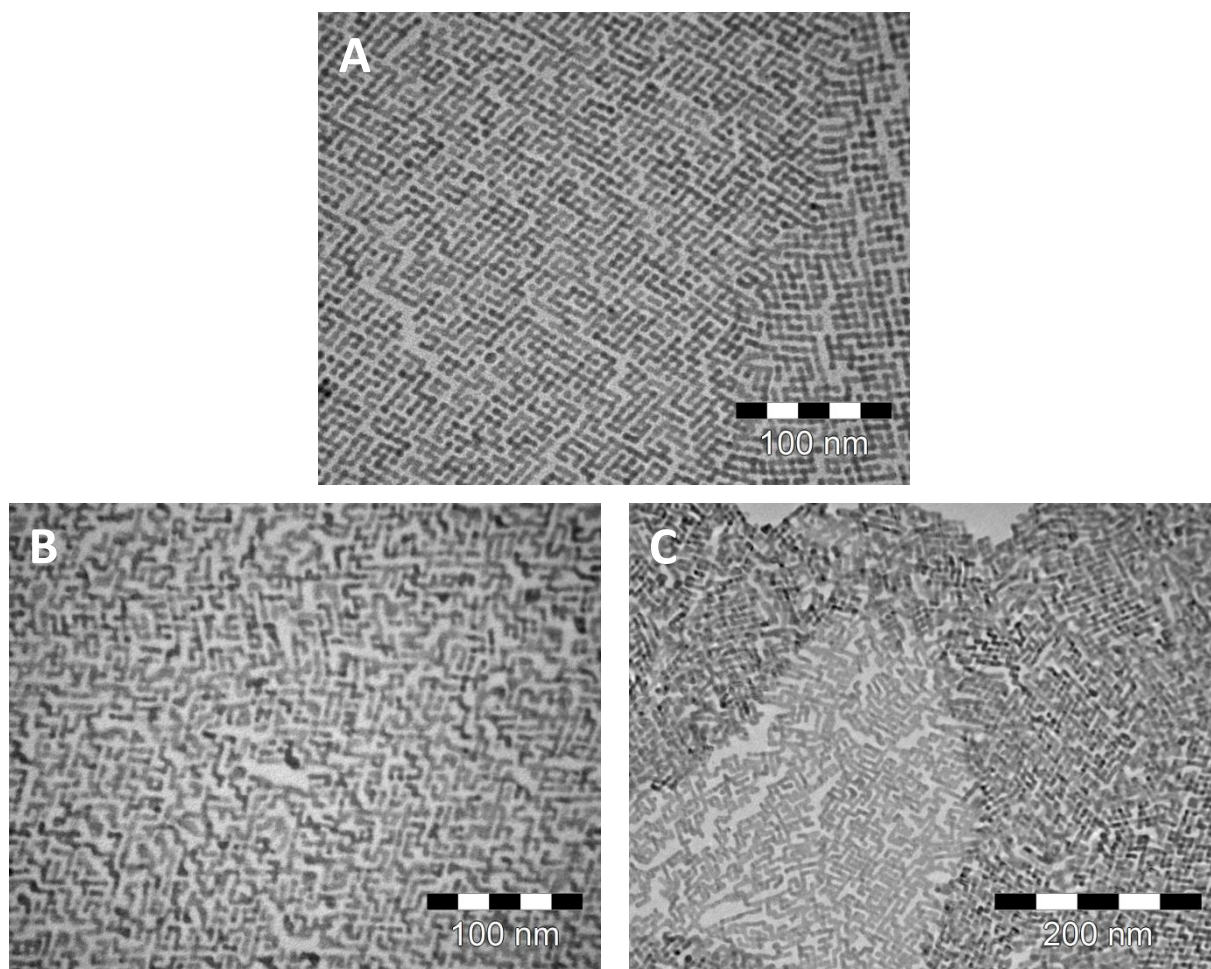
Figure 13. The effect of temperature on oriented attachment of PbTe, in (A) 20°C, (B) 25°C and in (C) 30°C.). A relative concentration of [40] was used with the addition of $2 \cdot 10^{-5} mol/L$ OA in the EG. The 'squere' structure of (A) slowly disappears due to melting.

5.3.C. GISAXS measurements.

As shown in the section 'Oriented attachment in air', PbTe quantum dots are very sensitive for oxidation by oxygen and water, so a closed environment is necessary for proper oriented attachment. Unfortunately this could not be applied in the setup which was built in Grenoble (figure 7A). An effort was made to purge the reaction chamber with a flow of nitrogen before the sample was dropped on the EG and during the evaporation. However, this was not enough to protect the particles from oxidation while measuring. After every measurement a TEM sample was taken, but it was impossible to prevent contact with air between the time of fishing and putting the fished sample under vacuum. Usually, it took approximately 2-3 minutes before vacuum could be applied, due to the location of the vacuum pump and the procedures getting there.
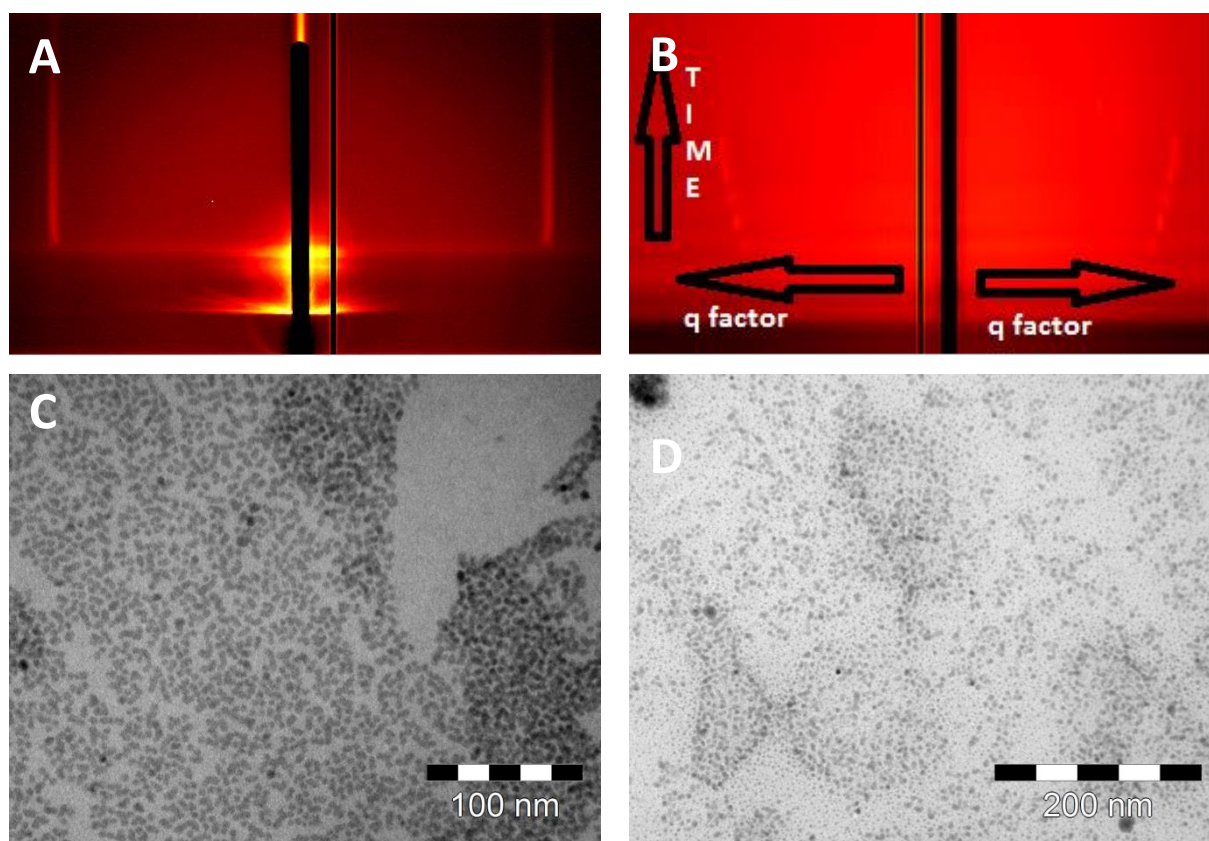
Figure 14. In (A) an example is given of run 12 of sample JG_5. In this sample 45 μL of stock solution diluted with 5 mL hexane was loaded on the Teflon sample holder filled with 25 mL EG. On the horizontal axe the q factor presented. In (B) an overview of the peak intensities over time is given. One can clearly see that the peak maximum intensity moves outwards which indicated that the structure elements come closer together. In (C) & (D) TEM images are shown from the heavily oxidized particles are visible. These TEM images were made after all runs were completed (the peak already vanished at that time).
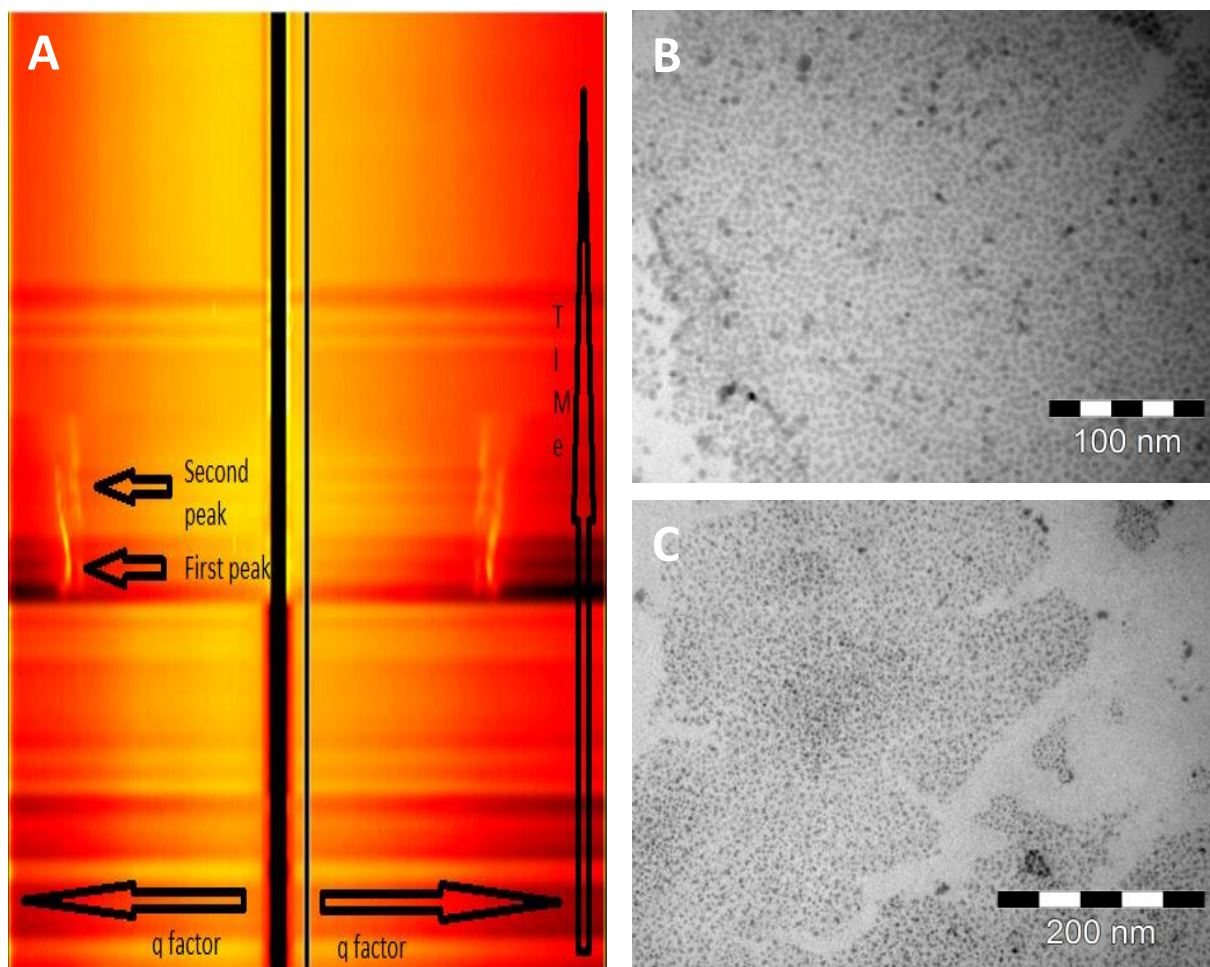
Figure 15. A). An overview of the peak intensities over time of sample JG 24. In this sample 25μl stock solution diluted in 5ml hexane was dropped on 23ml ethylene glycol which contained 0.02μl oleic acid. Time progresses in the vertical direction starting from below, the q factor is in the horizontal direction. In the beginning there are no peaks till a certain run peaks appear which vanish a few runs later. It is clear that both peaks move outwards which means that the structure shirks. B) A TEM image taken after run 45 (a the arrow of the second peak), which was at a moment that the peaks were still visible. Some contours of quantum dots are still recognizable but the particles are mostly damaged too much. C) A TEM image of the sample taken after all runs were passed. Quantum dots are not recognizable any more, the point in the image have an average diameter of ±4nm which is much smaller than the original 5.8nm. (JG 24)

Another problem we faced was that the height of maximum scattering intensity was hard to find. This was due to the poor wet ability of hexane on the ethylene glycol, which made the surface noticeable curved. Hence, the beam hit the Teflon sample holder instead of the surface of the sample.

Above two samples which were measured in the synchrotron in Grenoble are shown. In figure 14 A, a long scan is shown and a sharp peak is visible. In figure 14B and figure 15A the time trend of the peak plotted against the q-value is displayed.

In both figures narrow vertical peaks arise which indicate that there is ordering of a small object at the surface, without an periodicity in the z direction (perpendicular to the surface). Beside to the time trend of the peaks, TEM images are shown, these were fished after all runs were performed, except figure 15B. These pictures show that no attachment occurred and that the particles are thorough degraded by oxidation (there are similarities observed between the particles shown in the figures of the section 'Oriented attachment in air').

The peaks that move outwards, indicate that the self-assembled object move closer together. In figure 15A, a second peak appeared as well, which was also visible in other samples. However, there was not an unequivocal explanation for that. It could indicate that a second layer was underneath with slightly different distances between the particles. Another explanation can be that due to the curvature of the solvent and EG another distance is displayed in reciprocal space if the beam hits the front of the sample or the back of the sample.

In table 3 the q values and the corresponding length between the object are shown (extended in appendix 4). The peak probably comes from a self-assembly pattern with a hexagonal packing, because that is also normally observed for spherical particles [117]. The distance between two neighboring quantum dots end up at values of 8.54 nm, 9.29 nm and 8.73 nm, which means approximately 2.64 nm, 3.39 nm and 2.83 nm was occupied by the ligand bilayer in between two quantum dots. In crystal structure studies the size of a monolayer of oleic acid is between 1.7-2.4 nm depending on the orientation of the double bound [118] [119] [120]. The exact size of a ligand bilayer is depending on the intertwining on the two layers. Schliebe et al. reported a densely packed bilayer with a thickness of 3.6 nm [91]. The results from the GISAXS experiment suggest that the two monolayers are strongly intertwined and therefore shorter. The particles are probably self-assembled while most solvent was evaporated and the monolayers of oleic acid molecules are 'touching' each other. After most solvent was evaporated, exposure to an air environment occurred and the particles crumble and the self-assembled structure is lost and the peak vanished. It was tried to stop the experiment while the peaks were still visible as shown in figure 13B. At that time, approximately half of the surface of the EG was dried up (visible by eye), even though peaks

were visible before and after the experiment was restarted, better TEM images were not obtained (probably due to oxidation while walking towards the vacuum pump). In the glovebox, the same chemicals and amounts did yield attachment, which suggests that oriented attachments takes place after self-assembly occurred and the structure was dried (example of result obtained in Utrecht, in appendix 4). Unfortunately, the exposure to air was too destructive to yield oriented attachment after the quantum dots were self-assembled in Grenoble.

Table 3. Overview of the starting and end value of the q factor at peak position and corresponding distances of the quantum dots in 2 types of lattices. Note that the first peak of JG-20 vanishes very quickly hence there is not much difference between the first and last q factor.

Sample	Q factor	Distance in hexagonal packing [nm]	Expected thickness of bilayer [nm]
JG-5	0.763-0.850	9.51-8.54	3.61-2.64
JG-24, peak 1	0.747-0.781	9.71-9.29	3.81-3.39
JG-24, peak 2	0.807-0.831	9.00-8.73	3.1-2.83

Conclusion and outlook.

The experiment failed to perform oriented attachment and to follow this process by the scattering of X-rays on the surface. The setup made for this purpose could not be tight enough to ensure oxygen and water free conditions. Particles which are more stable against oxidation should be used and also a setup which can be completely closed to prevent oxidation is necessary. Next to that, a vacuum pump close to the setup will be very useful. In this session, about 2 minutes exposure to air was unavoidable.

Nevertheless, self-assembly in which the particles 'touch' each other by their ligand layer was still observed. Unfortunately, the self-assembled structure could not lose all the oleic acid bound to the surface, thus oriented attachment could not occur. Before this could happen the structure and particles were destroyed by oxidation.

Two conclusions arise by these experiments. Although oriented attachment was not visible, it seems that oriented attachment is the next step after the particles were self-assembled at first. The self-assembly process start at the very end of the evaporation. This was observed when the runs were stopped while peaks were still detectable. At that moment, half of the sample was already dry, while a thin film of solvent was clearly visible on the other half, which was rapidly evaporating.

5.3.D. Top view.

With TEM it is easy to look at different magnification to see the big picture of the drying process. If patterns are recognized it is possible to follow the oriented attachment. In figure 16, oriented attachment of PbTe dissolved in hexane is visualized. The quantum dots are attached in a 'square' lattice with the relative concentration of [20] (at 20 °C and $2\cdot10^{-5}$ mol/l oleic acid added to the EG). The difference in figure 16A-D is the magnification of the TEM image, which is low in A and higher till D. The particles are dried in such a way that there are layers formed, one complete covering layer, which is probably the layer which is formed at the liquid-gas interface. A second layer and third layer on top visualized by arrows in figure 16B, which are probably particles which could not fit it the liquid-gas interface anymore and are therefore forced to form a second layer. This layer stacking is a recurrent phenomenon in all oriented attached samples and is also visible in appendix 5, in which it even occurs in dried unattached PbS particles. It is also very easy to see due to the density of the particles, in which the local concentration of particles is much higher in the second layer.
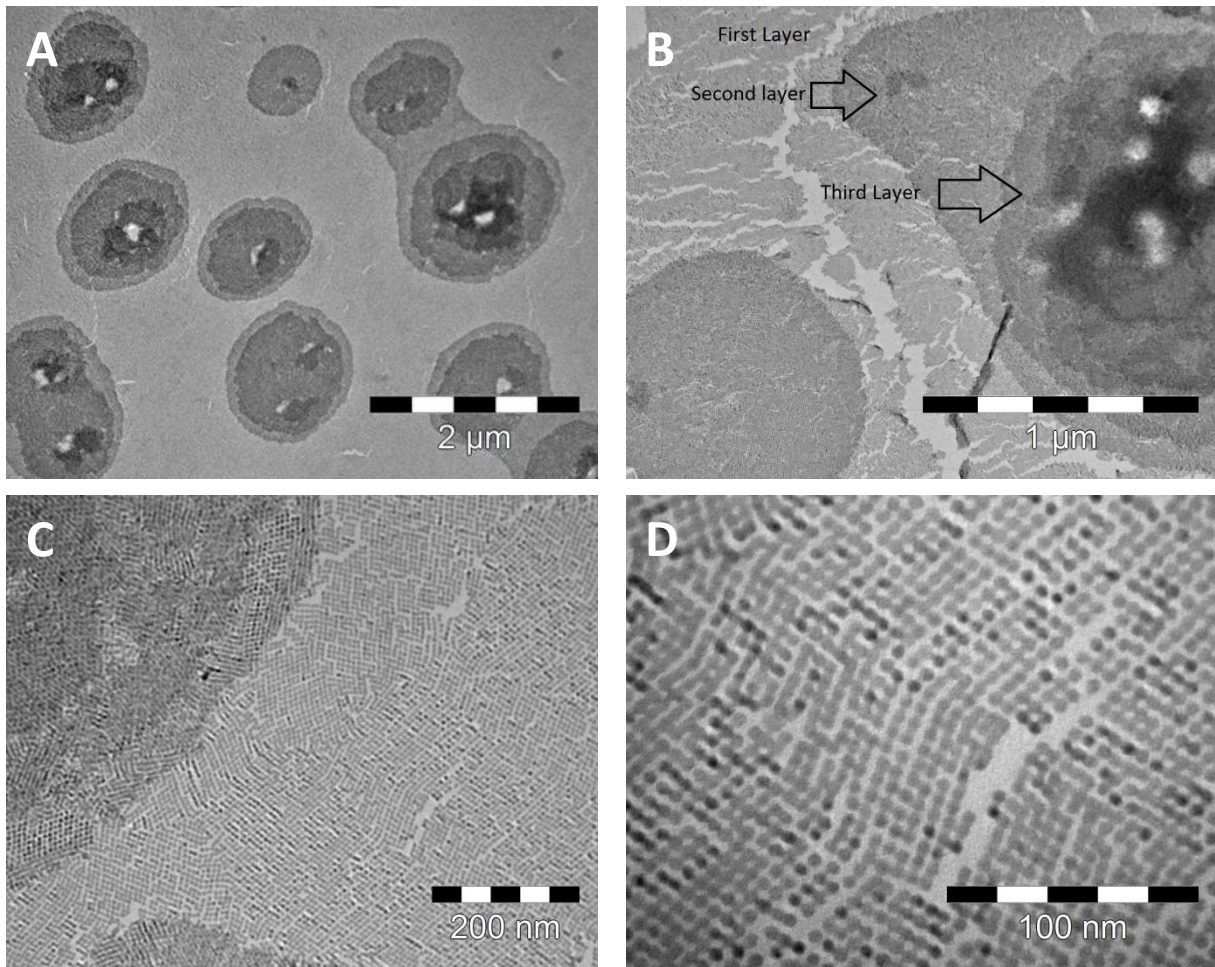
Figure 16. TEM images of oriented attached PbTe in a square lattice from different heights. The samples dry in one monolayer and a second or third layer in a circle on top of the first monolayer, visualized by the arrows in B. A concentration of 2·10⁻⁵ mol/l oleic acid in the EG was used at a temperature of 20 °C, while the sample was fished after 45 minutes.

5.3.E. The role of Oleic acid.

In the hot injection method, oleic acid is of huge importance for determining the size of the particles, the stability [13] and even the shape of the particle [51]. If quantum dots want to attach, the bounded oleic acid should be detached from the surface, so there is space for attachment of the opposing facet. It is not exactly known how this process of detachment is facilitated. Several authors suggest that this detachment is facilitated by small alcoholic molecules or pH, so no ions but just uncharged molecules are left behind [19] [20], this is shown by the reaction equations beneath.

Two equations, visualized in structural formulas, are shown. The first equation leaves a charged particle while the second equation leaves only uncharged molecules.
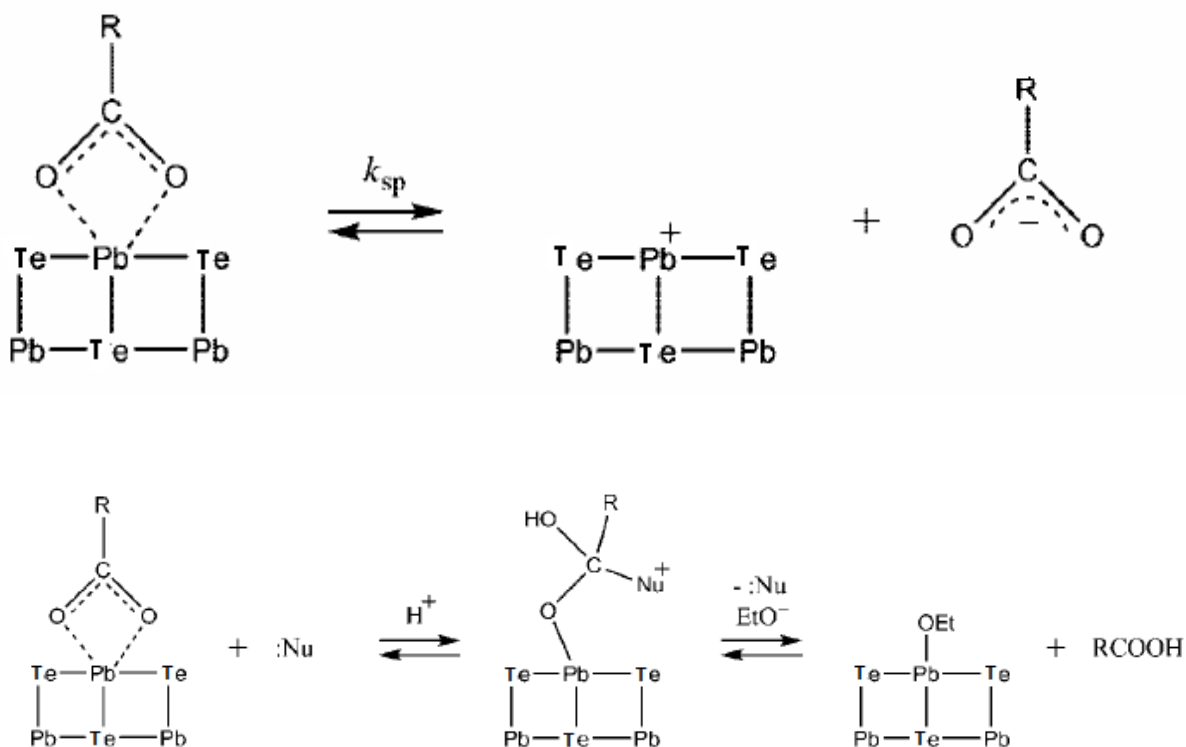
On the other hand, it is also possible that the oleic acid leaves in the form of lead-oleate, which leaves uncharged molecules behind [17]. From analysis (appendix 6) it seems that it is not the case. The binding length of two attached quantum dots should be somewhat shorter than two separate quantum dots (the length of two lead atoms, assuming both sides were shortened by one lead atom). This difference of 0,24 nm (length of two Pb atoms) is hard to

measure in a realistic way with TEM images [121], however an attempt is performed. The size of an attached quantum dot is 5.84 nm and of a single quantum dot 5.86 nm and it is not significant different from each other. It therefore seems that detachment of Pb-oleate is not the main mechanism, but more trustworthy research should bring more clear results.

Before we look at the effects of oleic acid additions, a few notes should be made. First of all, oleic acid is the cause of the only repulsive force in the system, it is therefore of mayor importance to know its location and strength. Attractive forces, in this experiment, are assumed to stay the same (but are distance dependent), so detachment of oleic acid is probably the main driven force behind oriented attachment in this experiment.

Second note is about the total amount of oleic acid. A very rough calculation is performed in appendix 7, to estimate the amount of oleic acid needed to bind the complete surface of all quantum dots in a typical experiment from the scratch. This amount is roughly 0,02 µL. This is of course an extremely small amount and this immediately explains the vulnerability nad complexity of the system. If such an amount is enough to fill up the complete surface of all quantum dots present in the system, very small changes in environmental factors, as in the composition of the EG or DEG layer can give different results. Even the partial pressure of several molecules in the glovebox can matter, especially by keeping in mind the relative large surface of an experiment ($0,25\pi$ cm^2) and diffusion speed [122]. Also the presence of small alcoholic molecule or small contaminations in the glasswork, like acid, should not be underestimated, due to the excessive use of those molecules in the gloveboxes [18] [19].

The third point of consideration is the starting material. Quantum dots made by the hot injection method contain a certain known amount of ligand during the reaction and at the end of a reaction. As a stock solution this precise knowledge is lost, due to differences in washing procedure. It can differ in, the amount of washing steps, amount of small alcohols used and in use of different alcohols. Small alcohols interfere with the ligand layer around quantum dots and thereby the amount of oleic acid present and the composition of the quantum dot surface [17] [18] [19] [20]. The different washing procedure of PbS (unwashed) and PbTe should be taken into account in the interpretation of the results in this thesis.
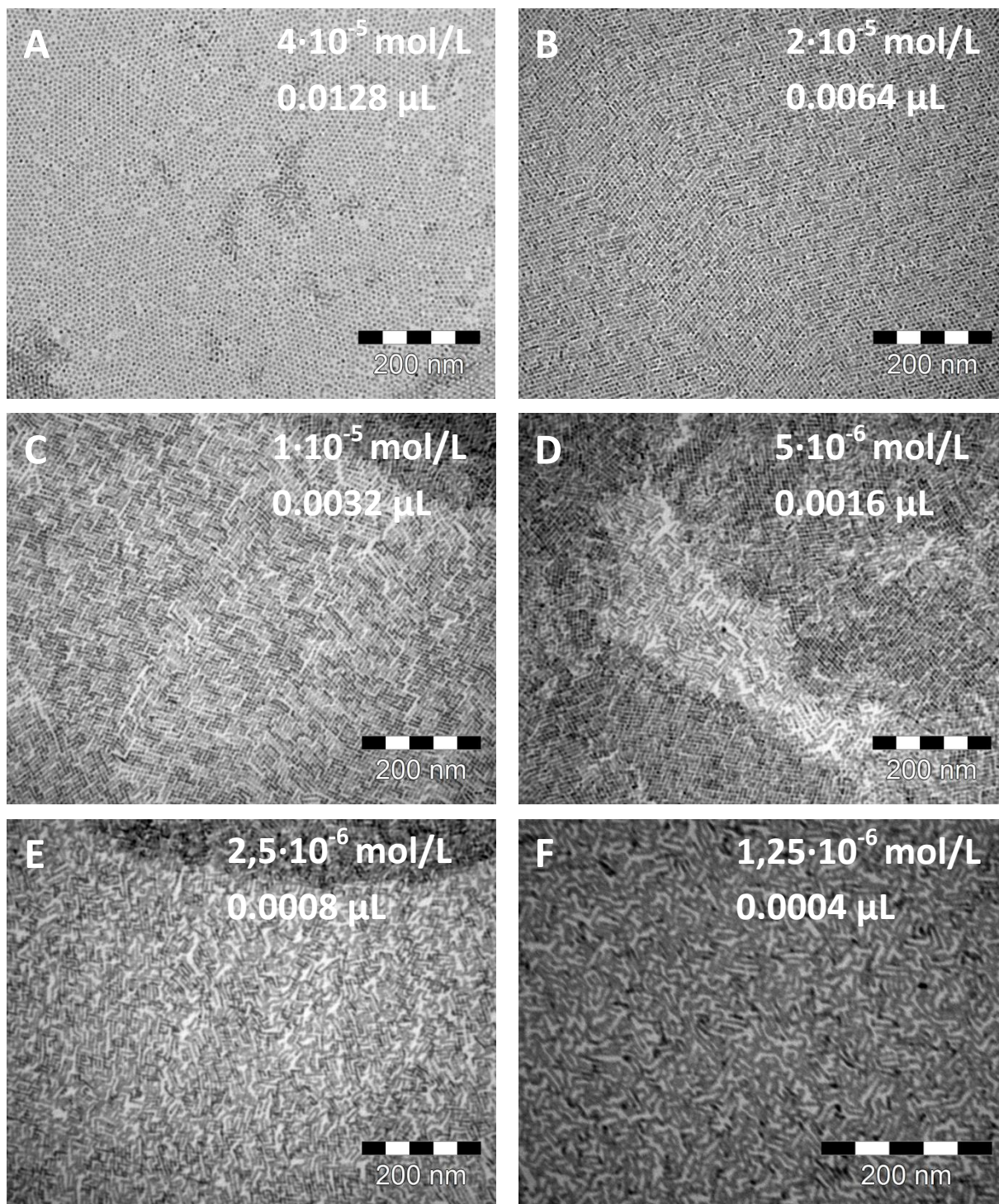
Figure 17. Evolution of the structure while decreasing the oleic acid concentration in EG, all at 20 °C and dried for 45 minutes with addition of the same relative concentration of [±20][2]. There is no structure visible in (A), where the quantum dots are protected from attachment due to the ligand shell around them. The structure arising in (B) becomes more melted and the clear structure vanish gradually. In (B) a long range 'square'

---

[2] The ± is added because this batch was made just before a moment that it was noticed that the concentration of the stock solution changed due to evaporation of the solvent. These samples were all taken in the same period, so the samples are comparable with each other, but the relative concentration is not comparable with other batches.

structure is visible which is already less pronounced in (C) and is completely vanished in (D) - (F). The oleic acid concentration in EG in shown in the upper right corner of each sample, all in mol/L or in µL added to 1 ml EG.

The concentration of oleic acid that was added to the EG decreased in figure 17 from (A) untill (F). The concentration is shown in the right upper corner of every TEM image and the amount of oleic acid added to 1 mL EG is shown. In (A) the amount of oleic acid added is the largest and the particles are protected in such a way that attachment was hindered completely. The long range 'square' structure clearly visible in (B) becomes less and less visible while decreasing the concentration of oleic acid in the sample. In the samples (D)-(F) the structure is almost not visible anymore. In these last samples the structures are almost completely melted before or after attachment took place.

In investigating the effect of oleic acid on the attachment of PbTe quantum dots also much larger amount of oleic acid was added. Some interesting features revealed. It was already known by Z. Tang et al, that quantum dots can self-organize in free floating sheets [123]. By addition of 0.145 µl of oleic acid into the EG layer, it seems that these sheets are formed (appendix 8). Future research can point out if there is a relation between an excess of oleic acid and free floating sheet and maybe even the oriented attachment of those free floating sheets into 2D atomically connected materials, like nanoplatelets [91] [94].

Conclusion and outlook.

As was stated in the beginning of this sub-section, better knowledge on the amounts and position of oleic acid in the sample would be extremely useful. Due to the influence and the sensibility of oleic acid, it is hard to conclude what exact amount should be added to yield the best results. Concerning the influence of different partial pressure of gases in the gloveboxes, one should be careful with conclusions about structures of batches which are not made on the same day. In this thesis only repetitive samples with respect to each other, are compared with each other. Amount of oleic acid added can therefore differ in well-defined structures of different batches, but one should take figure 17 into account, so the pattern can be recognized. In the future, it would be very interesting to look at factors that influence the detachment of oleate from the surface of the quantum dot. One can think of three main ways to do this. First is the pH, this is the main driver of oriented attachment in nature and would therefore be interesting to look at in this experiment and oriented attachment experiment in general [69]. The second factor that can influence this layer of ligands, is the addition of small chlorine containing hydrocarbons, which bind stronger to the cation [54]. An example of this comes from Schliebe et al. who used small chlorine containing molecules who are assumed to bind strongly to the cation [91]. The third type of molecules that can influence this binding of oleate to the surface are small alcohols, which are also used in washing procedures [18] [19]. This was also tried, but was unfortunately unsuccessful, to induce precise attachment. However, some observations have been made (see appendix 9).

5.3.F. The three different structures.
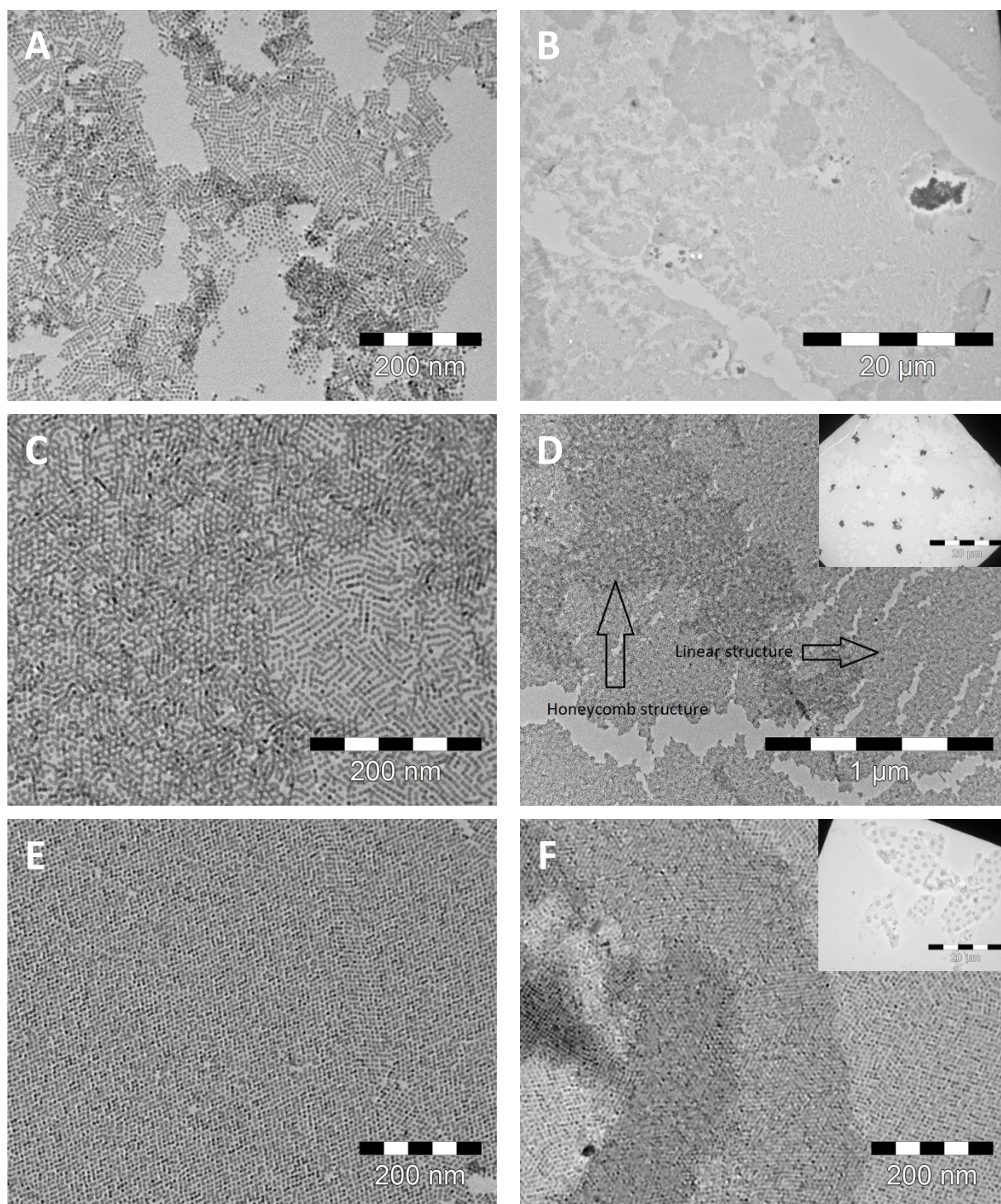
Figure 18. An overview of the three oriented attached structures that are possible. In A) & B) the linear structure is visible in which a relative concentration of 10 is used. In figure C) & D) the honeycomb structure is visible always in combination with the linear structure at a relative concentration of 15. In the denser part, a second layer came on the first layer whereby the honeycomb structure arose, while in the one layer part a linear structure is visible. In E) & F) the 'square' structure is visible at a relative concentration of 25. On the inset of D) & F) a top view is shown.

5.3.G. The linear structure.

In the relative concentration range lower than [~15] PbTe quantum dots oriented attach in a linear fashion, which is shown in figure 18 A & B and appendix 11. Attachment already starts at a temperature of 7 °C and destructive melting occurs at temperatures above 25 °C. For very low concentration [2], melting becomes less destructive due to the large amount of space between linear attach structures, although the linear strings become more curved (see appendix 11). In figure 19A an example of PbTe linear attached quantum dots are shown, with a higher magnification in the upper right corner. The spherical (truncated cubed) attached particles are still visible in this image. In Figure 19 B-D the possible facets of attachment are shown, which in fact, can be all three different facets of the truncated cube. Although due to the possibility of a dipole moment in the direction of the <111> facet, this is the most plausible facet of attachment [52]. But also the <110> facet can be the facet of attachment due to the high surface energy. This all makes the <100> facet the less probable, but high resolution TEM can give a decisive answer.
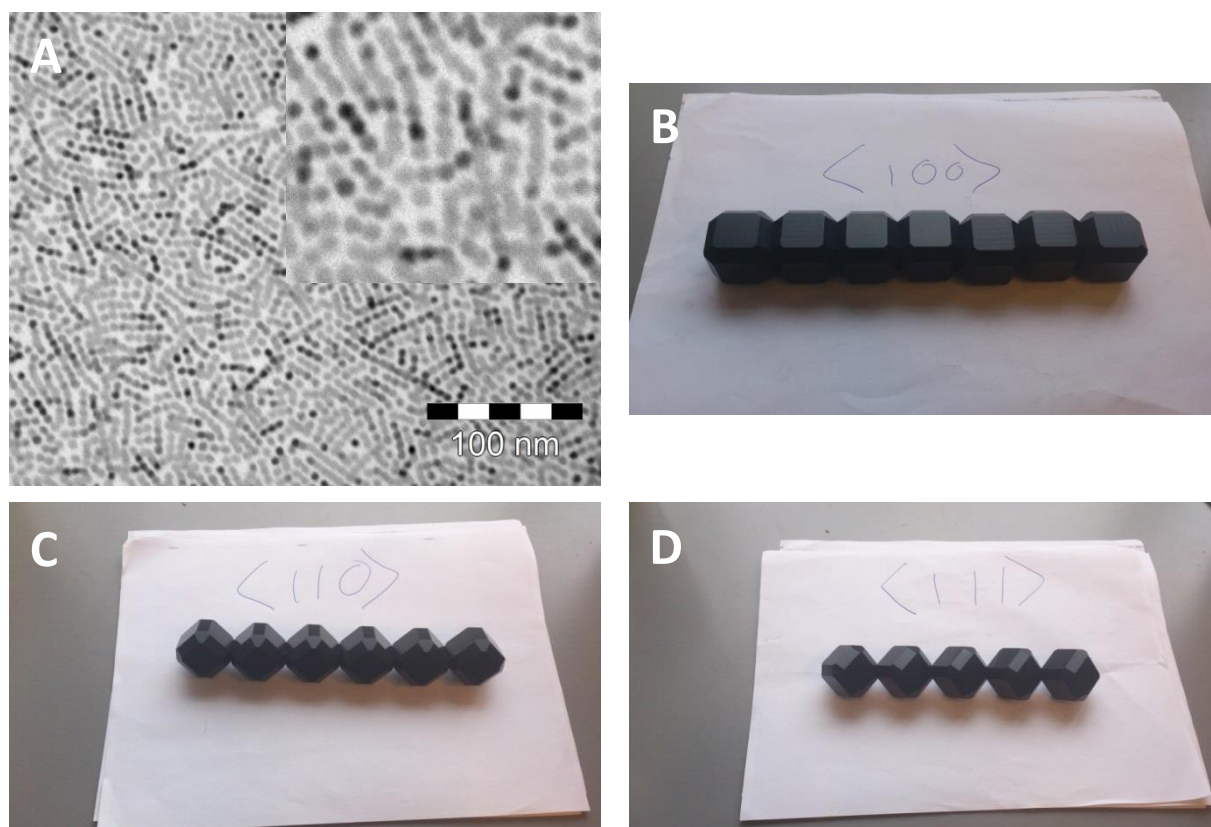
Figure 19. (A) An example of a linear structure with a magnification in the upper right corner which shows the attached dots. (B-C) A model to show the possible facets which are attached. In this case all facets can be used to get linear attachment, although the <111> facet is the most plausible due to the possibility of a dipole moment and it has the highest surface energy.
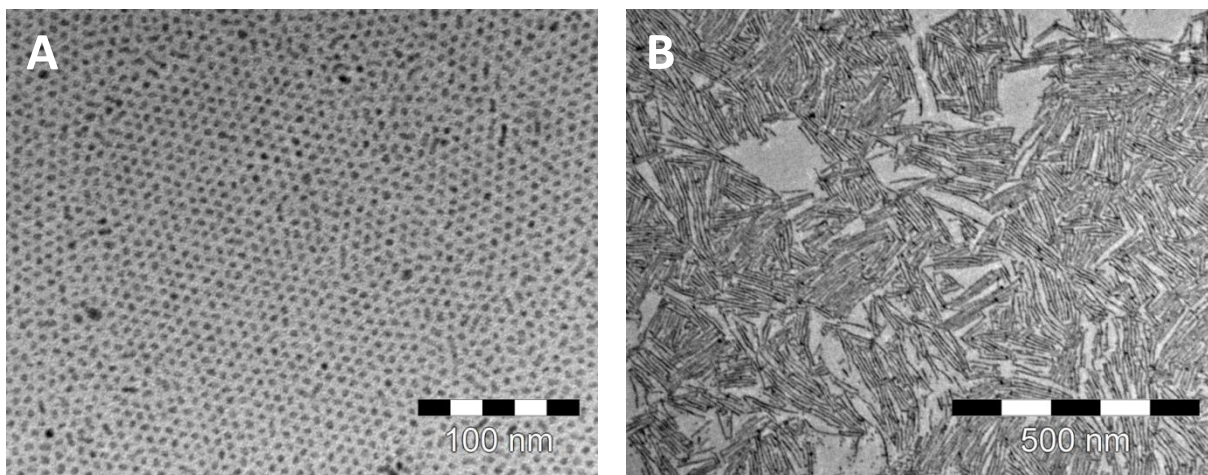
Figure 20. An example of a linear attach structure for PbS. A concentration of $1.87 \cdot 10^{-6} mol/L$ quantum dots is used (relative concentration of [20]). In a this is done at a temperature of 25°C and in B of 30°C.

Also for PbS it was tried to oriented attach quantum dots to varies structures. For these experiments particles of 4.9 ± 0.3 nm were used, obtained from Relinde Moes. These particles are nicely monodisperse and show typical absorption and emission characteristics (appendix 10). However the shape under TEM does not look completely spherical or like a truncated cube (this difference cannot be discernible) (appendix 10). Some particles are more like a triangle, which is a problem because the availability of all the specific facets is not likely in that case. In Figure 20 an example of linear attached PbS is shown. Attachment for PbS quantum dots starts at a temperature of 30 °C, below which no attachment occurs (figure 20B). At 35 °C the particles aggregate and form large undefined and uncontrolled structures. Again, for PbS all facets can be used for attachment in a linear fashion, but the <111> facet is the most probable due to a possible dipole moment and the high surface energy of the <111> facet. Also here, high resolution TEM can answer the question, which facet is attached.

5.3.H. The 'square' structure.

As shown in figure 18 E & F and appendix 12 it was also possible to make a square like structure for PbTe. The structure arises at approximately a relative concentration [20] or higher at a temperature of 20 °C. Also in this structure a clear layered structure is always visible, but mostly with two 'square' structures on top of each other (figure 18F). It looks similar as an contour map with isolines, in which clear circles are present where a second layer starts. It was possible to make these structures on a very large areas as shown in the inset of figure 18F. However, there is a clear difference compared to the square structure Wiel Evers et al. made [82]. The square structure is in the case of PbTe, never really square, but there is always an angle ranging from 74°-85° between the two opposite rows which is clarify in figure 21 A&B. In figure 21C a zoomed picture of a 'square' lattice is shown. It is evident from this picture, that there is not one angle of attachment, but two. One angle is ~75° and the other is 90°. A combination of the two angles of attachment gives the range of angles shown in figure 21A&D. In figure 21D a model is built to explain the 75° angle. This angle can only be made by attaching the <111> facet while the truncated cubes are lying on their side with the <110> plane pointing upwards. A 90° angle can be made by either attaching the <110> facet or the <100> facets as shown in figure 21E&F. It is not possible to get a 90° angle by connection of the <111> facet, so at least two different facets are involved in this 'square' structure. Attachment by the <110> plane is the most plausible to get a 90° angle, due to the higher surface energy of that facet. A clear recipe or regularity to make this 'square' structure with a certain on forehand predicted angle was not found. Even within one TEM sample small differences can be found. This unpredictable behavior has probably to do with very small differences in reaction conditions, even composition of the EG or the air in the glovebox.
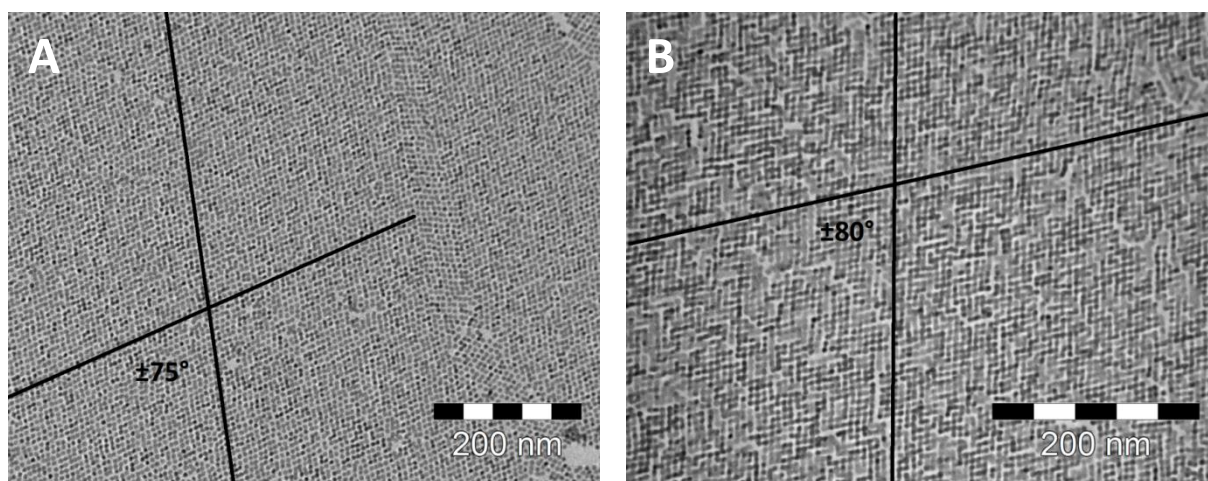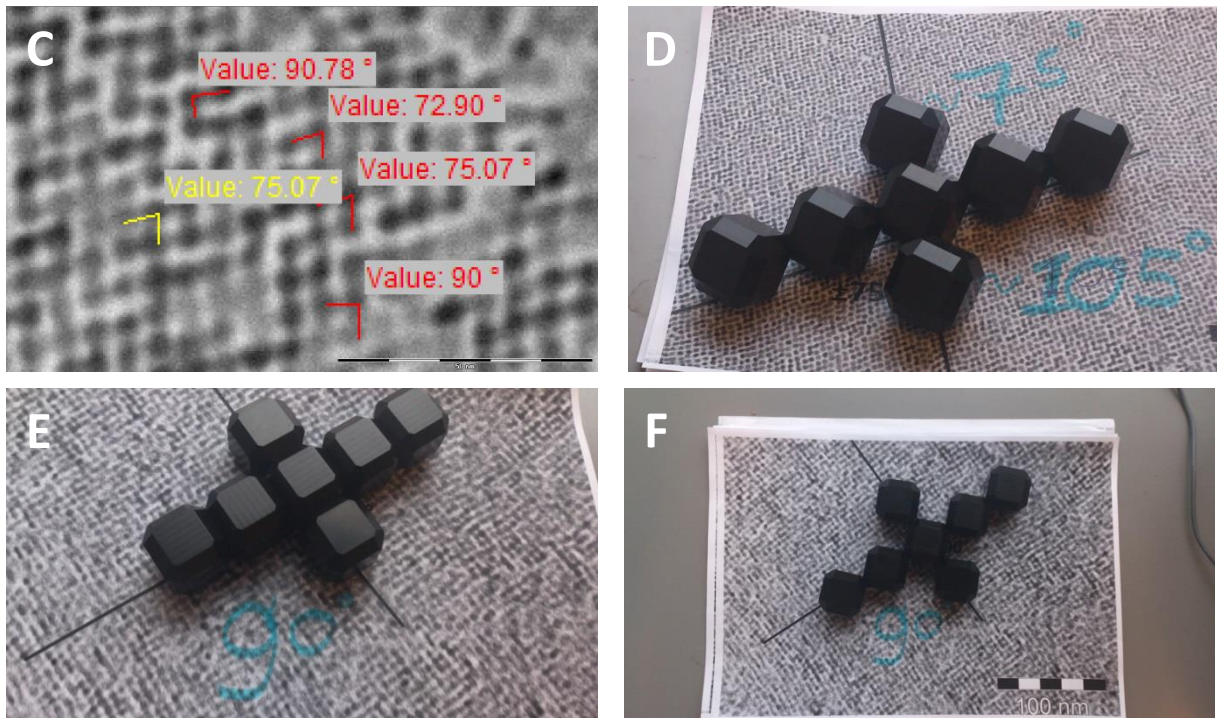
Figure 21. In A & B two examples of the 'square' structure is shown. It is clear by the black lines that the angle between the two rows is not exactly 90°, but always in between 74°-85°. In (C) a highly magnified picture of a 'square' lattice displayed. From this picture it is clear that there is not one angle of attachment but there are two, one of ~75° and one of 90°. In (D) a model is used to explain a 75° angle between two attached rows. This is only possible by attachment via the <111> plane, with the <110> plane pointing upwards. In (E) & (F) the two possible facets of attachment with a 90° is shown. This way of attachment is only possible by the <100> or <110> facet.

It was also possible to make a square lattice for PbS, which is shown in figure 22. This structure is made with a concentration of $2.81 \cdot 10^{-6} \; mol/l$ (relative concentration of [30]) at 30 °C. In contrast with PbTe this lattice has always an 90° angle between the opposite rows. This lattice is therefore made by attachment of the <110> or <100> facet, in which again the <110> facet is the most plausible due to the higher surface energy [59].
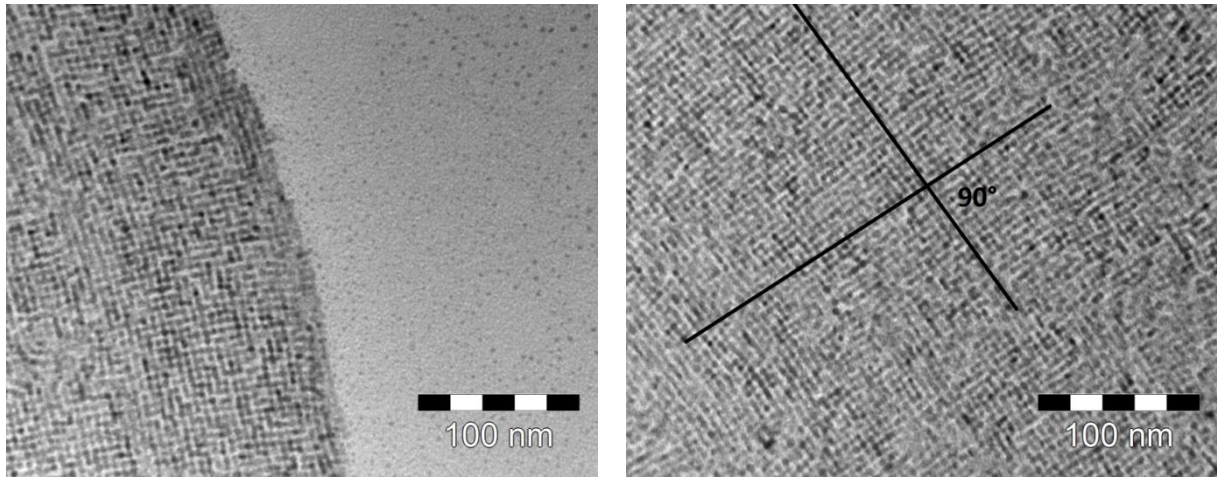
Figure 22. The square lattice of PbS is shown. This lattice is only observed with a 90° angle between the two opposite rows.

5.3.I. The honeycomb structure/siliceen lattice.

In this section the honeycomb/siliceen lattice is discussed. Besides giving my results, also a model is presented which should explain several open questions of this structure. This structure was first found by Wiel Evers et al. and is also the most promising one, due to the similarities with the graphene atomic lattice [82]. At first, it was conceived that the structure should look like the model shown in figure 23A. This structure is flat and connected by the <110> facets, although there is a small mismatch in the atomic lattice by this connection. It was though, that this structure arises by, in plane attachment of several quantum dots by their <110> facet [82]. Crucial in this explanation is that the quantum dots should all orient similar in an interface with their <111> plane pointing upwards. This orientation of separate quantum dot in this way should be energetically favorable over other orientations [82]. Calculations showed that there was indeed a small energy difference between different orientations in an interface (liquid-gas), but it still could not explain all questions. The most pressing question still was, why the structure in figure 23A was formed and not the structure of figure 23B. In the model of figure 23B a quantum dot is placed exactly in the middle of the honeycomb and this fits perfectly; all <110> facets are now atomically connected. It was therefore suprising that not B was formed but A, because attachment in the middle should always be more energetically favorable due to the large reduction of surface energy. Later on, tomography was performed on the structure which resulted in a different structure shown in figure 23C. In this model structure, not the <110> but <111> facets are atomically connected. However, the

most striking difference is the height difference in the structure and therefore this structure was called the siliceen lattice instead of honeycomb lattice. This structure is also much more complicated compared to the honeycomb, for example the lengths of the structure in horizontal as well as vertical direction depends on the truncations on the truncated cube (see figure 8C). Also the formation of the structure cannot be explained by purely 2D systems any more, otherwise no height difference could arise. In figure 23D, figure 18 C&D and appendix 13 examples of the siliceen lattice made by 5.9 nm PbTe quantum dots are presented. These lattices arise at a relative concentration between [15]-[20], at a temperature of 20 °C. The structure is very vulnerable for environmental changes in air and EG, which makes it hard to compose. Small changes in these conditions can change the way oleic acid is attached to the surface of the quantum dots and therefore reduce, for example, the layer of steric hindering and attachment can take place too early or even melting can occur. To have more control of these factors oleic acid can be added to the EG to influence the equilibrium constant of the adsorption and desorption of oleic acid on the surface of the quantum dots.

It did not work to make the siliceen lattice for PbS. It was expected that a siliceen structure should arise for PbS in the concentration range between linear and square as is the case for PbTe and PbSe. In this range, between $1.87 \cdot 10^{-6}$ mol/l and $2.81 \cdot 10^{-6}$ mol/l (relative concentration of ([20]-[30]), a combination of linear and square structures are formed, this is shown in the appendix 14. There can be multiple reasons for this. The first one is that the shape of the PbS quantum dots is too irregular to really bind to the <111> facet. Another reason can be that the right conditions were not found. The sample contained a lot of oleic acid molecules, which might not be detached in the right way. Another reason, which will become more clear after the section 'ideal size', is that the size of the quantum dot is too small. The ideal size is likely around 5.5 nm and the particles used here are around 4.9 nm, which is significantly smaller. This will be explained in more detail in section 'ideal size'.
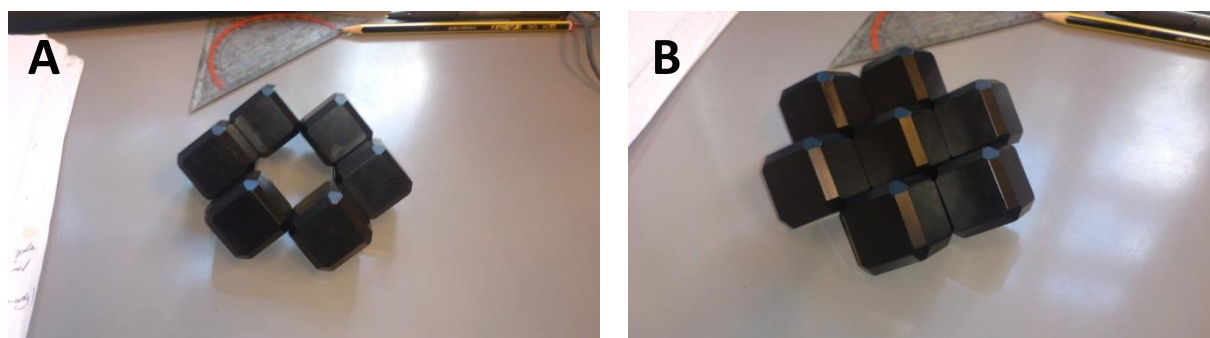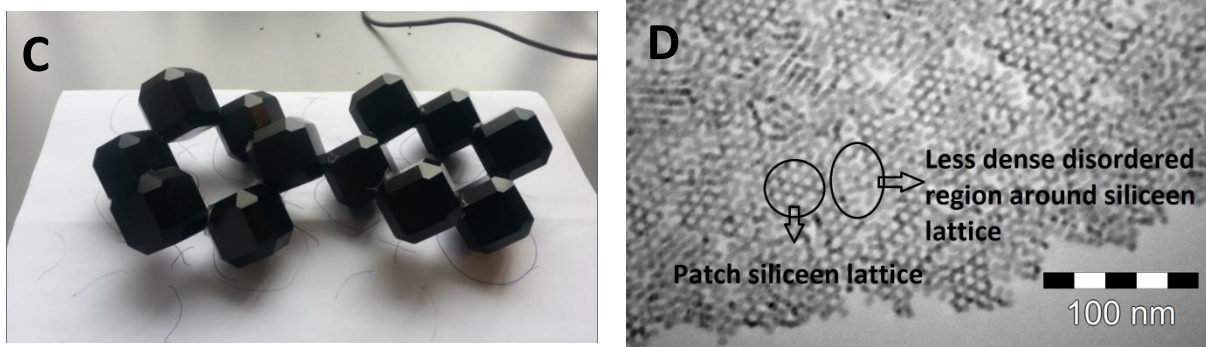
Figure 23. In (A) the honeycomb lattice, formed by the attachment of the <110> facet of truncated cubes. In (B) the honeycomb structure with a fully connected quantum dot in the middle. In (C) the model of the siliceen lattice is shown and in (D) PbTe siliceen lattices are shown.

A few notes which will be explained later on in the model section and the analyzing section.

- First the siliceen lattice is always in combination with the linear lattice as shown in figure 18C&D.

- The second important point is that the siliceen lattice always arises on the more 'denser' part of the TEM images, where the amount of original quantum dots is higher compared to the linear part (figure 18C&D).

- The last point to notice is that the siliceen lattice has never large areas in the case of PbTe (5.9 nm), but always consist of patches of the siliceen structure with a less dense disordered part around the patches, which is visualized in figure 23D.

5.3.J. The model.

Now a model is used to explain the growth of the siliceen lattice which results eventually in a prediction of the size of quantum dot/oleic acid for siliceen lattice fabrication. Starting in figure 24A, first a hexagonal plane of particles is packed at the liquid-gas interface by self-assembly. The distance between the particles depends on the length and amount of the ligands (oleic acid) around the quantum dots. This distance is hard to estimate because no direct measurement can be used for this purpose and it depends strongly on the intertwining of the two monolayers (see section 'GISAXS measurements'). TEM gives the best approximation, although the length measured by TEM is always someway shorter than in reality, due to shrinking of the structure while it is dried under vacuum.

If the solution is drying and the particles self-assembly at the interface, than it can be that there is not enough space for all the particles. In that case a second layer of hexagonal self-assembled particles will be deposited below the first hexagonal plane (see section 'top view'). This is visualized by crosses in Figure 24B. In figure 24C a glass plate is put in between the two layers to illustrate that there are two separate planes. In figure 24D the situation is displayed as if you look to it with a TEM. Now a siliceen lattices arise, although the layer are not atomically connected. In figure 24E the top hexagonal plane is replaced by the siliceen lattice and it fits completely in such a way that one cannot see any difference between the two. It is proposed here that the classical oriented attachment mechanism plays a role [49]. This is displayed in figure 25D first a mesocrystal is formed, in which the building blocks are not atomically connected. This is followed by the detachment of oleic acid from the surface and the building blocks are fused together. In this fusion process the <111> planes are connected. In this way the siliceen lattice of figure 24F arises. The reason that linear structures are also visible in siliceen samples, is that in the part with only a single plane of hexagonal packed quantum dots, oriented attachment occurs in a linear fashion, while in the denser part siliceen lattices growths. In the section 'ideal size' it will be explained why the siliceen structure is not a long range in my case and why there is a less dense part around it, but first an experimental example is given.
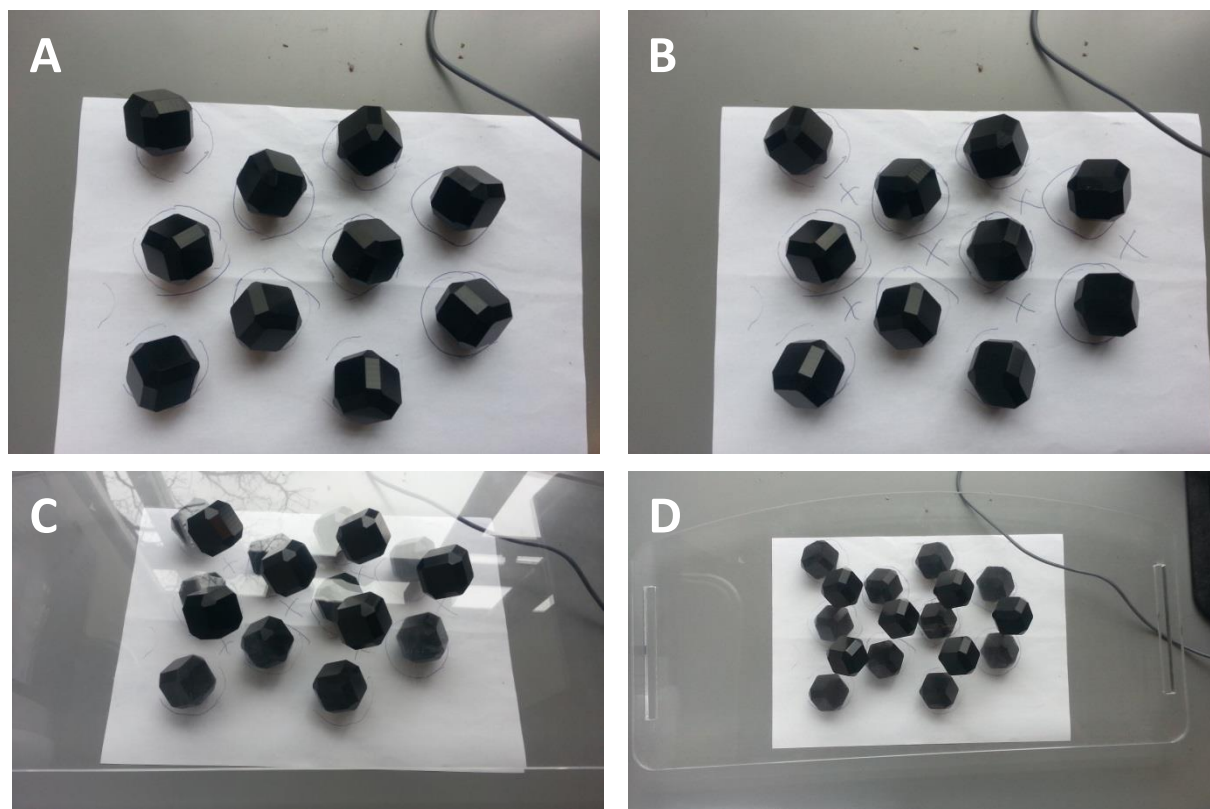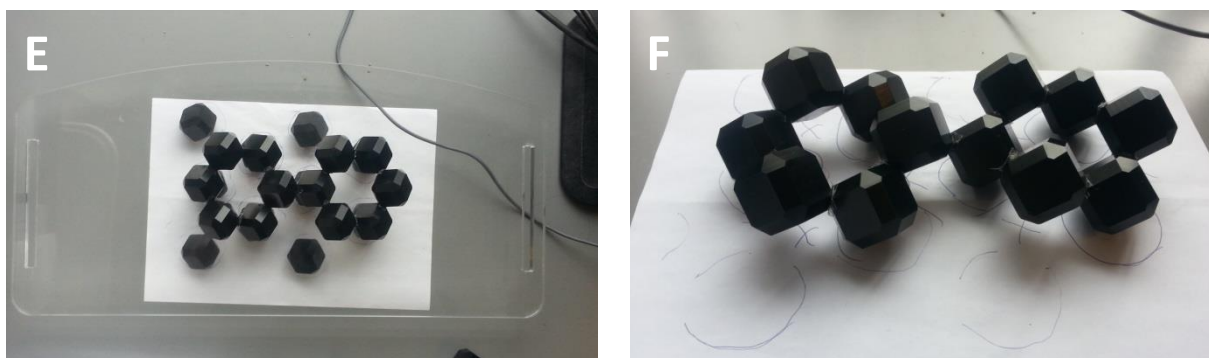
Figure 24. A model is used to explain the arise of the siliceen lattice. In (A) a hexagonal packed lattice of quantum dots is visualized. In (B) a second unattach layer of quantum dots comes on top of the first layer indicated by the crosses and this is further visualized in (C) with a glass plate between the two layers. In (D) a top view, like one does with TEM, is made. Here a seemingly siliceen lattice arises, but this are actually to hexagonal planes on top of each other. In (E) the top hexagonal plane in replaced by the siliceen lattice which clearly fits perfectly. In (F) the two hexagonal planes are fused together to the siliceen lattice.

Because of the weak temperature dependence of PbTe for oriented attachment (oriented attachment starts already at 7 °C), it was hard to experimentally prove that this model was correct. At a certain moment, it was also tried to perform oriented attachment on DEG instead of EG. This was also done in the article where this experiment was first proposed, but used as template for self-assembly [124] [125]. Unfortunately, only a few experiments could be performed on this DEG, because there was only a small amount left and newly ordered DEG gave totally different results. This again proved the vulnerability of these experiments, in which the composition of the liquid template is of major importance. On this DEG, the PbTe quantum dots experienced an enormous stability. At room temperature, with a small amount of oleic acid ($2 \cdot 10^{-5} mol/L$) dissolved in DEG, the particles didn't attach at all, as shown in figure 25A. Here a hexagonal plane of self-assembled quantum dots is shown with a second hexagonal plane on top. These two layers are not attached, because otherwise also in the single layer attachment should be visible. In figure 25B&C an oriented attachment experiment is performed at a temperature of 25 °C with no oleic acid on the same DEG. It is clear that some parts are heavily melted, but also small patches of siliceen lattices are visible. Unfortunately the DEG was finished after those experiment and the relative concentration of the sample used in figure 25A and figure 25B&C is not exactly the same ([20] in (A) and [15] in (B)&(C)), but both are in the 'siliceen range' of relative concentrations. In figure 25D the proposed mechanism is again shown, in which first a mesocrystal of two hexagonal planes on top of each other is formed which eventually fuse together to form the siliceen lattice.
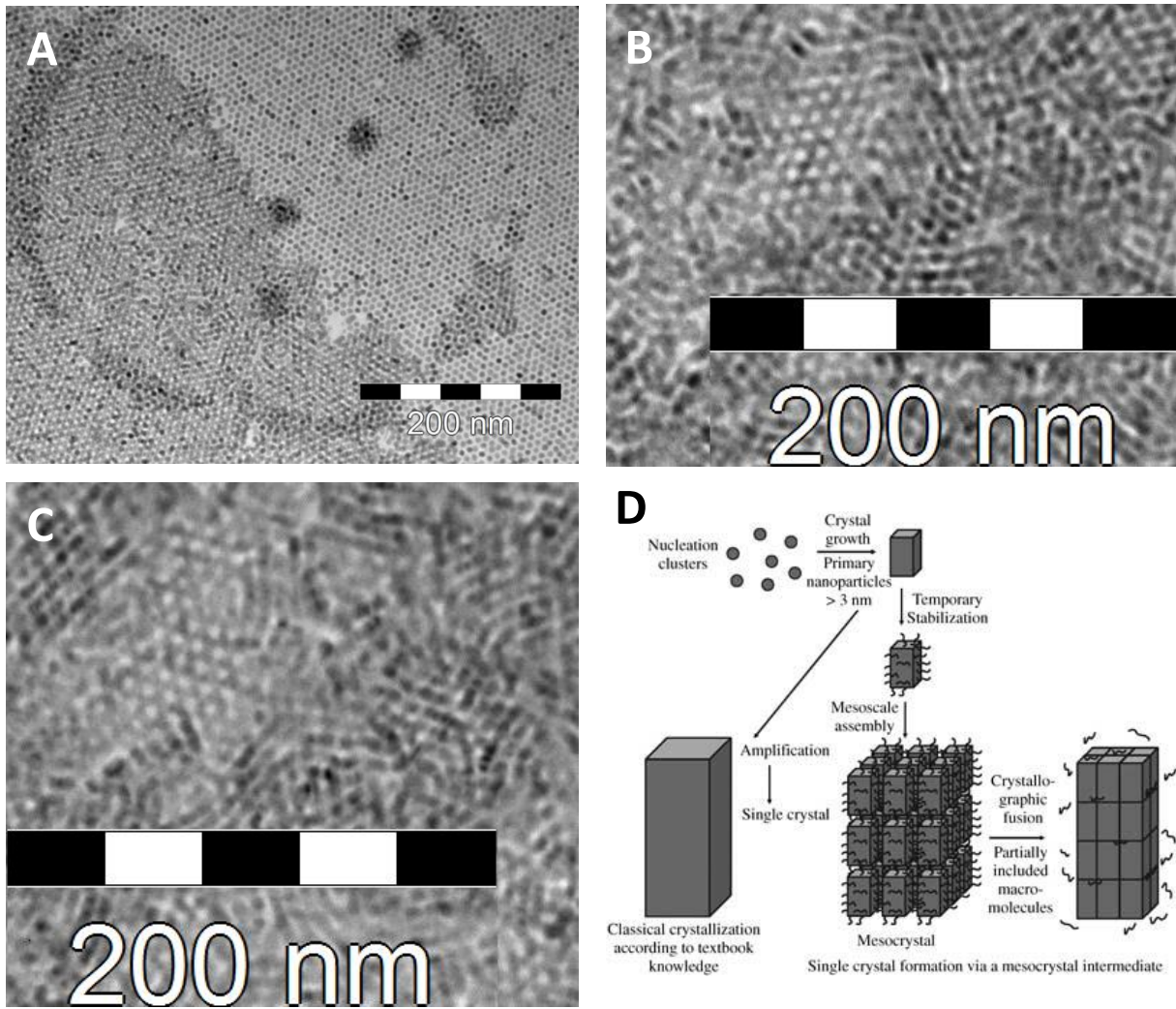
Figure 25. (A) Oriented attachment experiment of PbTe on DEG at 20 °C with addition of $2 \cdot 10^{-5} mol/l$ oleic acid in the DEG. A relative concentration of [20] was used. A layer of hexagonal packed quantum dots is visible with a second unattached layer on top of it. (B) & (C) This oriented attachment experiment is performed at 25 °C on DEG (same as in (A)). Quite some melted areas are visible but also small areas of siliceen lattices are visible. The relative concentration is somewhat lower, [15], but still in the 'siliceen range'. In (D) the mechanism behind the formation of the siliceen lattice is shown.

5.3.K. Ideal sizes to get the siliceen lattice.

In this part an analyses is performed to explain why the siliceen lattice consist only of patches and not of long range siliceen lattices. It will also be explained why there is a somewhat less denser region around a patch of siliceen lattice (figure 23D). To get a perfect long range siliceen lattice, two hexagonal planes should fuse together in such a way that it fits. In figure 26A two hexagonal packed planes of quantum dots are separated by a glass plate. The <111> facets point upwards so three <111> facets are in the right position for attachment and the layers fuse together to form figure 26C. The distance between two neighboring quantum dots is exactly right so that fusion will lead to a regular structure. In figure 26B&D two examples are shown where that requirement is not met.
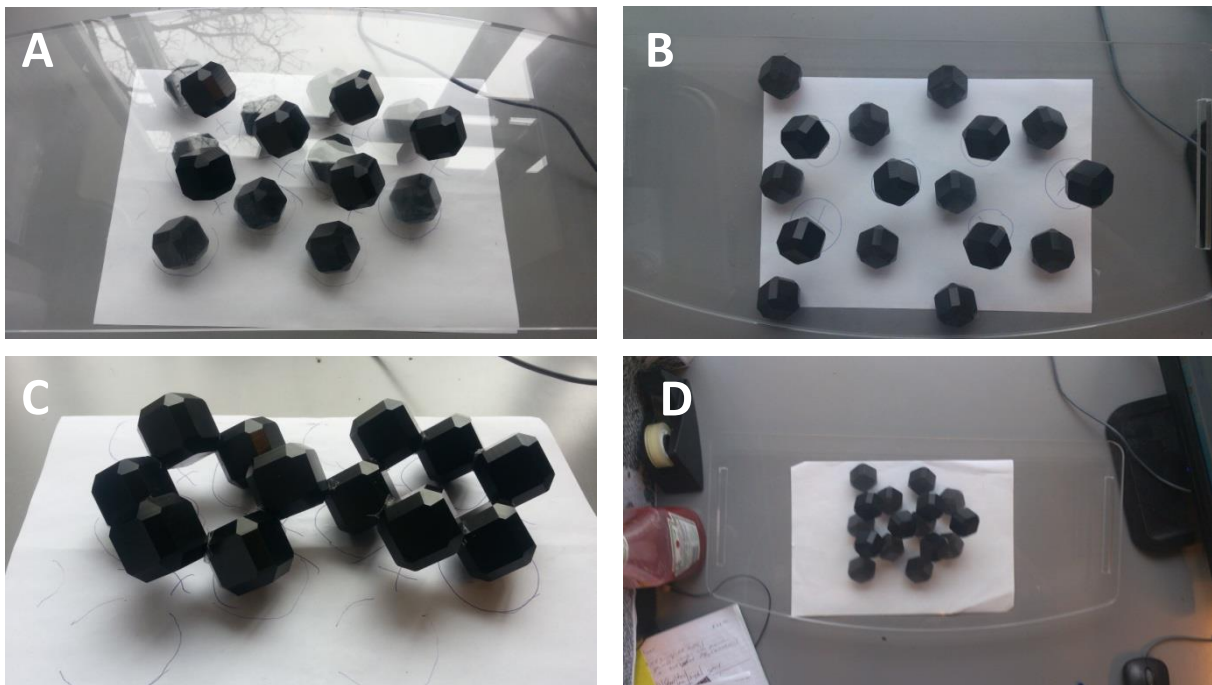
Figure 26. In (A) two hexagonal planes are on top of each other separated by a glass plate. In (C) the same picture is made from a top view, but now the distance between two neighboring particles is much larger. Fusion of the two layers cannot occur anymore because the <111> facets are not directed towards each other. In (B) the two hexagonal planes are fused together to form a siliceen lattice. In (D) also two unattach hexagonal planes are on top of each other but now the distance between the particles is very short. In the particles try to fuse, an unregular structure will be formed because the <111> planes are not facet to each other.

In figure 26B the distance between two neighboring quantum dots is too large (or the ligand is too long). If the ligands will be detached from the surface it will not lead to fusion because particles are too far from each other. The opposite is illustrated in figure 26D. The particles in

the two self-assembled hexagonal planes are now to close to each other. The <111> facet are not pointing perfectly towards each other, so no long range superstructure can be made if self-assembly occurs like this.

In this section, a comparison is made between an unattached hexagonal packed sample (figure 24D) and a siliceen lattice (figure 24E) to see if the samples presented are perfectly aligned or not. If one wants to make a large area siliceen lattice; alignment should be perfect and no length difference should be present between both situation. If there is a deviation from the optimum alignment, strain will develop and the structure will break up. To test if this is the case in PbTe of 5.9 nm, the length of the siliceen lattice will be compared with the length of the structure where it arises from, two hexagonal planes on top of each other. The measurements are shown in appendix 15 and the results in table 4. To be sure it was not influenced by an error in the TEM image, it was tested on several different siliceen lattices and TEM images with two hexagonal planes on top of each other. Before we go to the results, one note should be made. A TEM image is made by putting the sample under vacuum to make sure that all solvents and EG are evaporated. This will results in a contraction of the image of two hexagonal planes on top of each other, not on the siliceen lattice because it is atomically connected. As shown in table 4, this difference in average distance is highly significant on a smaller than 0.1% significant level (t-value = 5.15). The distance in two hexagonal planes is already bigger without taking into account, the increase in the quantum dot distance caused by drying the TEM grid under vacuum, which probably even increases the distance. This means that PbTe of 5.9 nm is in the situation which deviates from the optimum alignment towards figure 24B (although not that extreme). The distance in the unattached case is bigger compared to the distance in the siliceen lattice. One can now see, why there is a less dense part around a patch of siliceen lattice. A few quantum dots will attach, but till a certain moment, a quantum dot cannot reach it neighboring <111> facet anymore and no attachment will follow.

Table 4. Statistics on the distance measurements.

PbTe (nr. 116)	Mean [nm]	Nr.	σ
two flat hexagonal planes on top of each other	25.04	103	1.14
Measured distances in a siliceen,	24.51	102	1.04

This means, for making the honeycomb structure with 5.9 nm particles there will be strain caused by the contraction while the quantum dots try to attach. Therefore there will be defects in the structure, in which there is a place left over. This is also visible in the TEM images of honeycomb in which areas of honeycomb are interspersed with disordered/linear structures. Although there is an ideal size to make siliceen lattices (probably ~5.4 nm, due to pictures of Wiel Evers [82]), it does not mean that no siliceen lattice of other sizes can be made. If the length of the ligand is also adjusted one can in principle make the siliceen lattice of several sizes of quantum dots and thereby vary the size of the repeating unit of siliceen.

6. Conclusion.

A wide range of sizes of PbTe colloidal nanocrystals was made, which show clear absorption and emission features. Many oriented attachment experiments were done with these particles. Linear structures were made of PbTe and PbS. Also square structures were made from both compounds, although the square structure made from PbTe was not completely 90°, but an explanation was given to explain this ranging angle. It seems that not one facet is involved in attachment of these particles, but two. This is quiet unusual for oriented attachment experiments, but proven to be possible here. Besides these structures patches of siliceen lattices were also made including their growth model. I propose that this structure arise by the classical oriented attachment theory, in which first a mesocrystal is formed which eventually fuses together to form an atomically connected ultra-thin superstructure. Quantum dots, in this model, first self-assembly into a mesocrystal, in which the quantum dots are packed in two heaxagonal planes. After this structure of the hexagonal packed planes on top of each other is formed, oleic acid is detached from the surface and the siliceen lattice arises. This explanation would explain a few crucial un explained observations; why there is a hole in the middle and why this structure can only be made with a good ratio of quantum dot diameter and ligand length. It also predicts that it is possible to make the siliceen unit cell smaller or larger by changing the size of the quantum dot and the length of the ligand simultaneously.

7. Outlook.

The synthesis of SnTe is very complex. For further use, it would therefore be wise to search for ways to increase the stability, by searching for better stabilizing ligands (TOP was tried but did not work). Also one has to take into account that the synthesis is at low temperatures which increases the mobility of the monomers and increases the possibility of particles melting together. Making the complex $Pb_{1-x}Sn_xTe$ is probably very hard in a one-step method, but can be done by cation exchange after SnTe is made.

It is clear that small changes in the environment can majorly change the conditions of oriented attachment. Controlling the environment is therefore a key point in making the experiments more reproducible and controllable.

Oriented attachment occurs when the repulsive force of the steric hindering and the attractive forces are almost similar. If the ligand shell is reduced or taken away completely, slow and precise growth can be achieved. In the experiment presented in this thesis, oleic acid is slowly dissolved in the EG layer below the oriented attachment interface. This detachment of oleic acid of the surface of the quantum dots can maybe be controlled more by making use of other complexing agents. This was illustrated by the article of Schliebe et al., in which small cation complexing agents are used to induce oriented attachment, but the exact mechanism is not known [91]. It is also thought that nanoplatelets can arise from the oriented attachment of quantum dots, which is similar to the article of Schliebe et al. [92] [93] [94].

Another way to influence the detachment of ligand is the way nature does it; making use of difference in pH. The pH influences the binding of the ligand to the quantum dot surface [69]. Also small alcohols have an influence on the surface of quantum dots, which is know from washing procedures [18] [20]. These molecules and mechanisms which influence the steric hindering can be extremely useful in the future to design new materials. More knowledge on this complicated topic of detachment of the ligand is very useful for further research.

A more fundamental research area will be the extension of knowledge about the forces which play a role in the oriented attachment process. Especially the attractive forces are still quite mystic [59]. A focused research to answer the question which attractive force is the dominant one in which situation, would be very useful and lead to better understanding is different cases.

The last interesting and useful subject will be the gathering of more knowledge about the exact shape of the quantum dot in every situation. In this way it is possible to see which facet is available for attachment and which not. This process is probably quite complex and it is even claimed that it can be changed after the quantum dot synthesis by the availability of ligands [51].

When there is more knowledge about all these factors it can be possible to model new structures, by logical thinking or even computer modeling.

8. Acknowledgement.

9. References.

[1]   A. Geim and K. Novoselov, "The rise of graphene.," *Nature Materials,* vol. 6, pp. 183 - 191, 2007.

[2]   Y. Tung and M. Cohen, "Relativistic Band Structure and Electronic Properties of SnTe, GeTe, and PbTe," *Physical Review,* vol. 180, no. 823, pp. 823-825, 1969.

[3]   R. Dalven, "A review of the semiconductor properties of PbTe, PbSe, PbS AND PbO.," *Infrared Physic,* vol. 9, pp. 141-184., 1969.

[4]   J. Dimmock, I. Melngailis and A. Strauss, "Band and structure and laser action in PbxSnx-1Te," *Physical review letters,* vol. 16, no. 26, p. 1193, 1966.

[5]   I. Arachchige and M. Kanatzidis, , "Anomalous Band Gap Evolution from Band Inversion in Pb1-xSnxTe Nanocrystals," *nanoletters,* vol. 9, no. 4, pp. 1583-1587, 2009.

[6]   L. Fu and C. Kane, "Topological insulators with inversion symmetry," *Physical review B,* vol. 76, p. 045302, 2007.

[7]   G. Grzybowski and B. Whitesides, "Self-Assembly at All Scales," *science,* vol. 29, no. 295, p. 2418, 2002.

[8]   R. Penn and J. Banfield, "Imperfect Oriented Attachment: Dislocation Generation in Defect-Free Nanocrystals," *Science,* vol. 14, no. 281, p. 969, 1998.

[9]   H. Zheng, R. Smith, Y.-W. Jun, C. Kisielowski, U. Dahmen and A. Alivisatos, "Observation of Single Colloidal Platinum Nanocrystal Growth Trajectories.," *Science,* vol. 324, no. 5932, pp. 1309-1312, 2009.

[10]   C. Murray, D. Noms and M. Bawendi, "Synthesis and Characterization of Nearly Monodisperse CdE (E = S, Se, Te) Semiconductor Nanocrystallites.," *J. Am. Chem. Soc. ,* vol. 115, no. 19, pp. 8706-8715, 1993.

[11]   H. Vehkamäki, Classical Nucleation Theory in Multicomponent Systems, England: Springer, 2006.

[12]   Z. Peng and X. Peng, "Formation of High-Quality CdTe, CdSe, and CdS Nanocrystals Using CdO as Precursor," *J. Am. Chem. Soc.,* vol. 123, pp. 183-184, 2000.

[13]   C. d. M. Donega , "Synthesis and properties of colloidal heteronanocrystals," *Chemical Society Reviews,* vol. 40, p. 1512, 2011.

[14]   C. Burda , X. Chen, R. Narayanan and M. El-Sayed, "Chemistry and Properties of Nanocrystals of

Different Shapes," *Chem. Rev. ,* vol. 105, pp. 1025-1102, 2005.

[15] V. Lamer and R. Dinegar, "Theory, production and mechanism of formation of monodisperse hydrosol," *J. Am. Chem. Soc.,,* vol. 72, p. 4847–4854, 1950.

[16] T. Trindade, P. O'Brien and N. Pickett, "Nanocrystalline Semiconductors: Synthesis, Properties, and Perspectives," *Chem. Mater. ,* vol. 13, pp. 3843-3858, 2001.

[17] I. Moreels, B. Fritzinger, J. Martins and Z. Hens, "Surface Chemistry of Colloidal PbSe Nanocrystals," *J. AM. CHEM. SOC.,* vol. 130, no. 9, p. 15081–15086, 2008.

[18] A. Hassinen, I. Moreels, K. de Nolf, P. Smet, J. Martins and Z. Hens, "Short-Chain Alcohols Strip X-Type Ligands and Quench the Luminescence of PbSe and CdSe Quantum Dots, Acetonitrile Does not," *Journal of the American Chemical Society,* vol. 134, no. 51, p. 20705–20712, 2012.

[19] M. Sliem, A. Chemseddine, U. Bloeck and R. Fischer, "PbSe nanocrystal shape development: oriented attachment at mild conditions and microwave assisted growth of nanocubes.," *CrystEngComm,* vol. 13, pp. 483-488, 2011.

[20] M. Law, J. Luther, Q. Song, B. Hughes, C. Perkins and A. Nozik, "Structural, optical and electrical properties of PbSe Nanocrystal Solids Treated Thermally or with Simple Amines," *JACS,* vol. 130, no. 18, pp. 5970-5985, 2008.

[21] E. Groeneveld, Synthesis and optical spectroscopy of (hetero)-nanocrystals: An exciting interplay between chemistry and physics, Utrecht: University of Utrecht, 2012.

[22] J. Urban, D. Talapin, E. Shevchenko and C. Murray, "Self-Assembly of PbTe Quantum Dots into Nanocrystal Superlattices and Glassy Films," *JACS,* vol. 128, no. 10, pp. 3248-3255, 2006.

[23] E. Roduner, Nanocopic materials; Size-dependent Phenomena, cambridge: RCS publishing, 2006.

[24] J. Yuk, J. Park, P. Ercius, K. Kim, D. Hellebusch, M. Crommie, J. Lee, A. Zettl and A. Alivisatos, "High-Resolution EM of Colloidal Nanocrystal Growth Using Graphene Liquid Cells.," *Science,* vol. 336 , no. 6077 , pp. 61-64 , 2012.

[25] I. Lifshitz and V. Slyozov, "The kinetics of precipitation from supersaturated solid solutions," *J. Phys. Chem. Vol.,* vol. 19, no. 1-2, pp. 35-50,, 1961.

[26] D. Talapin, A. Rogach, M. Haase and H. Weller , "Evolution of an Ensemble of Nanoparticles in a Colloidal Solution: Theoretical Study.," *J. Phys. Chem. B,* vol. 105, no. 49, pp. 12278-12285, 2001.

[27] T. Schaaff and R. Whetten, "Controlled Etching of Au:SR Cluster Compounds.," *J. Phys. Chem. B ,* vol. 103, pp. 9394-9396, 1999.

[28] K. Edinger, A. Golzhauser, K. Demota, C. Woll and M. Grunze, "Formation of Self-Assembled Monolayers of n-Alkanethiols on Gold: A Scanning Tunneling Microscopy Study on the Modification of Substrate Morphology," *Langmuir,* vol. 9, pp. 4-8, 1993.

[29] X. Lin, C. Sorensen and K. J. Klabunde, "Ligand-Induced Gold Nanocrystal Superlattice Formation in Colloidal Solution.," *Chem. Mater.,* vol. 11, pp. 198-202, 1999.

[30] X. Lin, G. Wang, C. Sorensen and K. Klabunde, "Formation and dissolution of gold nanocrystal superlattices in a colloidal solution.," *J. Phys. Chem. B,* vol. 103, no. 26, pp. 5488-5492, 1999.

[31] A. Smetana, K. Klabunde and C. Sorensen, "Synthesis of spherical silver nanoparticles by digestive ripening, stabilization with various agents, and their 3-D and 2-D superlattice formation.," *Journal of Colloid and Interface Science ,* vol. 284, no. 2, pp. 521-526, 2005.

[32] S. Stoeva, K. Klabunde, C. Sorensen and I. Dragieva, "Gram-scale synthesis of monodisperse gold colloids by the solvated metal atom dispersion method and digestive ripening and their organization into two- and three-dimensional structures.," *Journal of the American Chemical Society ,* vol. 124, no. 10, pp. 2305-2311, 2002.

[33] Q. Zhang, J. Xie, J. Yang and J. Lee, "Monodisperse icosahedral Ag, Au, and Pd nanoparticles: Size control strategy and superlattice formation," *ASC nano,* vol. 3, no. 1, pp. 139-148, 2009.

[34] A. Samia, J. Schlueter, J. Jiang, S. Bader, C. Qin and X. Lin, "Effect of ligand-metal interactions on the growth of transition-metal and alloy nanoparticles.," *Chemistry of Materials,* vol. 18, no. 22, pp. 5203-5212, 2006.

[35] S. Cingarapu, Z. Yang, C. Sorensen and K. Klabunde, "Synthesis of CdSe Quantum Dots by Evaporation of Bulk CdSe using SMAD and Digestive Ripening Processes.," *Chem. Mater.,* vol. 21, no. 7, p. 1248–1252, 2009.

[36] D. Heroux, A. Ponce, S. Cingarapu and K. Klabunde, "Nanoparticles prepared by salt vapor-solvent vapor cocondensation and controlled nucleation: Metal sulfides (ZnS, CdS, CdSe, PbS), and metal halide (LiF). Size, aggregates, structures, digestive ripening, superlattices, and impregnations.," *Advanced Functional Materials ,* vol. 17, no. 17, pp. 3562-3568, 2007.

[37] D. Sidhaye and B. Prasad, "Many manifestations of digestive ripening: monodispersity, superlattices and nanomachining.," *NewJ. Chem.,* vol. 35, p. 755–763, 2011.

[38] D. Lee, S. Park, J. Lee and N. Hwang, "A theoretical model for digestive ripening," *Acta Materialia,* vol. 55, no. 15, pp. 5281-5288, 2007.

[39] H. Xin and H. Zheng, "In Situ Observation of Oscillatory Growth of Bismuth Nanoparticles.," *Nano Lett.,* vol. 12, no. 3, p. 1470–1474, 2012.

[40] K. Drexler, Engines of Creation: The Coming Era of Nanotechnology, New York: Oxford University Press, 1986.

[41] C. Peterson, "Foresight Institute," http://www.foresight.org/, Palo Alto, 1989.

[42] A. Alivisatos, "Semiconductor Clusters, Nanocrystals, and Quantum Dots," *science,* vol. 271, no. 5251, pp. 933-937 , 1996.

[43] E. Shevchenko, D. Talapin, N. Kotov, S. O'Brien and C. Murray, "Structural diversity in binary nanoparticle superlattices," *Nature ,* vol. 439, pp. 55-59, 2005.

[44] B. Korgel and D. Fitzmaurice, "Self-Assembly of Silver Nanocrystals into Two-Dimensional Nanowire Arrays," *advanced materials,* vol. 10, pp. 661-665, 1998.

[45] R. Penn and J. Banfield, "Oriented attachment and growth, twinning, polytypism, and formation of metastable phases: Insights from nanocrystalline TiO2," *American Mineralogist,* vol. 83, pp. 1077–1082,, 1998.

[46] J. Banfield, S. Welch, H. Zhang, T. Ebert and R. Penn, "Aggregation-Based Crystal Growth and Microstructure Development in Natural Iron Oxyhydroxide Biomineralization Products," *science,* vol. 2, no. 289, p. 751, 2000.

[47] D. Li, M. Nielsen, J. Lee, C. Frandsen, J. Banfield and J. De Yoreo, "Direction-Specific Interactions Control Crystal Growth by Oriented Attachment," *science,* vol. 25, no. 336, pp. 1014-1018, 2012.

[48] M. van Huis, L. Kunneman, K. Overgaag, Q. Xu, G. Pandraud, H. Zandbergen and D. Vanmeakelbergh, "Low-temperature nanocrystal unification through rotations and relaxations probed by in situ transmission electron microscopy," *Nanoletters,* vol. 8, no. 11, pp. 3959-3963, 2008.

[49] F. Meldrum and H. Colfen, "Controlling Mineral Morphologies and Structures in Biological and Synthetic Systems.," *Chem. Rev. ,* vol. 108, no. 11, p. 4332–4432, 2008.

[50] J. Zhang, F. Huang and Z. Lin , "Progress of nanocrystalline growth kinetics based on oriented attachment.," *Nanoscale,* vol. 2, pp. 18-34, 2010.

[51] C. Bealing, W. Baumgardner, J. Choi, T. Hanrath and R. Hennig, "Predicting Nanocrystal Shape through Consideration of Surface-Ligand Interactions.," *ACS Nano,* vol. 6, no. 3, p. 2118–2127, 2012.

[52] C. Fang, M. van Huis, D. Vanmaekelbergh and H. Zandbergen, "Energetics of Polar and Nonpolar Facets of PbSe Nanocrystals from Theory and Experiment," *ACS Nano,* vol. 4, no. 1, p. 211–218, 2010.

[53] Z. Zhang, S. Sun, X. Shao, D. Li and M. Han, "Three-dimentionally oriented aggregation of a few hunderd nanoparticles into manocrystalline architectures," *advanced materials,* vol. 17, no. 1, pp. 42-47, 2005.

[54] J. Polleux, N. Pinna, M. Antonietti and M. Niederbergen, "Ligand-Directed Assembly of Preformed Titania Nanocrystals into Highly Anisotropic Nanostructures.," *Advanced Materials,* vol. 16, no. 5, p. 436–439 , 2004.

[55] E. Lee , C. Ribeiro, E. Longo and E. Leite, "Oriented Attachment: An Effective Mechanism in the Formation of Anisotropic Nanocrystals.," *J. Phys. Chem. ,* vol. 109, no. 44, p. 20842–20846, 2005.

[56] J. Choi , C. Bealing , K. Bian , K. Hughes, W. Zhang, D.-M. Smilgies, R. Hennig, J. Engstrom and T. Hanrath, "Controlling Nanocrystal Superlattice Symmetry and Shape-Anisotropic Interactions through Variable Ligand Surface Coverage.," *J. Am. Chem. Soc.,* vol. 133, no. 9, p. 3131–3138, 2011.

[57] K. Bian, J. Choi, A. Kaushik , P. Clancy, D.-M. Smilgies and T. Hanrath , "Shape-Anisotropy Driven Symmetry Transformations in Nanocrystal Superlattice Polymorphs.," *ACS Nano,* vol. 5, no. 4, p. 2815–2823, 2011.

[58] R. Penn and J. Banfield, "Morphology development and crystal growth in nanocrystalline aggregates under hydrothermal conditions: Insights from titania," *Geochimica et Cosmochimica Acta,* vol. 63, no. 10, p. 1549–1557, 1999.

[59] H. Zhang and J. Banfield, "Energy Calculations Predict Nanoparticle Attachment Orientations and Asymmetric Crystal Formation.," *J. Phys. Chem. Lett.,* vol. 3, no. 19, p. 2882–2886, 2012.

[60] D. Talapin, E. Shevchenko, C. Murray, A. Titov and P. Kral, "Dipole-Dipole Interactions in Nanoparticle Superlattices.," *nano letters,* vol. 7, no. 5, pp. 1213-1219, 2007.

[61] 2. e. IUPAC, "Gold book, Compendium of Chemical Terminology,," in *Glossary of terms used in physical organic chemistry* , Oxford , ISBN 0-9678550-9-8, 1997, p. 1175.

[62] P. Atkins, Physical Chemistry, Fifth edition, Oxford: Oxford University, 1995.

[63] C. Chan and S. Warren, "Quantum Dot Bioconjugates for Ultrasensitive Nonisotopic Detection," *Science,* vol. 25, no. 281, p. 2016, 1998.

[64] A. P. Alivisatos, "Perspectives on the Physical Chemistry of Semiconductor Nanocrystals.," *J. Phys. Chem. ,* vol. 100, pp. 13226-13239, 1996.

[65] S. Wuister, C. Donega and A. Meijerink , "Influence of Thiol Capping on the Exciton Luminescence and Decay Kinetics of CdTe and CdSe Quantum Dots.," *J. Phys. Chem. B,,* vol. 108, no. 45, pp. 17393-17397, 2004.

[66] K. Szendrei, "Charge extraction from colloidal inorganic nanocrystals," Zernike Institute PhD thesis series , Groningen, 2011.

[67] B.-K. Pong, B. Trout and J.-Y. Lee, "Modified Ligand-Exchange for Efficient Solubilization of CdSe/ZnS Quantum Dots in Water: A Procedure Guided by Computational Studies," *Langmuir,,*

vol. 24, no. 10, pp. 5270-5276, 2008.

[68] X. Peng, J. Wickham and A. Alivisatos, "Kinetics of II-VI and III-V Colloidal Semiconductor Nanocrystal Growth: "Focusing" of Size Distributions," *J. Am. Chem. Soc.,* vol. 120, pp. 5343-5344, 1998.

[69] M. Niederberge and H. Cölfen, "Oriented attachment and mesocrystals: Non-classical crystallization mechanisms based on nanoparticle assembly," *physical chemistry chemical physics,* vol. 8, no. 28, pp. 3271-3271, 2006.

[70] P. Shen and W. Lee, "(111)-Specific Coalescence Twinning and Martensitic Transformation of Tetragonal ZrO2 Condensates," *Nano Lett.,* vol. 1, no. 12, p. 707, 2001.

[71] H. Colfen and M. Antonietti, "Mesocrystals: Inorganic Superstructures Made by Highly Parallel Crystallization and Controlled Alignment.," *Angew. Chem. Int. Ed.,* vol. 44, no. 35, p. 5576 – 5591, 2005.

[72] Q. Zhang, S.-J. Liu and S.-H. Yu, "Recent advances in oriented attachment growth and synthesis of functional materials: concept, evidence, mechanism, and future.," *Journal of Materials Chemistry,* vol. 19, pp. 191-207, 2009.

[73] H. Colfen and S. Mann, "Higher-Order Organization by Mesoscale Self-Assembly and Transformation of Hybrid Nanostructures.," *Angew. Chem. Int. Ed. ,* vol. 42, p. 2350 – 2365, 2003.

[74] H.-G. Liao, L. Cui, S. Whitelam and H. Zheng, "Real-Time Imaging of Pt3Fe Nanorod Growth in Solution," *Science,* vol. 336, no. 25, p. 1011, 2012.

[75] N. Pradhan, H. Xu and X. Peng, "Colloidal CdSe Quantum Wires by Oriented Attachment," *Nano Letters,* vol. 6, no. 4, p. 720, 2006.

[76] C. Pacholski, A. Kornowski and H. Weller, "Self-Assembly of ZnO: From Nanodots to Nanorods," *Angewandte Chemie,,* vol. 41, pp. 1188-1191, 2002.

[77] K.-T. Yong, Y. Sahoo, H. Zeng, M. Swihart, J. Minter and P. Prasad, "Formation of ZnTe Nanowires by Oriented Attachment," *Chem. Mater.,* vol. 19, no. 17, pp. 4108-4110, 2007.

[78] Z. Tang, N. Kotov and M. Giersig, "Spontaneous Organization of Single CdTe Nanoparticles into Luminescent Nanowires," *Science,* vol. 12, no. 297, pp. 237-240, 2002.

[79] B. Fitzmaurice and D. Korgel, "Self-Assembly of Silver Nanocrystals into Two-Dimensional Nanowire Arrays," *Adv. Mater.,* vol. 10, no. 9, p. 661, 1998.

[80] A. Halder and N. Ravishankar, "Ultrafine Single-Crystalline Gold Nanowire Arrays by Oriented Attachment," *Adv. Mater.,* vol. 19, p. 1854–1858, 2007.

[81] K.-S. Cho, D. Talapin, W. Gaschler and C. Murray, "Designing PbSe Nanowires and Nanorings through Oriented Attachment of Nanoparticles," *J. AM. CHEM. SOC.,* vol. 127, pp. 7140-7147, 2005.

[82] W. Evers, B. Goris, S. Bals, M. Casavola, J. de Graaf, R. van Roij, M. Dijkstra and D. Vanmaekelbergh, "Low-dimensional semiconductor superlattices formed by geometric control over nanocrystal attachment," *nanoletters,* vol. 13, no. 6, p. 2317–2323, 2013.

[83] M. Shim and P. Guyot-Sionnest, "Permanent dipole moment and charges in colloidal semiconductor quantum dots.," *J. Chem. Phys.,* vol. 111, no. 5, p. 6955, 1999.

[84] M. Klokkenburg, A. Houtepen, R. Koole, J. de Folter, B. Erné, E. van Faassen and D. Vanmaekelbergh, "Dipolar Structures in Colloidal Dispersions of PbSe and CdSe Quantum Dots.," *Nano Letters,* vol. 7, no. 9, p. 2931, 2007.

[85] D. Hapiuk, B. Masenelli, K. Masenelli-Varlot, D. Tainoff, O. Boisron , C. Albin and P. Melinon, "Oriented Attachment of ZnO Nanocrystals.," *Journel of physical chemistry,* vol. 117, pp. 10220-10227, 2013.

[86] C. Murray, C. Kagan and M. Bawendi, "Self-organization of CdSe nanocrystallites into three-dimensional quantum dot superlattices," *Science,* vol. 270, pp. 1335-1338, 1995.

[87] J. Chen, A. Dong, J. Cai, X. Ye, Y. Kang, J. Kikkawa and C. Murray, "Collective Dipolar Interactions in Self-Assembled Magnetic Binary Nanocrystal Superlattice Membranes.," *Nano Lett.,* vol. 10, no. 12, p. 5103–5108, 2010.

[88] C. Collier, R. Saykally, J. Shiang, S. Henrichs and J. Heath, "Reversible tuning of silver quantum dot monolayers through the metal- insulator transition," *Science,* vol. 277, pp. 1978-1981, 1997.

[89] V. Colvin, A. Goldstein and A. Alivisatos, "Semiconductor nanocrystals covalently bound to metal surfaces with self-assembled monolayers," *Journal of the American Chemical Society,* vol. 114, pp. 5221-5230, 1992.

[90] Y. Lin, Y. Lin, H. Skaff, T. Emrick, A. Dinsmore and T. Russell, "Nanoparticle assembly and transport at liquid-liquid interfaces," *Science,* vol. 299, pp. 226-229, 2003.

[91] C. Schliehe, B. Juarez, M. Pelletier, S. Jander, D. Greshnykh, M. Nagel, A. Meyer, S. Foerster, A. Kornowski, C. Klinke and H. Weller, "Ultrathin PbS Sheets by Two-Dimensional Oriented Attachment," *Science,* vol. 329, no. 30, pp. 550-53, 2010.

[92] S. Ithurria and B. Dubertret, "Quasi 2D Colloidal CdSe Platelets with Thicknesses Controlled at the Atomic Level," *J. Am. Chem. Soc.,* vol. 130, no. 49, p. 16504–16505, 2008.

[93] S. Ithurria, G. Bousquet and B. Dubertret, "Continuous Transition from 3D to 1D Confinement Observed during the Formation of CdSe Nanoplatelets.," *J. Am. Chem. Soc.,* vol. 133, no. 9, p.

3070–3077, 2011.

[94] S. Ithurria, M. Tessier, B. Mahler, R. Lobo, B. Dubertret and L. Efros, "Colloidal nanoplatelets with two-dimensional electronic structure.," *Nature Materials,* vol. 10, p. 936–941, 2011.

[95] N. Gehrke , H. Colfen, N. Pinna, M. Antonietti and N. Nassif, "Superstructures of Calcium Carbonate Crystals by Oriented Attachment," *Crystal Growth & Design,* vol. 5, no. 4, p. 1318, 2005.

[96] J. Murphy, M. Beard, A. Norman, P. Ahrenkiel, J. Johnson, P. Yu, O. Micic, R. Ellingson and A. Nozik, "PbTe Colloidal Nanocrystals: Synthesis, Characterization, and Multiple Exciton Generation," *JACS,* vol. 128, no. 10, pp. 3241-3247, 2006.

[97] M. Kovalenko, W. Heiss, E. Shevchenko, J.-S. Lee, H. Schwinghammer, A. Alivisatos and D. Talapin, "SnTe Nanocrystals: A New Example of Narrow-Gap Semiconductor Quantum Dots," *JACS,* vol. 129, no. 37, pp. 11354-11355, 2007.

[98] G. Renauda, R. Lazzari and F. Leroy, "Probing surface and interface morphology with Grazing Incidence Small Angle X-Ray Scattering," *Surface Science Reports ,* vol. 64, pp. 255-380, 2009.

[99] R. Leitsmann, F. Bechstedt, H. Groiss, F. Schaffler, W. Heiss, K. Koike, H. Harada and M. Yano, "Structural and electronic properties of PbTe (rocksalt)/CdTe (zinc-blende) interfaces.," *Applied Surface Science,* vol. 254, no. 1, p. 397–400, 2007.

[100] H. Shen, H. Wang, X. Chen, J. Niu, W. Xu, X. Li, X.-D. Jiang, Z. Du and L. Li, "Size- and Shape-Controlled Synthesis of CdTe and PbTe Nanocrystals Using Tellurium Dioxide as the Tellurium Precursor.," *Chem. Mater.,* vol. 22, no. 16, p. 4756–4761, 2010.

[101] W. van de Stam, "Colloidal Nanostructures for application in Quantum Dot Sensitized Solar Cells," University of Utrecht, Utrecht, 2012.

[102] Y. Yuan, F.-S. Riehle, H. Gu, R. Thomann, G. Urban and M. Krüger, "Green Chemistry for Large-Scale Synthesis of Semiconductor quantum dots," *J. Nanosci. Nanotechnol.,* vol. 10, no. 9, p. 6041, 2010.

[103] M. Kanehara, H. Arakawa, T. Honda, M. Saruyama and T. Teranishi, "Large-Scale Synthesis of High-Quality Metal Sulfide Semiconductor Quantum Dots with Tunable Surface-Plasmon Resonance Frequencies," *Chem. Eur. J.,* vol. 18, p. 9230 – 9238, 2012.

[104] J. Niua, H. Shen, X. Li, W. Xu, H. Wang and L. Li, "Controlled synthesis of high quality PbSe and PbTe nanocrystals with one-pot method and their self-assemblies.," *Colloids and Surfaces A: Physicochem. Eng. Aspects,* vol. 406, p. 38–43, 2012.

[105] S. Ferreira, E. Abramof, P. Motisuke, P. Rappl, H. Closs, A. Ueta, C. Boschetti and I. Bandeira, "Experimental observation of band inversion in the PbSnTe synstem," *Journel of applied physics,* vol. 85, no. 12, p. 7189, 1999.

[106] M. Kovalenko, D. Talapin, M. Loi, F. Cordella, G. Hesser, M. Bodnarchuk and W. Heiss, "Quasi-Seeded Growth of Ligand-Tailored PbSe Nanocrystals through Cation-Exchange-Mediated Nucleation," *Angewandte Chemie,* vol. 47, no. 16, p. 3029 –3033, 2008.

[107] D. Son, S. Hughes, Y. Yin and A. Alivisatos , "Cation Exchange Reactions in Ionic Nanocrystals.," *SCIENCE,* vol. 306, pp. 1009-1012, 2004.

[108] D.-K. Ko and C. Murray, "Probing the Fermi Energy Level and the Density of States Distribution in PbTe Nanocrystal (Quantum Dot) Solids by Temperature-Dependent Thermopower Measurements.," *ACS Nano,* vol. 5, no. 6, p. 4810–4817, 2011.

[109] H. Haug and S. Koch, Quantum theory of the optical and electronic properties of semiconductors, Singapore: World scientific publishing Co., 2004.

[110] J. Lim, R. Tilton, A. Eggeman and S. Majetich, "Design and synthesis of plasmonic magnetic nanoparticles," *Journal of Magnetism and Magnetic Materials,* vol. 311, no. 1, pp. 78-83, 2007.

[111] C. Liu, Y. Shau, Y. Zhu and K. Chen , "Magnetic monolayer film of oleic acid-stabilized Fe3O4 particles fabricated via Langmuir-Blodgett technique," *Thin Solid Films,* vol. 518, no. 1, p. 324–327, 2009.

[112] A. de Kergommeaux, J. Faure-Vincent, A. Pron , R. de Bettignies, B. Malaman and P. Reiss , "Surface oxidation of tin chalcogenide nanocrystals revealed by 119Sn-Mössbauer spectroscopy.," *J Am Chem Soc. ,* vol. 134, no. 28, pp. 11659-66, 2012.

[113] I. Moreels, K. Lambert, D. Smeets, D. De Muynck, T. Nollet, J. Martins, F. Vanhaecke, A. Vantomme, C. Delerue, G. Allan and Z. Hens, "Size-Dependent Optical Properties of Colloidal PbS Quantum Dots," *ACS Nano,* vol. 3, no. 10, p. 3023–3030, 2009.

[114] M. Sykora, A. Koposov, J. McGuire, R. Schulze, O. Tretiak, J. Pietryga and V. Klimov, "Effect of Air Exposure on Surface Properties, Electronic Structure, and Carrier Relaxation in PbSe Nanocrystals," *ASC Nano,* vol. 4, no. 4, p. 2021–2034, 2010.

[115] Q. Dai, Y. Wang, Y. Zhang, X. Li, R. Li, B. Zou, J. Seo, Y. Wang, M. Liu and W. Yu, "Stability Study of PbSe Semiconductor Nanocrystals over Concentration, Size, Atmosphere, and Light Exposure.," *Langmuir,* vol. 25, no. 20, pp. 12320-4, 2009.

[116] N. Greenwood and A. Earnshaw, "Selenium, Tellurium and Polonium," in *Chemistry of the Elements* , (2nd Edition), Elsevier, 1997, p. section 16.1.

[117] J. Park, H. Zheng, W. Lee, P. Geissler, E. Rabani and P. Alivisatos, "Direct Observation of Nanoparticle Superlattice Formation by Using Liquid Cell Transmission Electron Microscopy.," *acsnano,* vol. 6, no. 3, p. 2078, 2012.

[118] S. Abrahamsson and I. Ryderstedt-Natiringbauer, "The Crystal Structure of the Low-Melting Form of Oleic Acid.," *Acta Cryst.,* vol. 15, pp. 1261-1268, 1962.

[119] S. Craig, K. Roberts, J. Sherwood, K. Sato, Y. Hayashi, M. Iwahashi and R. Cernik, "Using in-situ synchrotron radiation powder diffraction to characterize growth-related structural polymorphic phase transformations in cis-9-c0-octadecenoic acid.," *Journal of Crystal Growth* , vol. 128, pp. 1263-1267, 1993.

[120] F. Kaneko, K. Yamazaki, K. Kitagawa, T. Kikyo and M. Kobayashi, "Structure and Crystallization Behavior of the â Phase of Oleic Acid.," *J. Phys. Chem. B* , vol. 101, pp. 1803-1809, 1997.

[121] D. W. Ball, Physical chemistry, United states of America: Inc. Thomas Learning, 2003, p. 752.

[122] C. Wilke, "Diffusional properties of multicomponent gases," *Chemical Engineering Progress,* vol. 46, pp. 95-104, 1950.

[123] Z. Tang, Z. Zhang, Y. Wang, S. Glotzer and N. Kotov, "Self-assembly of CdTe nanocrystals into free-floating sheets.," *Science,* vol. 314, no. `, pp. 274-278, 2006.

[124] A. Dong, J. Chen, P. Vora, J. Kikkawa and C. Murray, "Binary nanocrystal superlattice membranes self-assembled at the liquid–air interface," *NATURE,* vol. 466, p. 474, 2010.

[125] A. Dong, X. Ye, J. Chen and C. Murray, "Two-Dimensional Binary and Ternary Nanocrystal Superlattices: The Case of Monolayers and Bilayers," *nano letters,* p. 1804–1809, 2011.

[126] D. V. T. E. V. S. C. B. M. Jeffrey J. Urban, "self-assembly of PbTe quantum dots into nanocrystal superlattices and glassy films," *JACS, 128, ,* pp. 3248-3255, 2006.

[127] M. H. S. F. A. K. A. W. H. Nage, "Synthesis of monodisperse PbS nanoparticles and their assembly into highly ordered 3D colloidal crystals," *Zeitschrift fur Physikalische Chemie, 221 ,* p. 427, 2007.

[128] D. V. T. W. G. a. C. B. M. Kyung-Sang Cho, "Designing PbSe Nanowires and Nanorings through Oriented Attachment of Nanoparticles," *J. AM. CHEM. SOC., 127 ,* pp. 7140-7147, 2005,.

[129] S. A. W. H. Z. T. T. E. R. L. P. Jillian F. BanÞeld, "Aggregation-Based Crystal Growth and Microstructure Development in Natural Iron Oxyhydroxide Biomineralization Products," *SCIENCE, VOL 289,* p. 751, 2000.

[130] L. Zhang, R. He and H.-C. Gu, "Oleic acid coating on the monodisperse magnetite nanoparticles," *Applied Surface Science, 253,* vol. 253, no. 5, p. 2611–2617, 2006.

[131] H. Colfen and m. Antonietti, "Mesocrystals: Inorganic Superstructures Made by Highly Parallel Crystallization and Controlled Alignment.," *Angew Chem Int Ed Engl. 2005 Sep 5;44(35):5576-91.,* vol. 44, no. 35, pp. 5576-91, 2005.

[132] F. Meldrum and H. Colfen, "Controlling Mineral Morphologies and Structures in Biological and Synthetic Systems".

[133] H.-G. Liao, L. Cui, S. Whitelam and H. Zhang, "Real-Time Imaging of Pt3Fe Nanorod Growth in Solution," *SCIENCE,* vol. 336, no. 25, p. 1011, 2012.
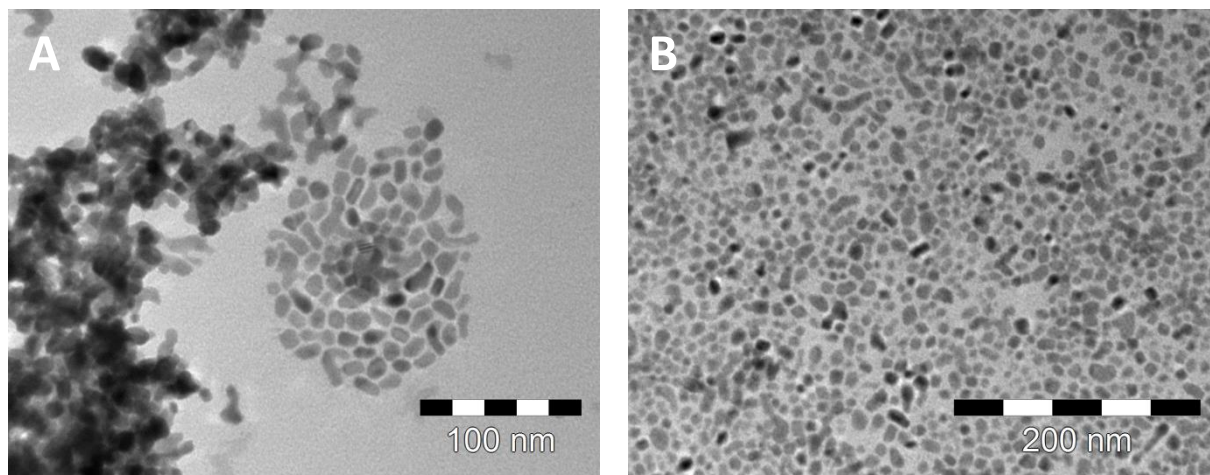
Appendix 1.

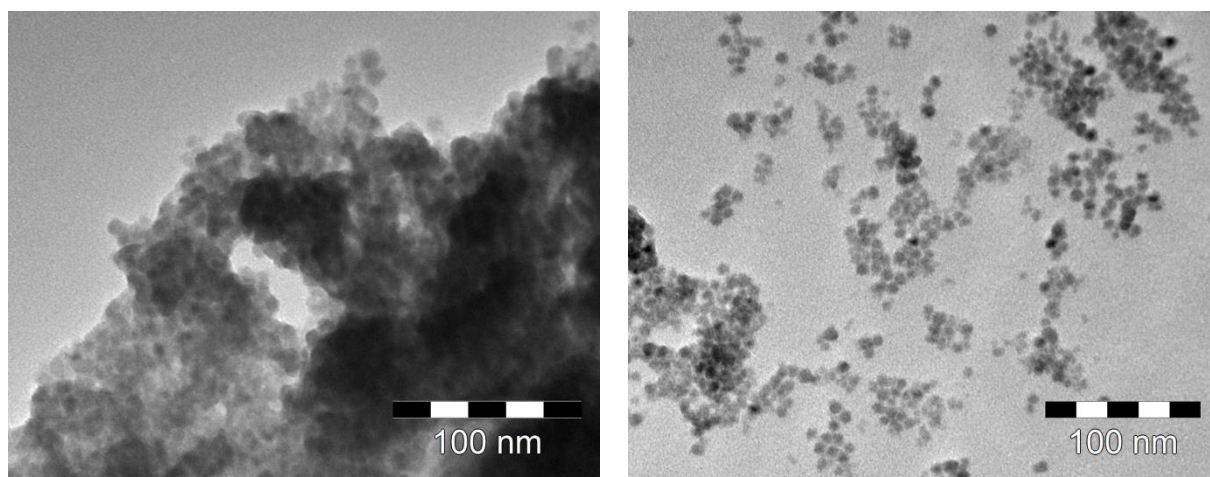*Figure 27. A failed attempt to get monodispersed $Pb_{1-x}Sn_xTe$ quantum dots.*

Figure 28. Sample SnTe 29-11-12 Large lumps of aggregated particles often arose.

Appendix 2.

PbTe in tolune.

For a nice self-assembly and also oriented attachment a slower evaporation would be favorable, thereby giving the particles more time to find the ideal positions. Also in the articles of W.Evers et al, it was stated that oriented attachment works better in toluene compared to hexane [82]. Therefore it was also tried to perform oriented attachment of PbTe in toluene. This was exactly harder than it looked like in the beginning. It seemed that the particles slowly dissolve in toluene into monomers. In figure 29, a few examples are visualized. Particles seem to disintegrate and form smaller particles with less spherical shapes.

Also PbTe did not attach in any oriented attachment experiment performed in toluene. It was also tried to add oleic acid to the EG and therefore indirectly to the drying solution, to protect the particles this is visible in figure 30. In these TEM images one can see that for the lowest two amounts of oleic acid added, the particles still demonstrate disintegration. In the samples where a high amount of oleic acid is added, the particles form long range sheets of hexagonal packed PbTe. In these samples also Ostwald ripening (even at room temperature!!) is clearly visible. It seems therefore that oleic acid in toluene can etch monomers from the quantum dots. More research on this topic should bring more clarity.
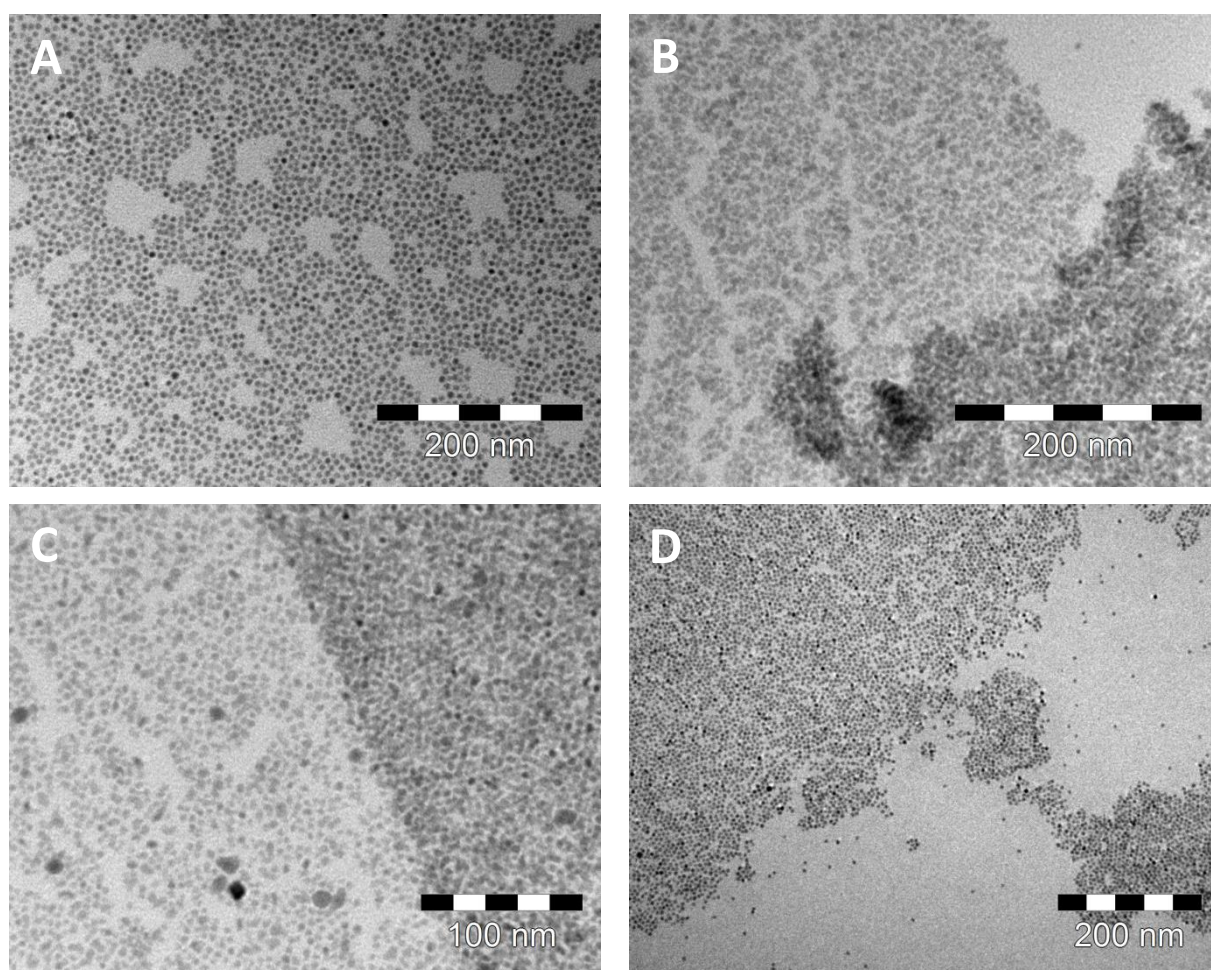
Figure 29. The development by increasing temperature of PbTe oriented attachment experiments in toluene. In A) 20 °C, B) 25 °C and C) 30 °C all three are dried for 120 minutes with the same concentration [18]. The shape of the particles changes completely when the temperature is increased, but it should be noted that also in A the is decreased by ~0.5nm compared to the starting particles. In D) almost the same experiment is performed as in B) with a slightly higher concentration (20) at the same temperature but with shorter time before the sample was fished, 90 minutes. This preserved the shape of the particles considerable, although in detailed images one can see that the sizes decreased (~1 nm).
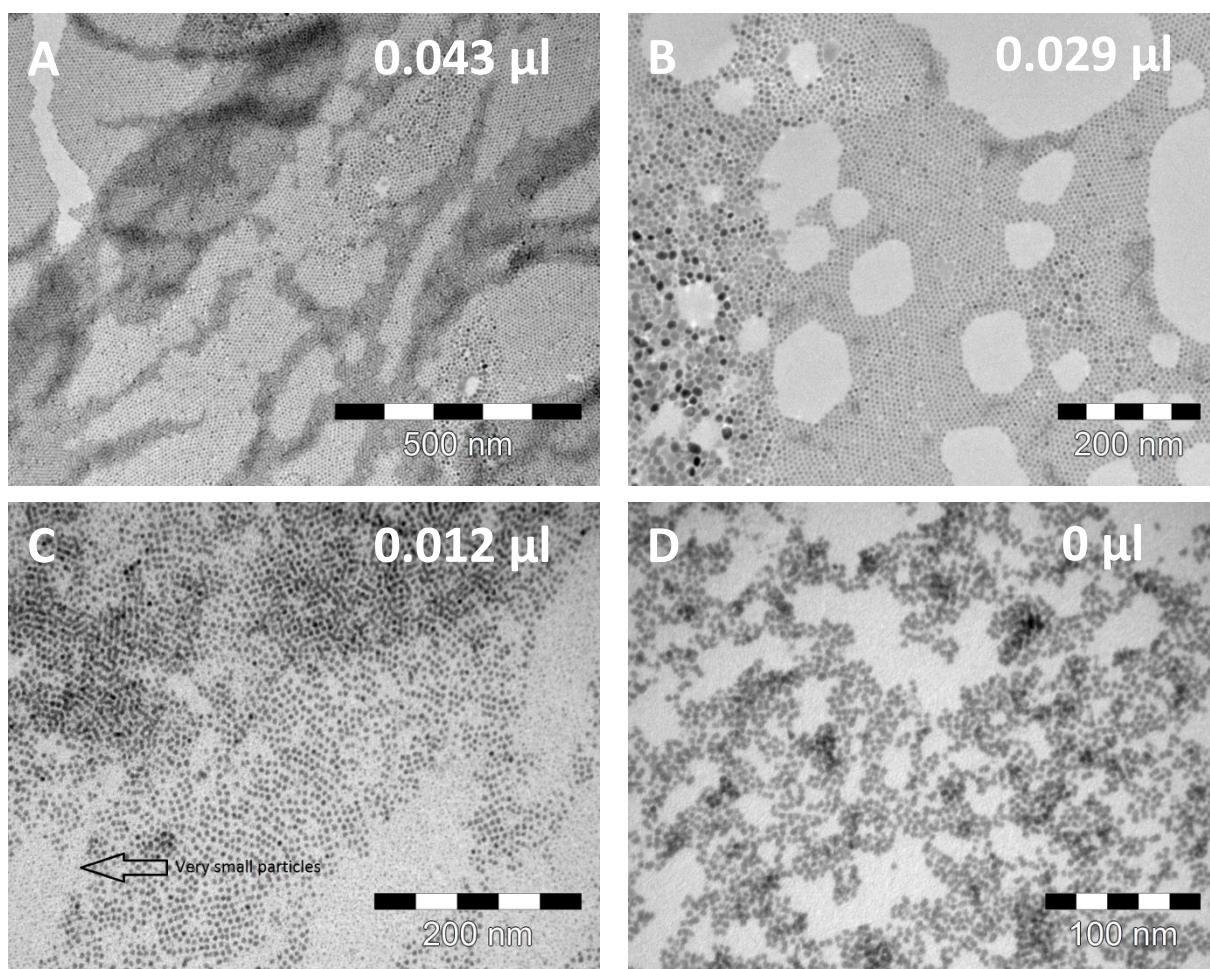
Figure 30. The development of oriented attachment experiments by addition of oleic acid in ethylene glycol, in A) 0.043 μl, B) 0.029 μl, C) 0.012 μl and in D) nothing. In A) and B) the particle shape is preserved and long range single layered hexagonal packing's are formed, but at some places, starting from a middle point , Ostwald ripening is discernible. In C) & D) the particle shape is not preserved. The particles start to decompose in smaller particles and the shapes are changing dramatically.

Appendix 3.
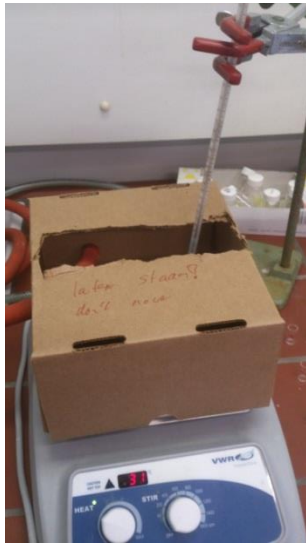
Figure 31. The setup for a simple test if oriented attachment could be performed in a semi-closed environment with a flow of oxygen pumped in the box by the brown hose. This experiment was tried to probe (in a worst case scenario) the conditions at the synchrotron.

Appendix 4.

GISAXS

Table 5. An overview of the peak positions and the corresponding distance between quantum dots in a hexagonal ordered lattice. The peak distance are calculated by $\frac{4\pi}{(\sqrt{3})*q-factor}$. Only the runs with visible peaks were used, after run 49 the peaks vanished.

run	Q factor peak 1	Distance according peak 1 [nm]	Q factor peak 2	Distance according peak 2 [nm]
35	0.747	9.71	0.807	9.00
36	0.750	9.67	0.798	9.09
37	0.750	9.67	0.798	9.09
38	-	-	0.799	9.08
39	-	-	0.805	9.01
40	-	-	0.810	8.96
41	0.758	9.57	0.812	8.93
42	0.762	9.52	0.821	8.84
43	0.763	9.51	0.823	8.82
44	0.769	9.43	0.827	8.77
45	0.783	9.27	0.831	8.73
46	0.772	9.40	-	-
47	0.775	9.36	-	-
48	0.778	9.33	-	-
49	0.781	9.29	-	-
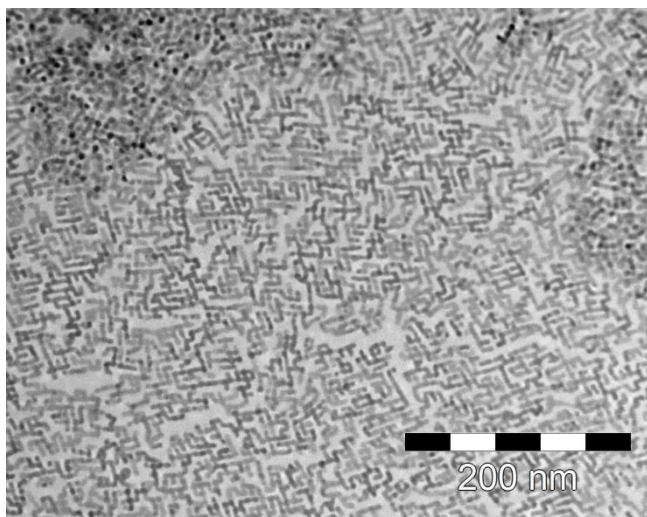
Figure 32. In this sample 45 µl of stock solution dissolved in 5 ml hexane was dropped on 5 ml EG in the same equipment as in Grenoble but setup in the glovebox in Utrecht. Disordered but attached quantum dots are visible, which extended on a large area.

Appendix 5.
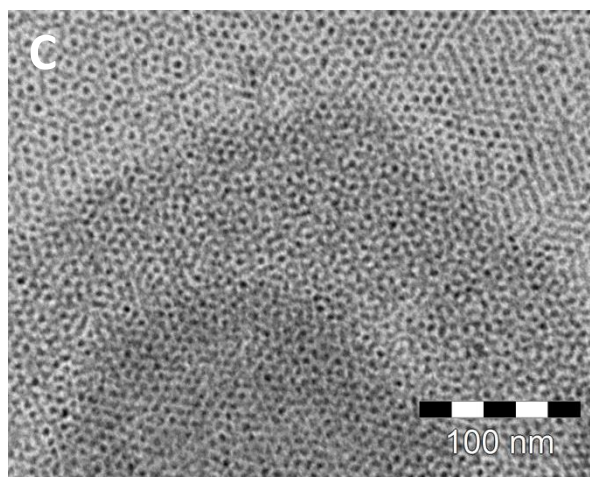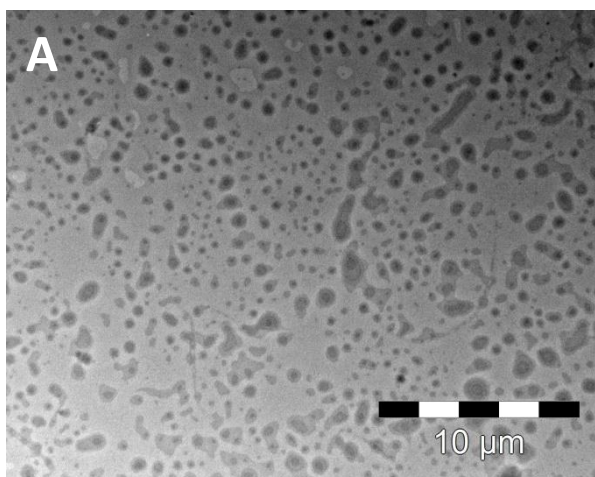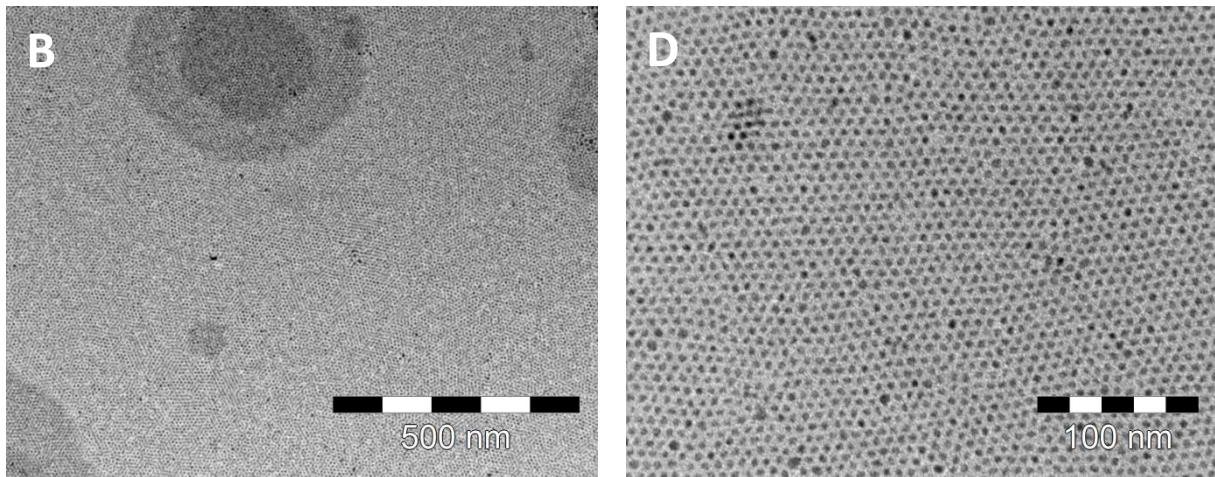
Figure 33. TEM image of PbS unattached particles. The same drying pattern is visible. A-D are dried at 20 °C for 120 minutes with a relative concentration of [25] for different magnifications.

Appendix 6.
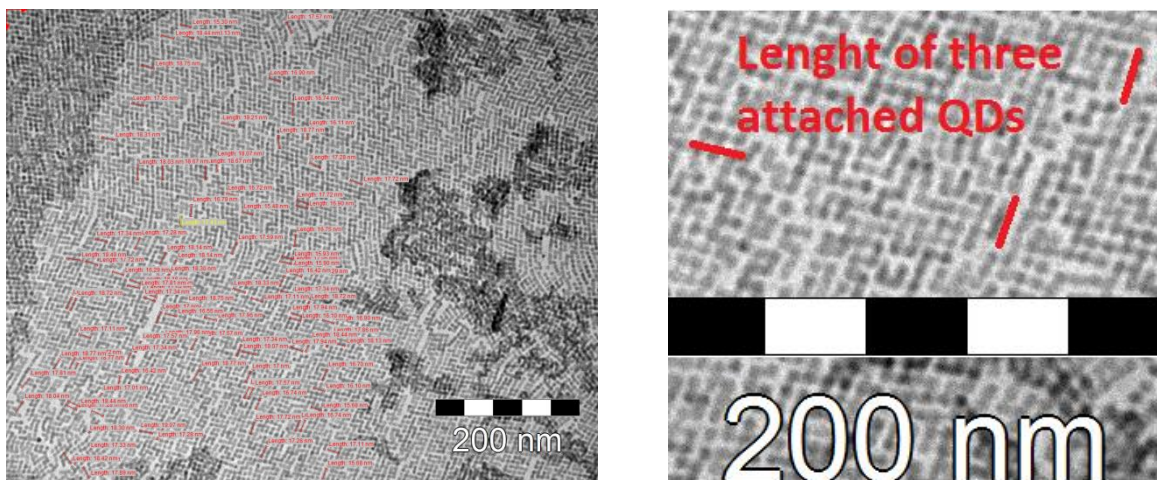
Appendix figure 34. (A) Overview of the measurements done in a 'square' lattice. Every time the total length of 3 clearly attached particles are measured as shown in figure (B).

Table 6. Line trace of 3 attached particles in a square lattice and statically measures.

PbTe	Mean, μ [nm]	Mean /3	Nr.	σ [nm]
17.53	5.84	100	0.91

Overview of line traces. The average length of 1 attached quantum dot is about 5.84 nm. The difference in this measurement and the size of a quantum dot measured after the synthesis (5.86 nm) is not significant different on a 1% level, with a t-value of 3.390, n=100 and

σ=0.91.It therefore does not seem that detachment of oleate from the surface of a quantum dot is due to the detachment of Pb-oleate. Although this analysis is too simple to draw a 'hard' conclusion. Other more directed measurement should be considered to be sure about this hypothesis.

Appendix 7.

Rough calculation of the total amount of oleic acid needed to fill up the complete surface of all quantum dots availably in a standard experiment.

Amount of quantum dots*Surface of a sphere in nm*4.2 = total amount of oleic acid to fill the complete surface.

4.2 is the average amount of oleic acid molecules on one nm^2 [17]. The amount of quantum dots is been estimated by the concentration given by Wiels Evers et al. for the siliceen lattice [82]. Other estimations, like for example calculate the amount of particles to cover the complete surface or uses the concentration of PbS, give approximately the same result.

$5.23*10^{16}$. => $8.69*10^{-8}$ mol oleic acid=> $2.456*10^{-5}$g => $2.1*10^{-5}$ ml oleic acid => 0.02 µl oleic acid

Even though this calculation is very rough, it gives an idea about the order of the amount. This incredible low amount (0.02 µl) explains way this system is so vulnerable for environmental changes, like the atmosphere, washing procedures of the glass, pollutions in compounds used etc.

Appendix 8.
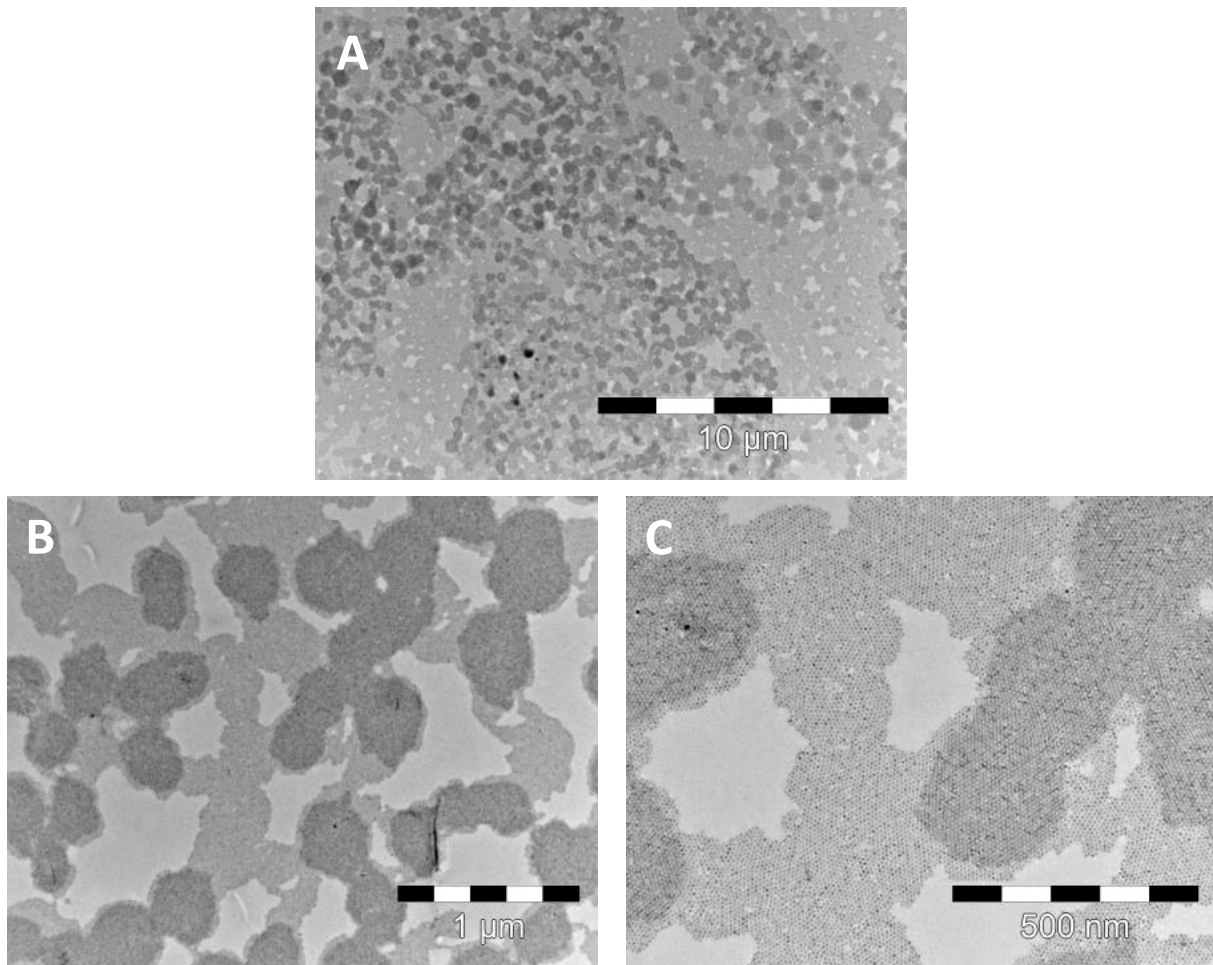
Figure 35. TEM images of an PbTe oriented attachment sample, with a relative concentration of [17], with the addition of 0.145 µl oleic acid to the EG. In this oleic acid rich sample particles were to protected for attachment but they form two dimensional spherical hexagonal packed sheets.

If it is true that at certain concentration hexagonal packed quantum dots in sheets arise, like in the article of Z. Tang et al. [123], there can be a connection with nanopletelets in the article of C. Schliebe at al. [91] and S. Ithuria et al. [94]. These self-assembled sheets can be the template to form an atomically connected nanoplatelet via oriented attachment. Attachment can than maybe be provoked, by chlorine containing co-solvents 1,2-dichloroethane, 1,2-dichloropropane and 1,1,2-trichloroethane, an increase in pH or slightly higher temperature. Investigation if free floating sheets are formed can be very easily done in GISAXS experiments, by putting a quantum dot solution with different oleic acid concentrations in a capillary and see if self-assembled structures are visible.

Appendix 9.

Unsuccessful attempt to induce attachment by small alcohols.
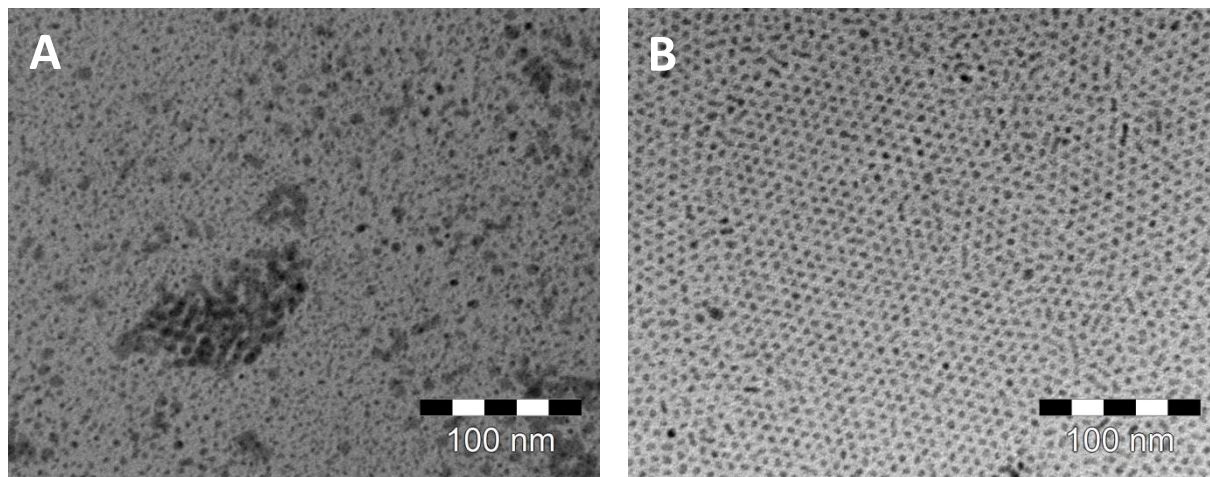
Figure 36. Both PbS samples (rel.[20]) are performed at room temperature (not the attachment temperature). In (A) however after 60 minutes 50 μL MeOH was added on the sample which resulted in aggregation and the break-up of particles. Nothing is done in (B) which resulted in normal hexagonal packed particles consistent with was is expected.

From figure it is clear that addition of MeOH has effect on the particles, but it was clearly not controlled enough to induce oriented attachment. When the MeOH was dropped the already dried structure was disorderd, by the droplet, which makes it not a good method. Injection of molecules in the EG layer would give more controllable conditions.
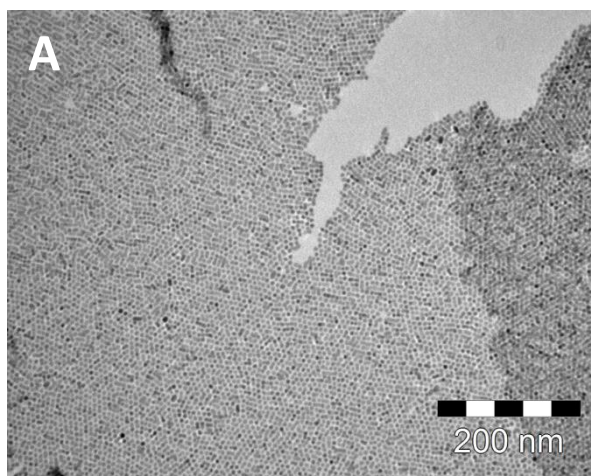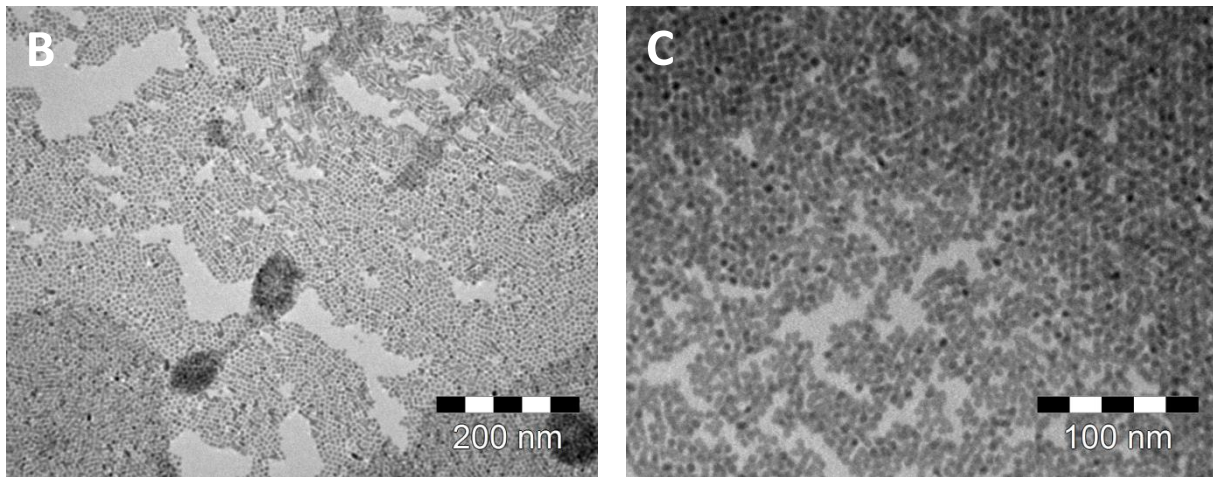
Figure 37. PbTe samples ([17]) with the addition of 0.025 μL oleic acid in the EG at 20 °C. (A) is performed in normal glovebox atmosphere, mostly separate unattached particles are visible. 5 mL MeOH was evaporated in the glovebox, 5 minutes before sample (B) was started, here also mostly separate particles are visible, but also small melted areas. In (C) another 5 mL was added in gaseous conditions to the glovebox. Now most particles are melted or attached together in a somewhat uncontrolled fashion.

Figure 35 shows what happened to PbTe samples when the glovebox atmosphere was changes by letting 5 mL of MeOH evaporate before starting the experiment (B). In (C) another 5 mL was evaporated which seem to change the attachment of the particles, from unattached to randomly attached. There are some changes in the shape of the particles, but there was no time to redo it and control it properly, more research is necessary.

Appendix 10.
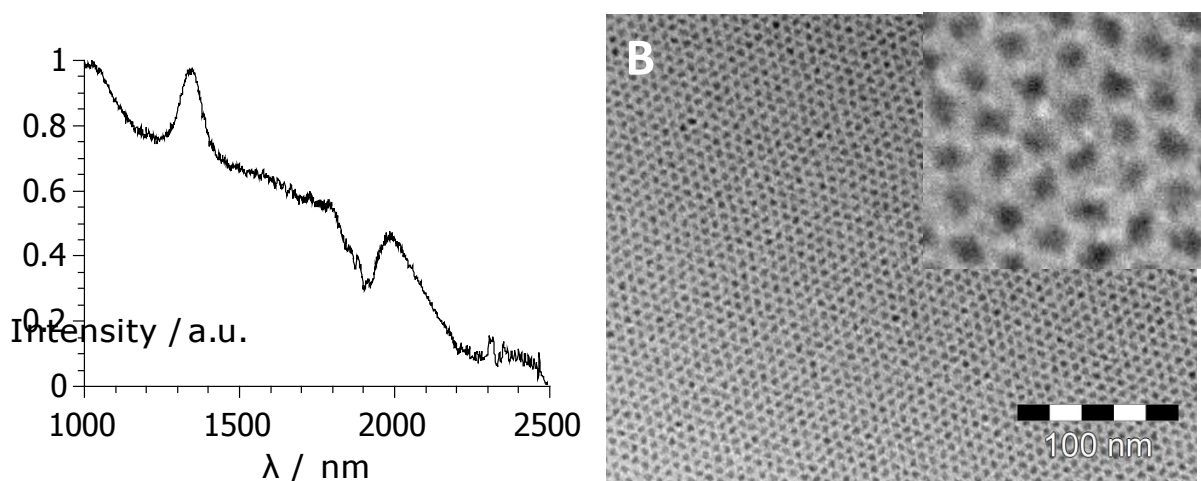
Fugure 38. In (A) the absorption of PbS (4.9 nm) is shown. The peak around 1325 nm is the first exciton peak

and the cove around 1900 nm is due to negative absorption of toluene (left over solvent). In (B) separate particles are shown in a TEM image. In the upper right corner a magnification of (B) is shown in which it is visible that not all particles look very spherical or truncated cube like, but there also exist undefined shaped particles.
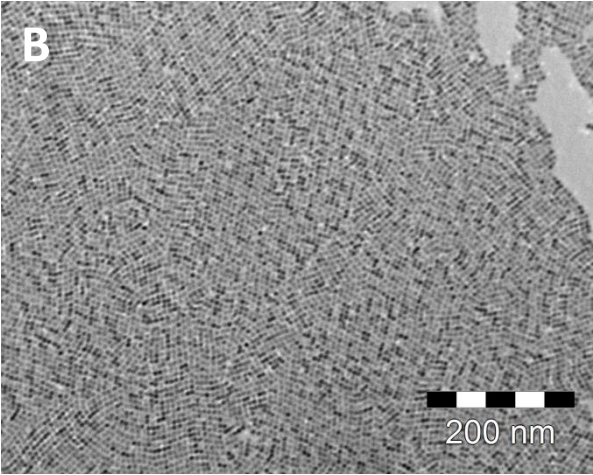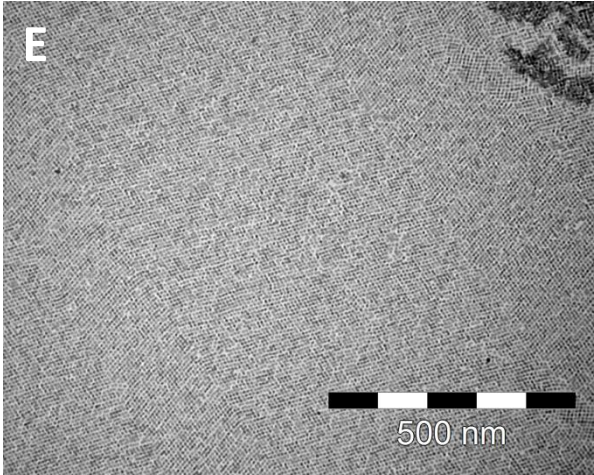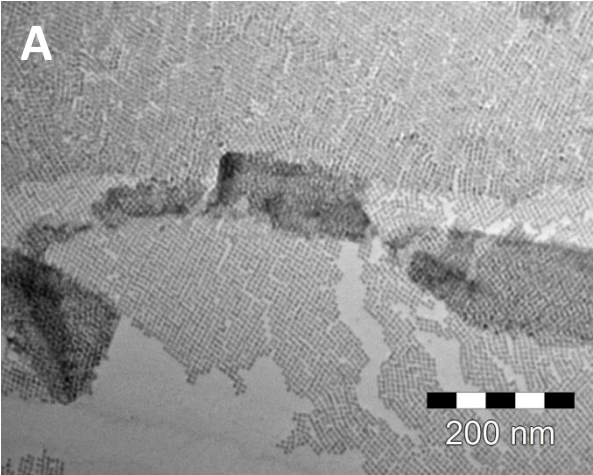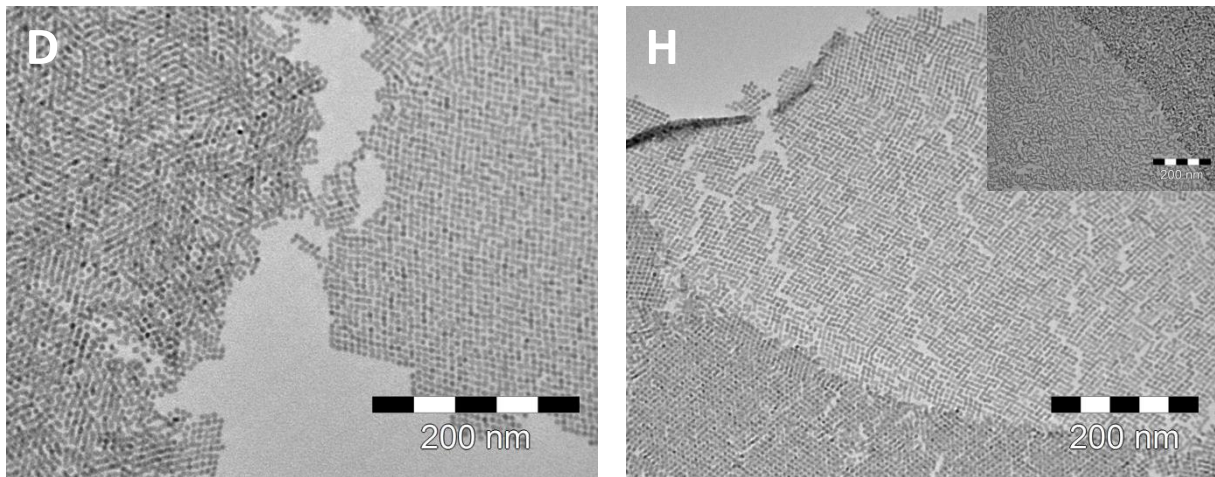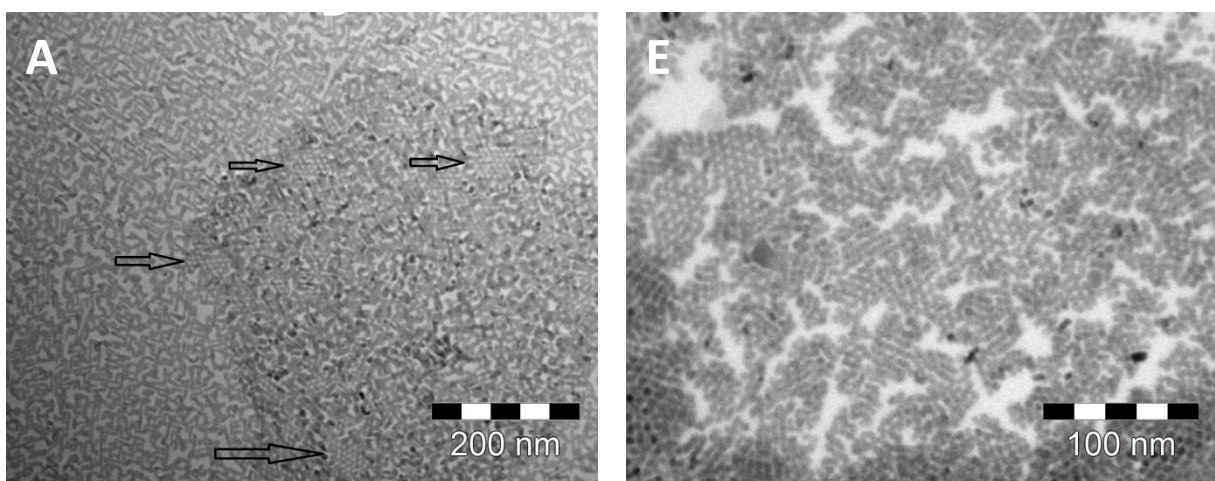
Appendix 11.
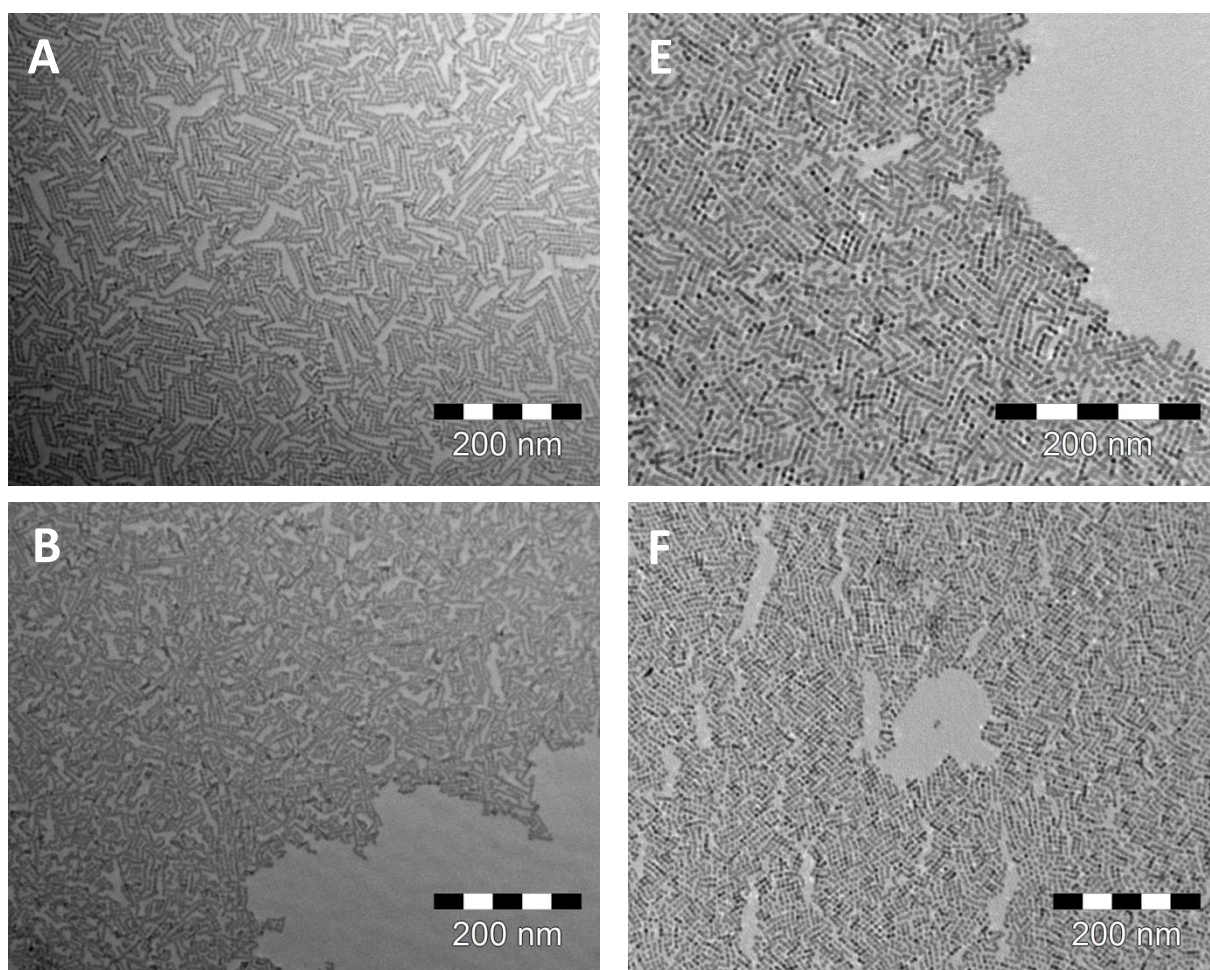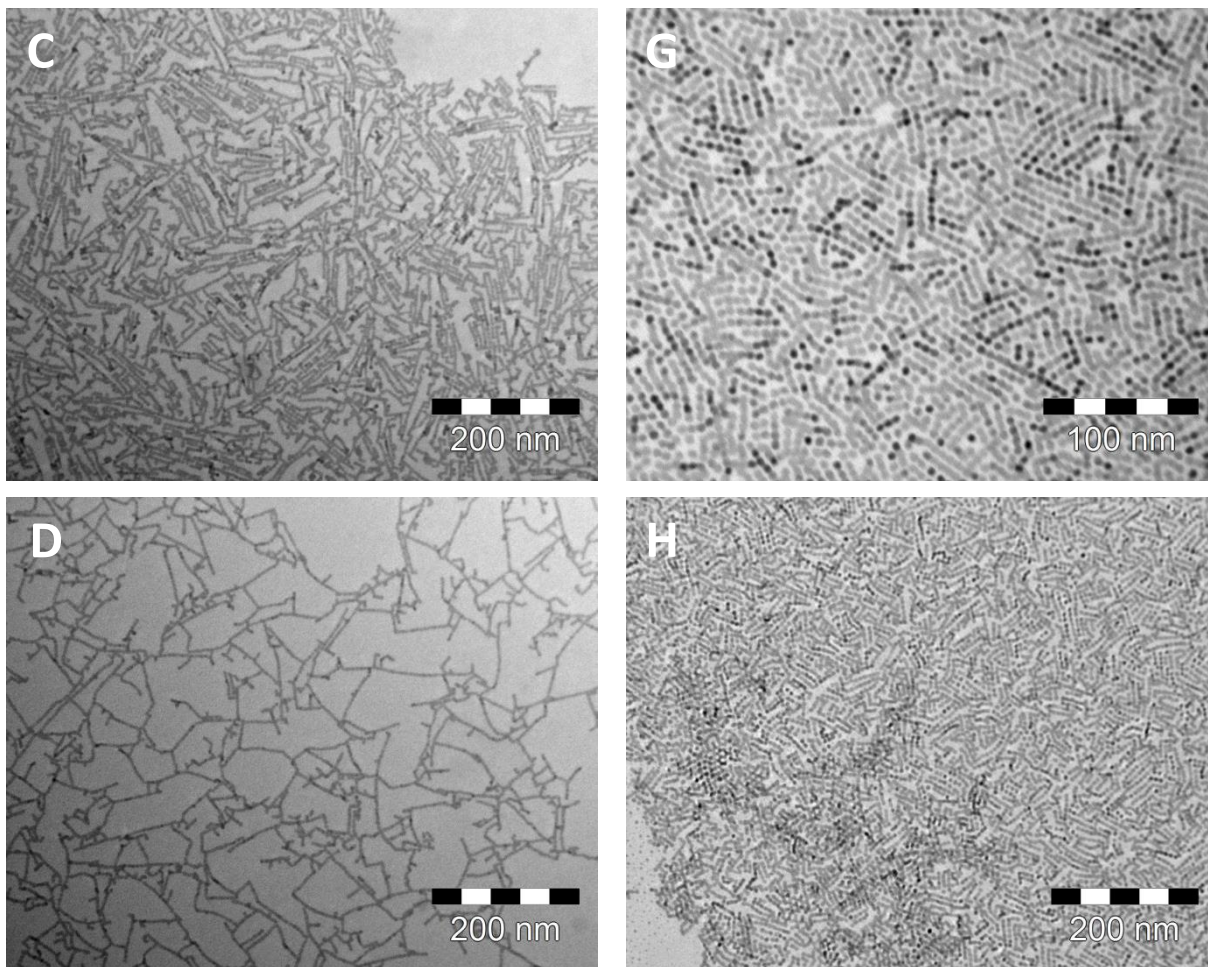
Figure 39. examples of linear attached quantum dots of PbTe. Some concentration be preceded by a ± sign, which indicate that the concentration can differ more. This is due to evaporation of the solvent of the stock solution. (A), at room temperature, [±10], also siliceen lattices visible in this sample (B), room temperature, [±2], (C), 40 °C, [±2], (D), 40 °C, [±1], (E) 20 °C, [15], (F) 7 °C, [±5], (G) 20 °C, [±12.5], with $2 \cdot 10^{-5}$ mol/l oleic acid in the ethylene glycol, (H) 20 °C, [18], was in combination with small parts of the siliceen lattice.
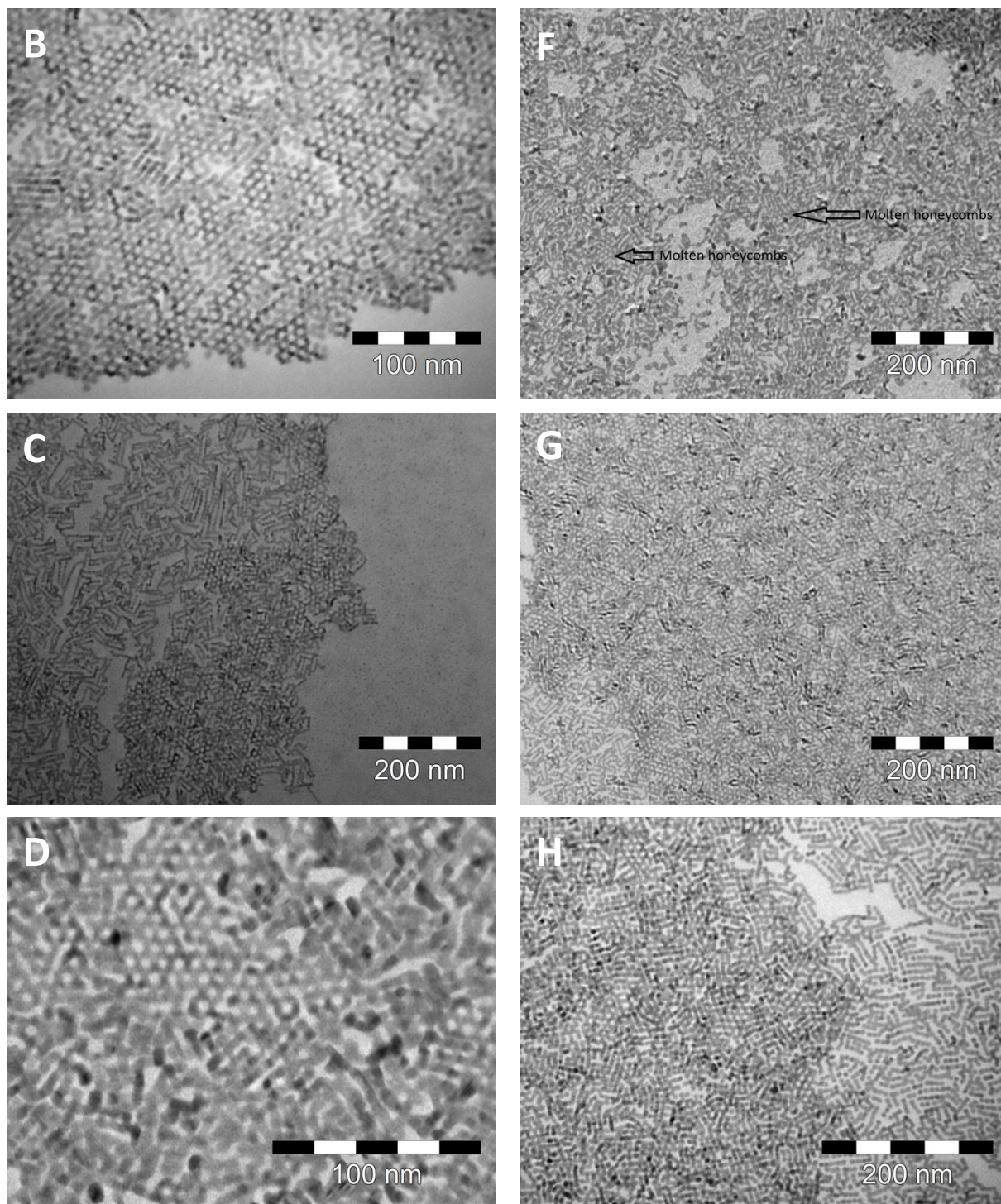
Appendix 12.
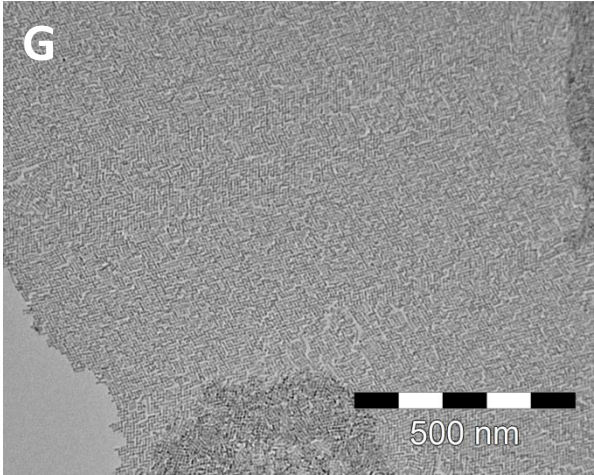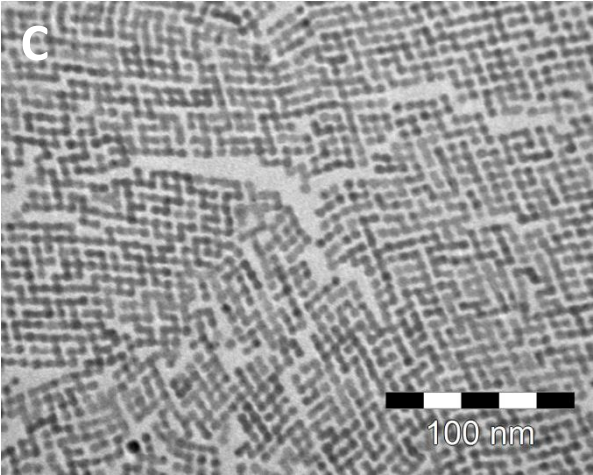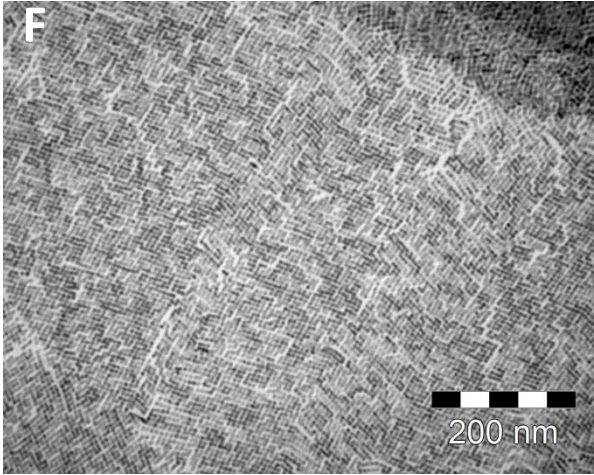
Figure 40. Examples of attached quantum dots in a 'squere' lattice. Some concentration be preceded by a ± sign, which indicate that the concentration can differ more. (A), at room temperature, [±50], (B), 7 °C [±50], (C), at room temperature, [±40], with 4·10⁻⁵ mol/l oleic acid in the ethylene glycol, (D), at room temperature, [±20], with 4·10⁻⁵ mol/l oleic acid in the ethylene glycol, (E) at room temperature, [±20], with 2·10⁻⁵ mol/l oleic acid in the ethylene glycol, (F) at room temperature, [±20], with 1·10⁻⁵ mol/l oleic acid in the ethylene glycol, (G) 20 °C, [±20], (H) 30 °C, [±40], with 2·10⁻⁵ mol/l oleic acid in the EG.

Appendix 13、

Figure 41. Examples of attached quantum dots in a siliceen lattice. Some concentration be preceded by a ± sign, which indicate that the concentration can differ more. (B), 40 °C, [±15], heavily melted, but siliceen lattice is still visible (B), at room temperature, [±20], (C), at room temperature [±10], (D), 40 °C, [±20], with $4 \cdot 10^{-5}$ mol/l oleic acid in the ethylene glycol, (E) 20 °C, [±20], on DEG, (F) 25 °C, [25], on DEG, (G) 20 °C, [16], (H) 20 °C, [15],
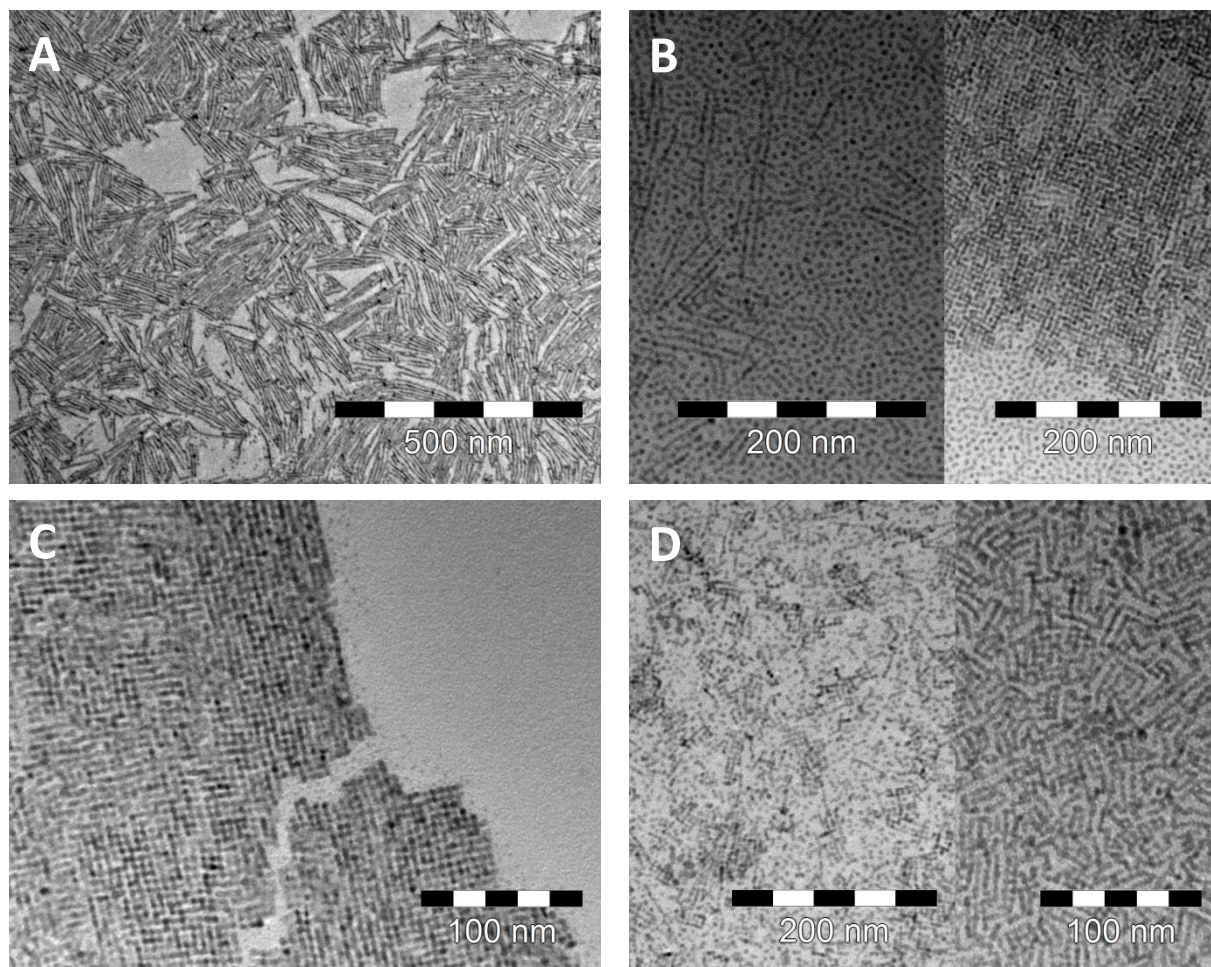
Appendix 14.

Figure 42. TEM images of oriented attached PbS quantum dots (5nm) at 30 °C. Relative concentrations are A) [20], B) [25], C) [30], D) [25] and 120 minutes was waited before fishing. A clear linear attachment is visible in A) a mix situation (linear, square and separate particles) is visible in B), a clear square structure is visible in C), and another very mix situation is visible in D). This sample was performed on other ethylene glycol in which $4*10^{-5}$ mol/l oleic acid was added to the EG.
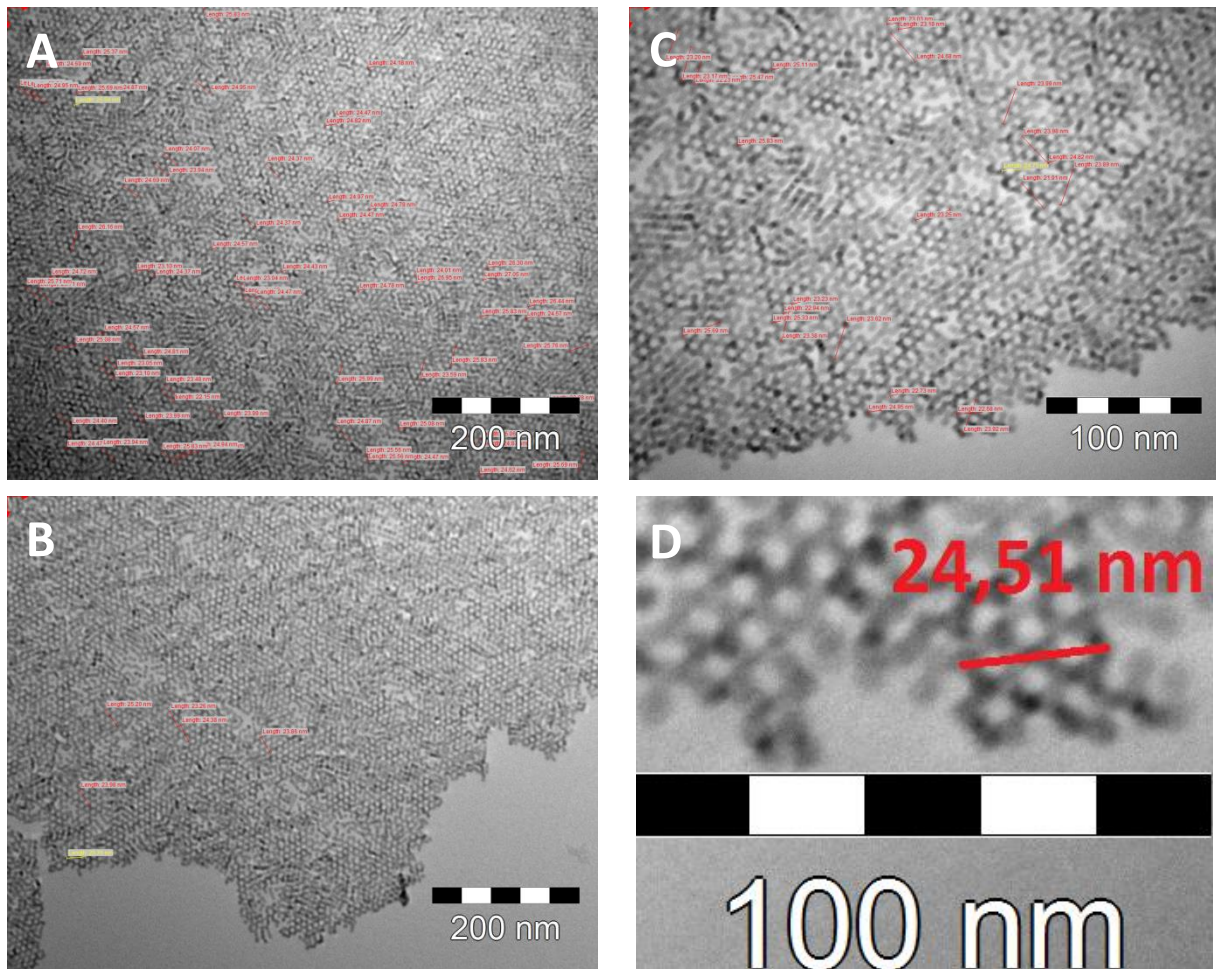
Appendix 15

Figure 43. A), B), C), give an overview of the length measurements of the honeycomb structure. D) in red a schematically overview over the measured line trace.
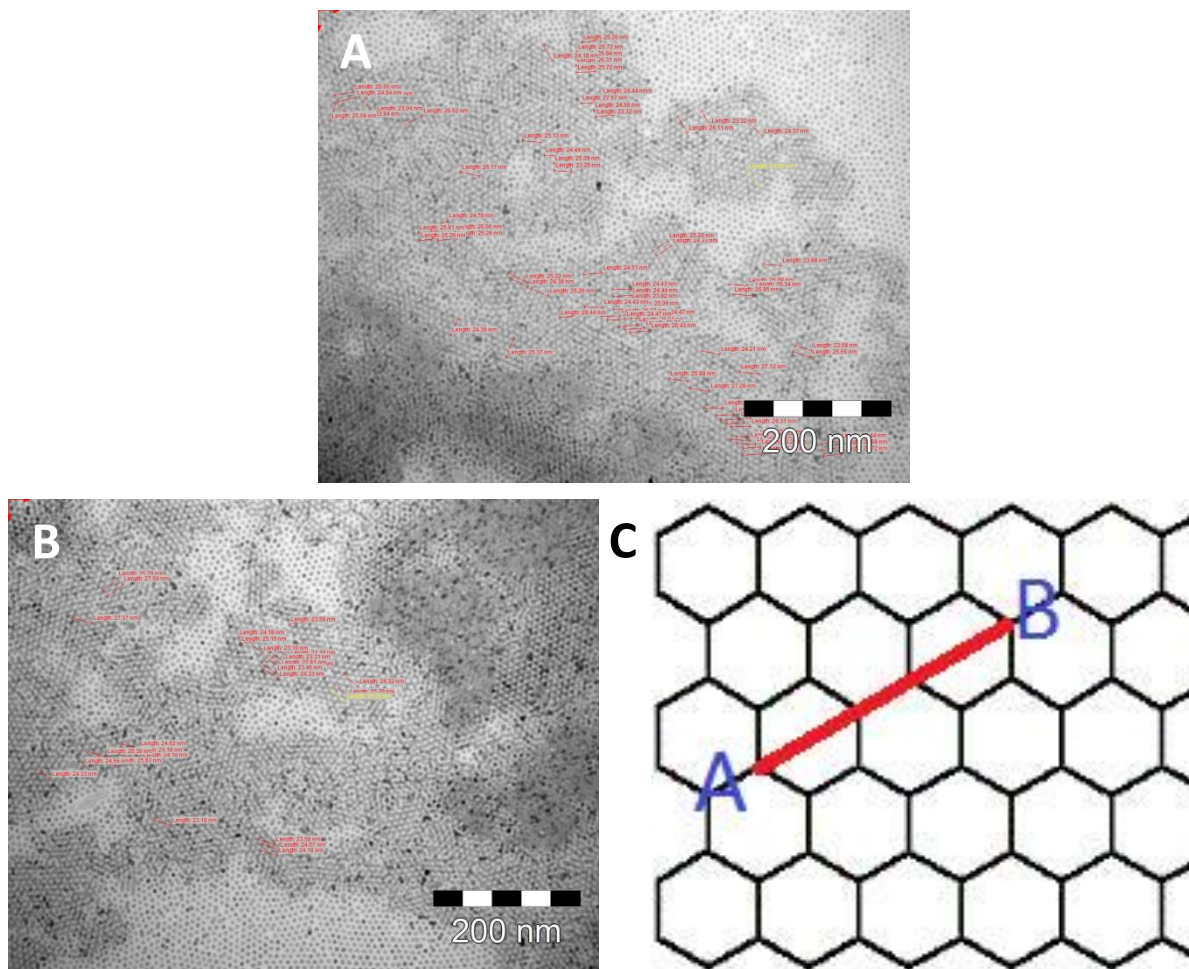
Figure 44. In (A) & (B) an overview of the length measurements of two overlapping hexagonal planes. C) A schematically overview of the measured line trace of the samples.